Solidification of Thin Liquid Films

Christopher T. Miles

Thesis submitted to The University of Nottingham
for the degree of Doctor of Philosophy

30th September 2019

Abstract

Understanding the dewetting and solidification of thin films is key in the fabrication of thin film solar cells, as a device with low percentage of surface coverage will have a greatly diminished efficiency. In this thesis we use Rational Continuum Mechanics to propose a thermodynamically-consistent framework for classes of models describing the evolution of solidifying thin films.

Starting from the key laws of the conservation of mass and the first and second laws of thermodynamics, and employing the Coleman Noll procedure, we derive a class of models for predicting the evolution of a thin liquid film in isothermal settings. We show that models existing in literature and derived using different techniques fit into these classes. This work is published in [1].

Invoking the same axioms we then consider non-isothermal settings, and first re-derive models for solidification in a bulk setting. Then we return to thin-film settings and derive a model for heat conduction in a rigid thin film by averaging the laws in the vertical direction to reduce the problem from d dimensions to $d-1$ dimensions, and then proposing a solution to the closure problem that arises due to fluctuations in the z direction. Culminating these techniques we discover, for the first time, a thermodynamically-consistent class of models for the solidification of thin films.

To allow proper numerical simulations, suitable choices for the constitutive relations within the new models are discussed. Simulations are discussed using linear finite elements for the spatial discretisation and energy-stable convex-splitting schemes as the time stepping algorithms. Parameters within the model are varied to investigate the effect they have on the dewetting of the thin film and the growth of holes, which gives implications on optimal manufacturing conditions for thin film solar cells.

Acknowledgements

I would like to express my greatest appreciation to my supervisors Dr Kris van der Zee and Dr Matthew Hubbard for their help and support throughout the four years of this project. I would also like to thank Professor Markus Owen and the Leverhulme Trust for funding the project.

Finally I would like to thank my family and friends for the endless moral support they have given to me throughout the project.

Contents

1 **Introduction** 1

1.1 Thin Film Solar Cells 2

1.1.1 Thin Film Solar Cells: Technological Importance . . 2

1.1.2 Fabrication of Thin Film Solar Cells: Surface Coverage Issue 3

1.1.3 Modelling Techniques 6

1.2 Achievements and Outline of Thesis 7

2 **Rational Continuum Mechanics** 11

2.1 Introduction to Rational Continuum Mechanics 11

2.2 Key Laws 14

2.2.1 Conservation of Mass 14

2.2.2 Conservation of Linear and Angular Momentum . 15

2.2.3 1st Law of Thermodynamics 18

2.2.4 2nd Law of Thermodynamics 19

2.2.5 Mechanical Version of the Second Law 20

2.3 Phase Field Variables 21

2.4 The Allen-Cahn and Cahn-Hilliard Equations 23

2.4.1 Allen-Cahn Equation 24

2.4.2 Cahn-Hilliard Equation 25

3 Numerical Methods for Phase Field Simulations 27

3.1 Gradient-Flow Model 27

3.2 Numerical Methods for Simulations 28

3.2.1 Spatial Discretisation 28

3.2.2 Convex Splitting Time Discretisation 30

3.2.3 Backwards Euler Time Discretisation 33

3.2.4 IEQ and SAV Methods 35

4 Isothermal Thin Film Dynamics 38

4.1 Nucleation and Growth of Holes in Thin Films 39

4.1.1 Simple Hole Growth Models 39

4.2 PDE Models Describing the Evolution of Thin Films 43

4.2.1 Classical Thin-Film Modeling 43

4.2.2 Energetic Modeling Approach in Thin Films 49

4.3 Rational Derivation of Isothermal Thin-Film Dynamics . . 50

4.3.1 Constitutive Dependence 52

4.3.2 Deriving Constraints 53

4.3.3 Choices 54

4.3.4 Connections 55

4.3.5 Regularisation of the Asymptotic Model 57

4.3.6 Conclusion 58

5 Solidification in a Bulk Fluid 62

5.1 Existing Work 62

5.1.1 Sharp Interface Model 63

5.1.2 Phase-Field Modelling 64
5.1.3 Adaptions to the Phase-Field Model 67
5.2 Rational Derivation of a Model 68
5.2.1 Deriving Constraints 68
5.2.2 Choices of Constituent Classes 70
5.2.3 The Free Energy Functional 74
5.3 Conclusions 76

6 Thin Film Heat Equation **78**
6.1 Geometry 78
6.2 Vertical Averaging 81
6.2.1 Conservation of Energy 81
6.2.2 Entropy Inequality 83
6.2.3 Applying Laws of Thermodynamics 84
6.3 Free Energy Functional 85
6.3.1 Defining the Dependent Variables 87
6.3.2 Final Equation 92

7 Thin Film Solidification **93**
7.1 Axiomatic Laws for a Solidifying Thin Film 94
7.1.1 Conservation of Mass 94
7.1.2 Conservation of Energy 96
7.1.3 Entropy Inequality 98
7.1.4 Solidification 99
7.1.5 The Reduced Dissipation Inequality 100
7.2 Choices of Constituent Classes and Dependent Variables . 101

7.2.1 Free Energy Functional 101
7.2.2 Choices of Dependent Variables 105
7.3 Internal Energy and the Free Energy 113
7.4 Specific Models 115
7.4.1 Latent Heat 115
7.4.2 Model A 116
7.4.3 Model B 117
7.5 Verification of the Models 119
7.5.1 Thermodynamical Consistency 119
7.5.2 Thin Film Heat Equation 120
7.5.3 Thin Film Flow 121

8 Numerical Simulations 123
8.1 Numerical Methods 123
8.2 A Non Volatile Liquid Film on a Substrate 124
8.3 Numerically-Suitable Function Extensions and Convex Splitting 125
8.4 Solidification of a Liquid Film 129
8.5 Solid Film Melting on a Heated Substrate 133
8.6 Volatile Film on a Heated Substrate 137
8.7 Conclusions 139

9 Conclusions and Recommendations for Future Work 140
9.1 Conclusions 140
9.2 Recommendations for Future Work 142

References 144

CHAPTER 1

Introduction

In a world in which non-renewable energy sources are rapidly depleting, and climate change caused by burning fossil fuels is having a devastating effect on the natural environment, it is becoming more important than ever to pursue cheap and clean renewable alternatives. Solar power offers an annual potential of over 1,500 exajoules of energy, around three times the total annual energy consumption in the world in 2012 [2]. However, by the end of 2016, only 1.8% of the world's electricity consumption came from solar power. Despite this, according to a 2014 study conducted by the International Energy Agency [3], solar power could be the largest source of energy by 2050.

Thin film solar cells, including those using perovskite material to absorb light, have the potential to greatly enhance the amount of solar energy harvested in society. They provide a cheap and lightweight alternative to silicon devices, and are currently the fastest developing photo-voltaic technology to date [4]. In addition to this, fabrication of these devices uses much less energy than their silicon counterparts, and they are constructed using materials abundant in nature.

The topic of this PhD thesis is the solidification of thin liquid films, which is one of the key processes in the fabrication of thin-film solar cells. To provide a proper context into the thesis, we next present in Section 1.1

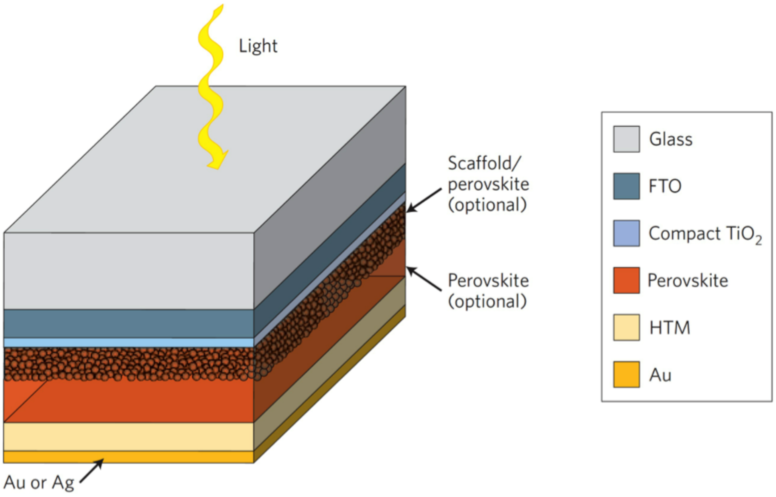

Figure 1.1: Diagram taken from [6] showing the layer structure of a thin film solar cell. Fluorine-doped Tin Oxide (FTO) is used as the electron transport material, while an optional metal oxide scaffold is shown [7]. In this case the absorbing layer is Perovskite.

a brief review on thin-film solar cells, issues with their fabrication, and approaches to their mathematical modelling. Then, Section 1.2 outlines the achievements obtained in this thesis.

1.1 Thin Film Solar Cells

1.1.1 Thin Film Solar Cells: Technological Importance

A standard thin film solar cell consists of three major components: an absorber for the absorption of light (for example Perovskite), an n-type semi-conductor such as FTO to accept electrons excited by the absorbed light, and a p-type semi-conductor (hole transporting material, HTM) for transporting holes [5], arranged as in Figure 1.1. During illumination, light excites electrons in the Perovskite material, which are injected into the conductance band of the n-type semi-conductor. The positive charge left on the Perovskite is then transferred onto the p-type semi-conductor and then on to the electrode.

Perovskite is an organic-inorganic compound that is attracting a large amount of attention in the field of photo-voltaic devices, due to the fact that the cells have the potential to be transparent, flexible, cheap and highly efficient. Details on the structure of the Perovskite material can be found in [6, 8–10]. There is a theoretical maximum limit, known as the 'Shockley-Queisser' limit, for single junction solar cells. For Perovskite based cells, the limit of efficiency is 31%, which is close to the 33% limit of gallium arsenide cells [11]. Current issues with the technology include rapid degradation of the devices, particularly in damp conditions [12]; however large strides have been taken to rectify this issue, such as in [7, 13].

Issues needing to be overcome during the fabrication process of a thin-film solar cell are the thickness of the absorbing layer [14, 15] and the size of the crystalline grains formed during solidification of the layer [16–18]. The final issue is the dewetting of the absorbing layer during fabrication [19]. The *surface coverage* issue [20, 21] is the basis of the research in this thesis and is discussed in greater detail in the next subsection.

1.1.2 Fabrication of Thin Film Solar Cells: Surface Coverage Issue

One of the major factors dictating the efficiency of a thin film solar cell is the percentage of the device that is covered by the absorbing material. Fabrication of perovskite solar cells involves mixing chemicals in a solvent to produce the Perovskite compound (the most studied Perovskite mixes methylammonium iodine, MAI, and lead iodide, PbI_2, in a solvent to produce methylammonium lead tri-iodie perovskite,$MAPbI_3$). The perovskite-solvent mixture is then deposited onto a substrate using a deposition technique which can include dip coating [22], spin coating [23, 24] or vapour deposition [17], as shown in Figure 1.2.

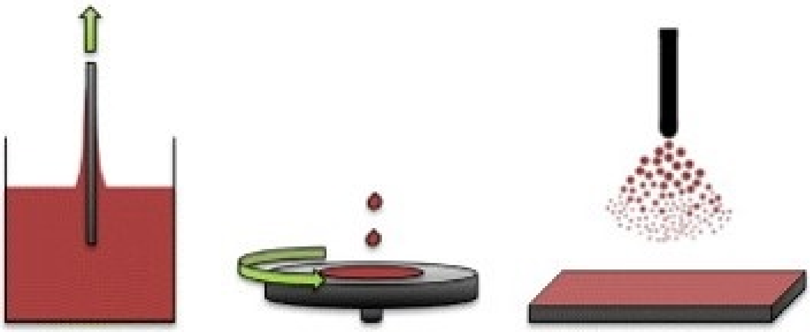

Figure 1.2: Three examples of deposition techniques, from left to right: dip coating, spin coating, vapour deposition. Image taken from [25].

Following deposition, the film is annealed by heating the device. This allows the Perovskite to fully crystalise [17], and also allows any unreacted reagents and the solvent to evaporate off. This evaporation drives a dewetting phenomenon [26] during which the thin film flows and solidifies, resulting in the final morphology of the thin film absorbing layer. It is this dynamic process of changing thin film morphology that the research carried out in this thesis is directed towards.

Poor surface coverage causes a reduction in device efficiency for two major reasons. Most obvious is that light cannot be absorbed by the areas uncovered by the absorber layer. Thus if only 70% of the cell is covered by the thin film, a maximum of 70% of light hitting the device can be absorbed while the rest passes through, assuming a uniform distribution of photons [14]. Secondly, a hole in the absorber layer allows the contacts on either side of the absorbing material to touch, creating 'shunt paths', in which recombination [27] of released electrons becomes much more likely, reducing the cell efficiency [28]. Many works agree that to achieve the maximum possible efficiency from a perovskite solar cell, carefully controlling the morphology of the film is key [9, 14, 29].

Some methods have been proposed to help avoid this issue. In 2014, Eperon et al. conducted a series of experiments to obtain maximal surface coverage by optimising annealing temperature and initial film thick-

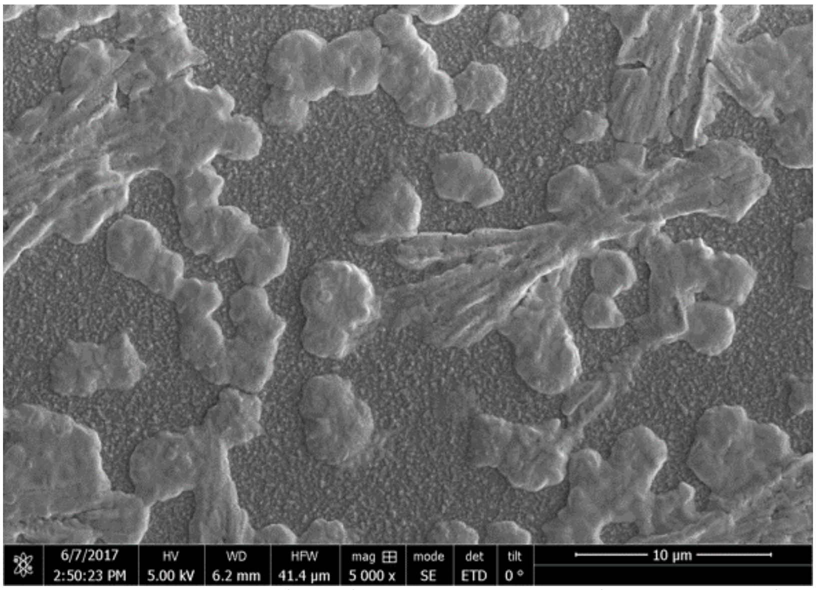

Figure 1.3: An example of the final morphology of a solar cell after annealing. The light areas are islands of perovskite while the darker area is the substrate uncovered by the absorber layer. Courtesy of a collaboration with the University of Amsterdam

ness [14]. They also discovered that using a solvent that evaporated more slowly reduces the surface coverage. Xu et al. suggested a method involving pumping away the solvent before the device is annealed [30]. This has the effect of greatly reducing the influence of solvent evaporation on film evolution and resulted in an average increase in film efficiency of 2%. Another method is to use a scaffold as a support for encouraging surface coverage [31–33], although this requires the use of much higher temperatures than fabrication of planar cells [34], incurring a higher energy cost.

It is well known that solid films in the as-deposited state are often thermodynamically unstable, causing them to dewet or agglomerate during annealing [35]. During the annealing phase, the absorber layer dewets and forms islands of perovskite surrounded by areas where the substrate is uncovered by the absorber layer. Figure 1.3 highlights this effect. Works cite various reasons for poor surface coverage. Fast crystallization of the perovskite material with solvent evaporation has been considered by Huang et al. [36], while the effects of film thickness [29] and the choice of halide anion [9] have also been investigated.

1.1.3 Modelling Techniques

The evolution of an unstable thin film has been well studied in a variety of ways. Many of these studies consider asymptotically manipulating bulk Navier-Stokes equations. A key work in this field is from Burelbach et al. [37] which is an underlying work to many further modelling attempts for the phenomenon. However, the asymptotic handling of bulk equations does not always guarantee that a model is consistent with the laws of thermodynamics. More recent methods of modelling thin film evolution are gradient flow based, for example [38]. These models, while thermodynamically consistent, make specific choices, while there exists whole families of models for describing thin film evolution which align with the laws of thermodynamics.

Rational Continuum Mechanics [39] provides a framework for modelling that initiates from key axioms from physics, i.e. conservation laws and the laws of thermodynamics. Starting with these principles, a class of models can be derived which guarantees thermodynamic consistency, regardless of the material in question. To make a class of models specific to a particular material, constitutive classes can then be defined. The Coleman-Noll procedure [40] can then be applied to reduce the constituent class to ensure this thermodynamic consistency is maintained [41].

Rational Continuum Mechanics has become a leading method in the modelling of the solidification of materials [42, 43]. However its application to thin films has remained unexplored and is the topic of this thesis.

1.2 Achievements and Outline of Thesis

The main aim of this thesis is to provide a Rational Continuum Mechanics framework for the derivation of mathematical models for thin films and their solidification. The objectives achieved in this thesis are:

1. To derive a new elementary class of models for thin-film evolution in an isothermal setting, based on a rational framework using free-energy dissipation, and to show that this class supports existing models derived using asymptotics and gradient-flows.
2. To derive a class of models for solidification of a bulk liquid, based on a rational framework using the axioms of thermodynamics and a new constitutive dependence, and to show that this derivation is consistent with other existing rational frameworks.
3. To derive a new class of models for heat conduction in a rigid thin film, based on a rational framework using the axioms of thermodynamics, their vertical averaging, and suitable closure for vertical fluctuations.
4. To derive a new class of models for the solidification of thin films in a non-isothermal setting, by extending the framework obtained in Objective 3.
5. To demonstrate how to obtain stable numerical simulations for the new models and investigate the behaviour of a thin film in a variety of settings.

Chapters 2 and 3 introduce the method of Rational Continuum Mechanics and diffuse interface modelling. In these chapters, the five key axioms used in rational continuum mechanics are presented; the conservation of mass and linear and angular momentum and the first and second laws of thermodynamics. We also derive a mechanical version of the second law of thermodynamics that can be used in isothermal settings. Two important models, the non-conservative Allen-Cahn equation [44] and the conservative Cahn-Hilliard equation [45] are derived using these principles; these equations form the basis of the majority of phase-field type models. Finally, in Chapter 3, numerical methods for simulating phase-field models in an energetically stable manner are discussed. In particular, we show that the Convex Splitting scheme [46] is energy stable, but the Backward-Euler method is only conditionally energy stable despite it being fully implicit. The methods discussed in these chapters form the basis of all modelling and simulations carried out in this thesis.

In Chapter 4, we derive a class of thermodynamically consistent models for describing the evolution of a liquid thin film from the mechanical version of the second law of thermodynamics detailed in Chapter 2. We perform simple simulations using the convex splitting methods for time stepping and linear finite elements for the spatial discretisation, as described in Chapter 3. We investigate other attempts for modelling thin films, in particular the asymptotically derived model by Burelbach et al. [37] and the gradient flow method by Thiele [38]. We proceed to show that, for a non-volatile film, the models derived in these works fit within the class that we have derived, and therefore rectify these issues. In doing so, objective 1 is achieved. Our derivation and simulations presented in this chapter have been published in [1].

To approach objective 2, an non-isothermal class of models is derived in Chapter 5 to describe the solidification of a bulk liquid. Often during the modelling of solidification, the solidification model is derived in an isothermal setting and a temperature equation is added post-derivation [47], for example by considering Fick's Law [48]. We use rational continuum mechanics coupled with the Coleman-Noll procedure to derive a thermodynamically consistent class of models which is assumed to be non-isothermal to begin with. We consider the second law of thermodynamics, and follow the work of Fabrizio et al. [43] by considering additional terms in the entropy flux to account for entropy changes on the diffuse boundary of the phase change, and we adapt previous methods by allowing dependent variables to have a constitutive dependence on the chemical potential.

In Chapter 6 we derive a model for heat conduction in a d-dimensional rigid thin film based on a rational framework. We use the thin nature of the film to introduce the method of taking the average of the parameters in the vertical direction, resulting in reducing the model to $d-1$ dimensions. In doing so, a closure problem similar to that found in turbulance modelling [49] arises due to the existence of both vertically averaged terms and non-averaged terms in the laws of thermodynamics. Modelling a solution to this closure problem results in the achievement of objective 3.

Chapter 7 combines the methods from all previous chapters in order to derive a new class of models for a solidifying thin film in a non-isothermal setting, in doing so achieving objective 4. The issues with dealing with a non-isothermal setting, as well as the closure problem that arises from vertically averaging out parameters both reoccur, and are handled in similar way to Chapters 5 and 6 respectively. When considering a vertically averaged free energy, additional terms arise when employing the Coleman-Noll procedure; this results in the chemical potentials of the system needing to be modified. In order to achieve objective 4, we verify that the class of models is indeed thermodynamically consistent and that it reduces to the classes found in previous chapters when the scenario is simplified.

In order to provide numerical simulations in Chapter 8, we first choose parameters within the class found in Chapter 7 to obtain a specific model. This model requires regularisation in order to properly simulate it. The convex splitting method [46] is applied as a time stepping algorithm, while the model is discretised spatially using linear finite elements [50]. The simulations investigate both non-volatile and volatile films, and numerical experiments are run to investigate how changing parameters affects the growth of holes in the thin film.

Finally, concluding remarks are made in Chapter 9, and recommendations for future work are suggested.

CHAPTER 2

Rational Continuum Mechanics

In this chapter, we introduce the framework of Rational Continuum Mechanics and rational diffuse interface modelling, and discuss why they provide a better choice than sharp interface alternatives for the situations being modelled in this thesis. We then describe the five axiomatic laws that underlie all rational modelling, and conclude by deriving two simple models, the Allen-Cahn and the Cahn-Hilliard equations, the dynamics of which lie at the heart of the majority of rationally derived models.

2.1 Introduction to Rational Continuum Mechanics

Computational problems dealing with a moving boundary can be addressed using sharp or diffuse interface methods. Sharp interface models consider a jump in the values of the phase variable, whereas diffuse interface models consider a smooth transition between values on each side of the boundary. This is highlighted in Figure 2.1. While many problems, such as that of thin films (see Chapter 4) can be satisfactorily dealt with using both methods, there are certain advantages that diffuse interface modelling offers which make it applicable in the work presented

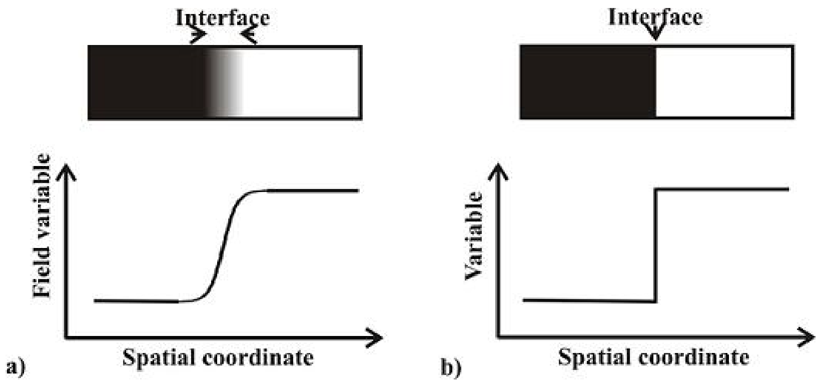

Figure 2.1: The difference between how a diffuse interface (a) and a sharp interface (b) model handles a jump at an interface, taken from [51].

here.

A major issue with sharp interface modelling is dealing with a change in the topology of the system under investigation. Consider, for example, a bead of water hanging from a surface, which separates to form a drop, or a thin liquid film on a surface rupturing and dewetting. Many sharp interface models that examine these phenomena break down at this point, as will be demonstrated later. However, diffuse interface modelling techniques naturally deal with this change of topology. This is demonstrated in Figure 2.2, which shows two growing holes in a liquid film coalescing to form a single, larger hole.

Rational continuum mechanics provides a rigorous framework for diffuse interface modelling. The method works from key axioms which are presented below, and through energetic considerations results in thermodynamically consistent partial differential equations for modelling the scenario in question. In this section we outline the theory of rational continuum modelling and state the five key axioms that form the basis of the method based on a complete work by Gurtin, Fried and Anand [39].

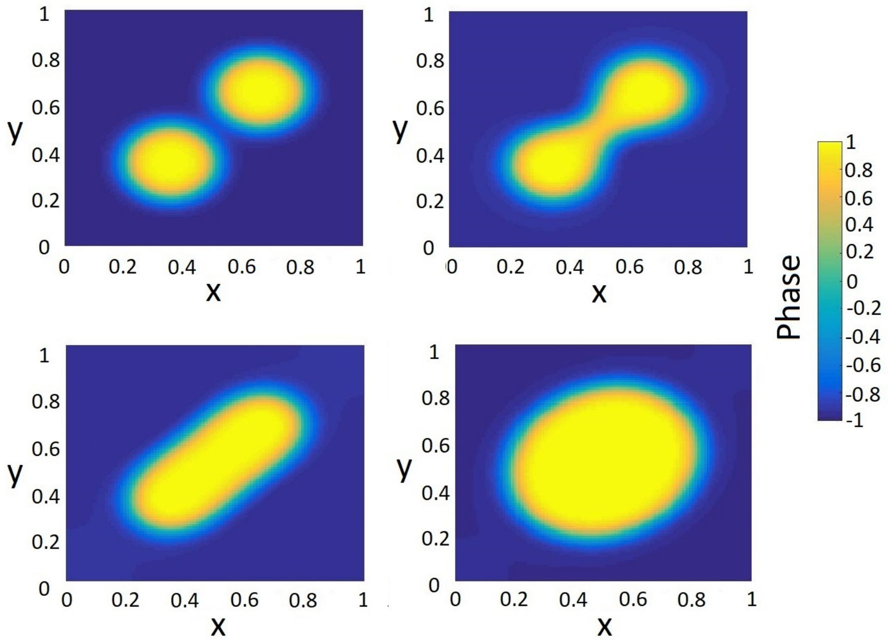

Figure 2.2: Two small holes in a liquid film growing and merging to form one larger hole. The change in topology is handled easily by a diffuse interface model, but a sharp interface model would come across difficulties between the panels in the top left and top right.

2.2 Key Laws

There are five key axioms that underlie rational continuum modelling: the conservation of mass, the conservation of linear and angular momentum, and the first and second laws of thermodynamics. For a model to be thermodynamically consistent, these five laws must hold in all physically realistic scenarios. In this section we present a general form for these five axioms.

We consider a d-dimensional body $\mathcal{B}_t \subset \mathbb{R}^d$, and a velocity field $\mathbf{v}(\mathbf{x}, t)$ for all points $\mathbf{x} \in \mathcal{B}_t$ and time t. We consider a reference body B to be $\mathcal{B}_t$ defined at a fixed point in time, and for any time t define a bijective deformation map $\chi_t : B \to \mathcal{B}_t$ such that for all $\mathbf{x} \in \mathcal{B}_t$, $\mathbf{x} = \chi_t(\mathbf{X})$ for some $\mathbf{X} \in B$.

2.2.1 Conservation of Mass

We take an arbitrary subset which convects with the body, $\mathcal{P}_t$, and define the reference subset $P \subset B$ such that $\mathcal{P}_t = \chi_t(P)$. Define $\rho_R(\mathbf{X}) > 0$ to be the density at reference point $\mathbf{X} \in B$. Then the total mass contained in P is given by

$$\int_P \rho_R(\mathbf{X}) dV_R. \tag{2.2.1}$$

Similarly, let $\rho(\mathbf{x}, t)$ define the density field of the body. Then the mass inside $\mathcal{P}_t \subset \mathcal{B}_t$ is given by

$$\int_{\mathcal{P}_t} \rho(\mathbf{x}, t)\, dV. \tag{2.2.2}$$

The balance of mass is then the statement that, for any time t,

$$\int_{\mathcal{P}_t} \rho(\mathbf{x}, t)\, dV = \int_P \rho_R(\mathbf{X})\, dV_R. \tag{2.2.3}$$

Noting that the right hand side of this equation is not dependent on time, we differentiate with respect to time to obtain

$$\frac{d}{dt}\int_{\mathcal{P}_t} \rho(\mathbf{x},t)\, dV = 0. \tag{2.2.4}$$

The local form of this equation can be found by applying the Reynolds Transport Theorem [52], resulting in

$$\int_{\mathcal{P}_t} \frac{d\rho}{dt} + \rho\left(\nabla\cdot\mathbf{v}\right)\, dV, \tag{2.2.5}$$

which, by the arbitrary nature of $\mathcal{P}_t$ results in

$$\dot{\rho} + \rho\left(\nabla\cdot\mathbf{v}\right) = 0. \tag{2.2.6}$$

2.2.2 Conservation of Linear and Angular Momentum

For a spatial region $\mathcal{P}_t \subset \mathcal{B}_t$, the linear and angular momentum is given by

$$\mathbf{L}(\mathcal{P}_t) = \int_{\mathcal{P}_t} \rho\mathbf{v}\, dV, \tag{2.2.7}$$

for some density $\rho = \rho(\mathbf{x},t)$. Taking the time derivative gives

$$\frac{d}{dt}\mathbf{L}(\mathcal{P}_t) = \frac{d}{dt}\int_{\mathcal{P}_t} \rho\mathbf{v}\, dV, \tag{2.2.8}$$

which becomes

$$\int_{\mathcal{P}_t} \frac{d}{dt}(\rho\mathbf{v}) + \rho\mathbf{v}\left(\nabla\cdot\mathbf{v}\right)\, dV \tag{2.2.9}$$

by applying the Reynolds Transport Theorem. Applying the product rule to the time derivative term and rearranging results in

$$\int_{\mathcal{P}_t} \rho\dot{\mathbf{v}} + \mathbf{v}\left(\dot{\rho} + \rho(\nabla\cdot\mathbf{v})\right)\, dV. \tag{2.2.10}$$

Here, $\dot{\mathbf{v}}$ represents the time derivative of $\mathbf{v}$. Finally, by applying (2.2.6) we obtain

$$\frac{d}{dt}\mathbf{L}(\mathcal{P}_t) = \int_{\mathcal{P}_t} \rho\dot{\mathbf{v}}\, dV. \tag{2.2.11}$$

The angular momentum for the same spacial region $\mathcal{P}_t$ is given by

$$\mathbf{A}(\mathcal{P}_t) = \int_{\mathcal{P}_t} \mathbf{r} \times (\rho\mathbf{v})\, dV, \tag{2.2.12}$$

where $\mathbf{r}$ is the position vector of a point $\mathbf{x}$ from an origin $\mathbf{o}$, defined as $\mathbf{r} = \mathbf{x} - \mathbf{o}$. Taking the time derivative and again employing the Reynolds Transport Theorem results in

$$\frac{d}{dt}\mathbf{A}(\mathcal{P}_t) = \int_{\mathcal{P}_t} \frac{d}{dt}(\mathbf{r} \times (\rho\mathbf{v})) + (\mathbf{r} \times \rho\mathbf{v})(\nabla \cdot \mathbf{v})\, dV. \tag{2.2.13}$$

We note that

$$\frac{d}{dt}(\mathbf{r} \times (\rho\mathbf{v})) = \mathbf{r} \times \frac{d}{dt}(\rho\mathbf{v}) + \dot{\mathbf{r}} \times (\rho\mathbf{v}), \tag{2.2.14}$$

and since $\mathbf{o}$ is not dependent on t this becomes

$$\frac{d}{dt}(\mathbf{r} \times (\rho\mathbf{v})) = \mathbf{r} \times \frac{d}{dt}(\rho\mathbf{v}) + \mathbf{v} \times (\rho\mathbf{v}) = \mathbf{r} \times \frac{d}{dt}(\rho\mathbf{v}). \tag{2.2.15}$$

Using this result, employing the product rule and rearranging in a similar way to that used for linear momentum, the right hand side of (2.2.13) becomes

$$\int_{\mathcal{P}_t} \mathbf{r} \times (\rho\dot{\mathbf{v}}) + \mathbf{r} \times (\mathbf{v}\,(\dot{\rho} + \rho(\nabla \cdot \mathbf{v})))\ dV. \tag{2.2.16}$$

Finally, applying (2.2.6) results in

$$\frac{d}{dt}\mathbf{A}(\mathcal{P}_t) = \int_{\mathcal{P}_t} \mathbf{r} \times (\rho\dot{\mathbf{v}})\, dV. \tag{2.2.17}$$

Forces acting upon a body can be split into two categories: contact forces exerted on the boundary of the body by its surroundings, and body forces, which act on the internal points of the body. We represent by

$\mathbf{t}(\mathbf{n})$ the contact force acting on the boundary oriented with the unit normal of $\mathcal{P}_t, \mathbf{n}$, and by $\mathbf{b}_0(\mathbf{x}, t)$ the body force acting on $\mathbf{x} \in \mathcal{P}_t$. Therefore the total contact and body forces acting on $\mathcal{P}_t$ are given by

$$\int_{\mathcal{P}_t} \mathbf{t}(\mathbf{n})\, ds \tag{2.2.18}$$

and

$$\int_{\mathcal{P}_t} \mathbf{b}_0\, dV \tag{2.2.19}$$

respectively. Similarly, the total moment exerted on $\mathcal{P}_t$ by the contact and body forces respectively are given by

$$\int_{\mathcal{P}_t} \mathbf{r} \times \mathbf{t}(\mathbf{n})\, ds \tag{2.2.20}$$

and

$$\int_{\mathcal{P}_t} \mathbf{r} \times \mathbf{b}_0\, dV. \tag{2.2.21}$$

Cauchy's theorem [53] states that there exists a spatial tensor field $\mathbf{T}$, known as the Cauchy stress tensor, such that

$$\mathbf{T}\mathbf{n} = \mathbf{t}(\mathbf{n}). \tag{2.2.22}$$

Given this, using the Reynolds Transport Theorem and applying the law of conservation of mass, we obtain from Newton's second law the final laws for the conservation of linear and angular momentum:

$$\int_{\mathcal{P}_t} \rho \dot{\mathbf{v}}\, dV = \int_{\partial \mathcal{P}_t} \mathbf{T}\mathbf{n}\, ds + \int_{\mathcal{P}_t} \mathbf{b}_0\, dV \tag{2.2.23}$$

and

$$\int_{\mathcal{P}_t} \mathbf{r} \times (\rho \dot{\mathbf{v}})\, dV = \int_{\partial \mathcal{P}_t} \mathbf{r} \times \mathbf{T}\mathbf{n}\, ds + \int_{\mathcal{P}_t} \mathbf{r} \times \mathbf{b}_0\, dV. \tag{2.2.24}$$

In this thesis, we consider inertial effects to be negligible, and so do not consider the conservation laws for linear and angular momentum. However, they have been included to give an overview of the full framework of Rational Continuum Mechanics.

2.2.3 1st Law of Thermodynamics

As in section 2.2.1 we consider a part $\mathcal{P}_t \subset \mathcal{B}$ to be an arbitrary region of $\mathcal{B}$. The first law can be written

$$\frac{d}{dt}\left(\mathcal{E}(\mathcal{P}_t) + \mathcal{K}(\mathcal{P}_t)\right) = \mathcal{W}(\mathcal{P}_t) + \mathcal{Q}(\mathcal{P}_t), \tag{2.2.25}$$

where $\mathcal{E}(\mathcal{P}_t)$ and $\mathcal{K}(\mathcal{P}_t)$ represent the internal and kinetic energies respectively, $\mathcal{W}(\mathcal{P}_t)$ is the external power applied to the boundary of $\mathcal{P}_t$ and $\mathcal{Q}(\mathcal{P}_t)$ is the rate of heat transfer to $\mathcal{P}_t$. The kinetic energy is written in the conventional way

$$\mathcal{K}(\mathcal{P}_t) = \int_{\mathcal{P}_t} \frac{1}{2}\rho|\mathbf{v}|^2 \, dV, \tag{2.2.26}$$

and the external power is given by

$$\mathcal{W}(\mathcal{P}_t) = \int_{\partial\mathcal{P}_t} \mathbf{Tn}\cdot\mathbf{v}\, ds + \int_{\mathcal{P}_t} \mathbf{b}\cdot\mathbf{v}\, dV, \tag{2.2.27}$$

where $\mathbf{T}$ is the Cauchy stress tensor and $\mathbf{b}$ is a body force. We now introduce the internal energy density e, and define

$$\mathcal{E}(\mathcal{P}_t) = \int_{\mathcal{P}_t} \rho e \, dV, \tag{2.2.28}$$

and we say that the change in heat energy in the body is made up of the flux of heat over the boundary $\mathbf{q}$ and an internal heat source q, written

$$\mathcal{Q}(\mathcal{P}_t) = -\int_{\partial\mathcal{P}_t} \mathbf{q}\cdot\mathbf{n}\, ds + \int_{\mathcal{P}_t} q \, dV. \tag{2.2.29}$$

These definitions are combined together to give the first law of thermodynamics:

$$\begin{aligned}\frac{d}{dt}\int_{\mathcal{P}_t}\rho\left(e+\frac{1}{2}|\mathbf{v}|^2\right)\,dV = \int_{\partial\mathcal{P}_t}\mathbf{Tn}\cdot\mathbf{v}\,ds+\int_{\mathcal{P}_t}\mathbf{b}\cdot\mathbf{v}\,dV\\ -\int_{\partial\mathcal{P}_t}\mathbf{q}\cdot\mathbf{n}\,ds+\int_{\mathcal{P}_t}q\,dV.\end{aligned} \tag{2.2.30}$$

It can be noted than in the case without motion, i.e. $\mathbf{v}\equiv 0$, this reduces to

$$\frac{d}{dt}\int_{\mathcal{P}}\rho e\,dV = -\int_{\partial\mathcal{P}}\mathbf{q}\cdot\mathbf{n}\,ds+\int_{\mathcal{P}}q\,dV. \tag{2.2.31}$$

2.2.4 2nd Law of Thermodynamics

Define the internal entropy of $\mathcal{P}_t$ to be $\mathcal{S}(\mathcal{P}_t)$ and the rate at which entropy is transferred to $\mathcal{P}_t$ to be $\mathcal{J}(\mathcal{P}_t)$. Then the rate of entropy production in $\mathcal{P}_t$, $\mathcal{H}(\mathcal{P}_t)$ is defined as

$$\mathcal{H}(\mathcal{P}_t) = \frac{d}{dt}(\mathcal{S}(\mathcal{P}_t)) - \mathcal{J}(\mathcal{P}_t). \tag{2.2.32}$$

The second law of thermodynamics states that this entropy production must be non-negative in all situations:

$$\mathcal{H}(\mathcal{P}_t) \geqslant 0. \tag{2.2.33}$$

We introduce the entropy density η, and write

$$\mathcal{S}(\mathcal{P}_t) = \int_{\mathcal{P}_t}\rho\eta\,dV. \tag{2.2.34}$$

We also write

$$\mathcal{J}(\mathcal{P}_t) = -\int_{\partial\mathcal{P}_t}\mathbf{j}\cdot\mathbf{n}\,ds+\int_{\mathcal{P}_t}j\,dV \tag{2.2.35}$$

for the entropy flux $\mathbf{j}$ and entropy source j. Finally, we introduce the temperature field $\theta > 0$, and we postulate that entropy is related to the heat energy by

$$\mathbf{j} = \frac{\mathbf{q}}{\theta}, \tag{2.2.36}$$

and

$$j = \frac{q}{\theta}. \tag{2.2.37}$$

Thus the final inequality for the second law of thermodynamics is given by

$$\frac{d}{dt}\int_{\mathcal{P}_t} \rho\eta \, dV \geqslant -\int_{\partial\mathcal{P}_t} \frac{\mathbf{q}}{\theta}\cdot\mathbf{n}\, ds + \int_{\mathcal{P}_t} \frac{q}{\theta}\, dV. \tag{2.2.38}$$

2.2.5 Mechanical Version of the Second Law

In this section, we investigate the meaning of the second law of thermodynamics in an isothermal situation, that is to say that $\theta = \theta_0$ is constant. Given this assumption and using (2.2.29), we note that

$$\mathcal{J}(\mathcal{P}_t) = \frac{1}{\theta_0}\left(-\int_{\partial\mathcal{P}_t} \mathbf{q}\cdot\mathbf{n}\, ds + \int_{\mathcal{P}_t} q\, dV\right) = \frac{\mathcal{Q}(\mathcal{P}_t)}{\theta_0}, \tag{2.2.39}$$

and so by multiplying through by θ_0 we see that

$$\frac{d}{dt}\int_{\mathcal{P}_t} \rho\theta_0\eta\, dV \geqslant \mathcal{Q}(\mathcal{P}_t). \tag{2.2.40}$$

Subtracting this from (2.2.30) we obtain the mechanical version of the second law of thermodynamics for use in isothermal cases:

$$\frac{d}{dt}\int_{\mathcal{P}_t} \rho\left(e - \theta_0\eta + \frac{1}{2}|\mathbf{v}|^2\right) dV \leqslant \mathcal{W}(\mathcal{P}_t). \tag{2.2.41}$$

By defining

$$\Psi = e - \theta_0\eta \tag{2.2.42}$$

to be the free energy density, then this can be written as

$$\frac{d}{dt}\int_{\mathcal{P}_t} \rho\left(\Psi + \frac{1}{2}|\mathbf{v}|^2\right) dV = \mathcal{W}(\mathcal{P}_t) - \mathcal{D}(\mathcal{P}_t) \tag{2.2.43}$$

for some $\mathcal{D}(\mathcal{P}_t) \geqslant 0$, which represents free energy dissipation.

2.3 Phase Field Variables

Rational continuum mechanics can be used for modelling numerous phenomena. For example, in [54] a derivation of the Navier-Stokes equations is given. In such scenarios, the quantities of interest, such as velocity or pressure, are continuous variables. However, in other cases such as the solidification of a liquid [55] or a crack propagating through a solid [56], the quantities of interest are discontinuous. In these cases, one can introduce a phase-field variable to distinguish between the phases of a region. Figure 2.3 shows an example of this for a liquid film which has partly solidified. In this case, the phase field variable $\phi(\mathbf{x})$ takes the value of 1 if the film is liquid at point $\mathbf{x}$ (represented by the white region), 0 if the film is solid (black region), and has a diffuse boundary of thickness ϵ separating the two distinct phases (grey region).

Advantages of phase field modelling include that surface tension is naturally included, topological changes such as pinching off or the merging of two bodies are easily handled and the boundary between the separate phases does not require tracking [54].

Models using phase field variables are often driven by the variational derivative of the free energy functional. This is defined such that the variational derivative of Ψ with respect to ϕ, written $\delta\Psi/\delta\phi$ satisfies

$$\frac{d}{dt}\int_{\mathcal{P}_t} \Psi \, dV = \int_{\mathcal{P}_t} \frac{\delta\Psi}{\delta\phi}\dot{\phi} \, dV. \tag{2.3.1}$$

Using phase field variables and the variational derivative of an energy functional, we are able now to derive two simple equations for describing non-conservative and conservative gradient flows that lie at the heart of phase-field modelling: the Allen-Cahn and the Cahn-Hilliard equa-

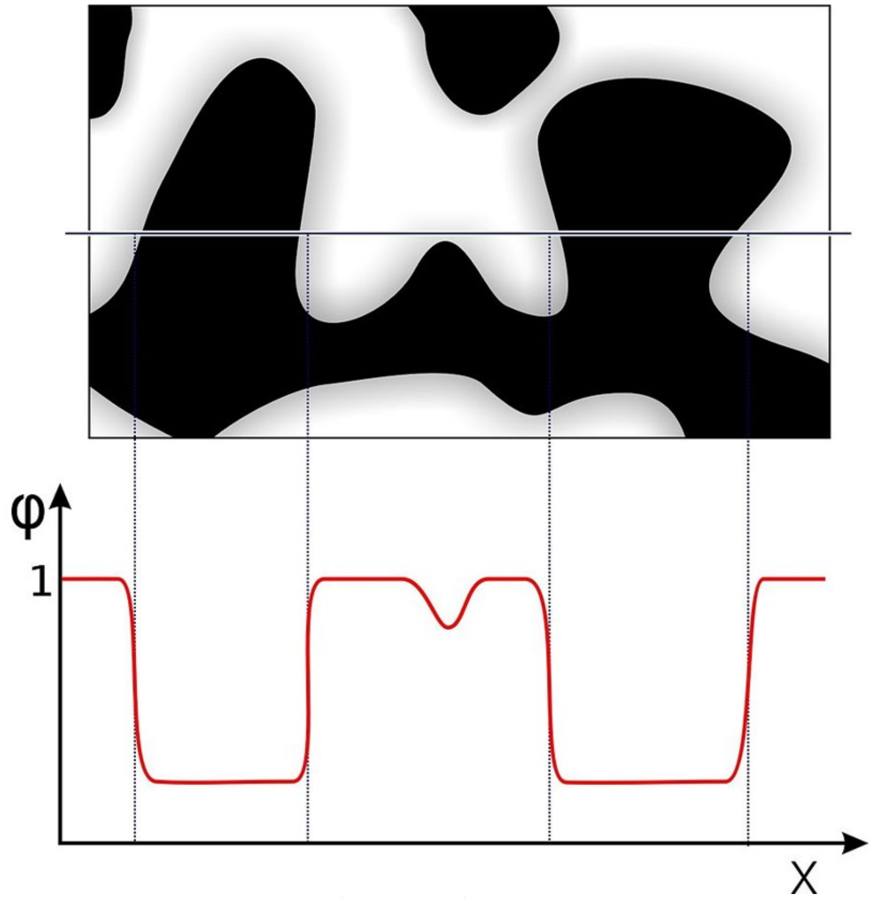

Figure 2.3: An example of a phase field parameter being used to identify the separate phases of a region. The parameter takes the value of 1 in the white phase, 0 in the black phase and has a smooth continuous interface between the two (grey areas)

tions.

2.4 The Allen-Cahn and Cahn-Hilliard Equations

In this section we use the above theories to derive two equations that are central to phase-field modelling, the non-conservative Allen-Cahn equation and the conservative Cahn-Hilliard equation. Consider a fixed domain $\Omega \subset \mathbb{R}^d$. For all points $x \in \Omega$, we introduce a phase-field parameter $\phi(x)$ and for the canonical free energy $\Psi(\phi, \nabla\phi)$ we define an energy functional $\mathcal{E}$ to be

$$\mathcal{E}[\phi] = \int_\Omega \Psi \, dV. \tag{2.4.1}$$

We assume that density is constant with $\rho(\mathbf{x}, t) = 1$, and that there is no velocity field $\mathbf{v} = 0$. With these assumptions, the mechanical version of the second law of thermodynamics, derived in Section 2.2.5, becomes

$$\frac{d}{dt} \int_\Omega \Psi(\phi, \nabla\phi) \, dV = \mathcal{W}(\Omega) - \mathcal{D}(\Omega), \tag{2.4.2}$$

for $\mathcal{D}(\Omega) \geqslant 0$. Assuming Ω is fixed, the time derivative can be moved inside the integral, and so by using the chain rule we can write

$$\frac{d}{dt} \int_\Omega \Psi \, dV = \int_\Omega \left(\partial_\phi \Psi \dot{\phi} + \partial_{\nabla\phi} \Psi (\dot{\nabla\phi}) \right) \, dV. \tag{2.4.3}$$

Changing the order of the time and space derivatives in the second term on the right hand side, and integrating this term by parts results in

$$\frac{d}{dt} \int_\Omega \Psi \, dV = \int_\Omega \left[\partial_\phi \Psi - \nabla \cdot (\partial_{\nabla\phi} \Psi) \right] \dot{\phi} \, dV + \int_{\partial\Omega} \partial_{\nabla\phi} \Psi \dot{\phi} \cdot \mathbf{n} \, ds. \tag{2.4.4}$$

From this, we define the variational derivative μ of $\mathcal{E}$ as

$$\mu = \frac{\delta}{\delta\phi}\left(\int_\Omega \Psi \, dV\right) = \partial_\phi \Psi - \nabla \cdot (\partial_{\nabla\phi}\Psi). \tag{2.4.5}$$

The derivation for both the Allen-Cahn and Cahn-Hilliard equations start with the Ginzburg-Landau energy functional, given by

$$\mathcal{E}[\phi] = \int_\Omega \Psi(\phi, \nabla\phi) \, dV = \int_\Omega \left(W(\phi) + \frac{\epsilon^2}{2}|\nabla\phi|^2\right) \, dV, \tag{2.4.6}$$

where $W(\phi)$ is a double well function with minima corresponding to the pure phases of ϕ and ϵ describes the width of the diffuse boundary between the phases.

2.4.1 Allen-Cahn Equation

The derivation for the Allen-Cahn equation starts by postulating the mass balance

$$\frac{\partial\phi}{\partial t} = -R, \tag{2.4.7}$$

which, along with (2.4.5) can be substituted into (2.4.4) to give

$$\frac{d}{dt}\int_\Omega \Psi \, dx = \int_\Omega -\mu R \, dx + \int_{\partial\Omega} \partial_{\nabla\phi}\Psi\dot{\phi} \cdot \mathbf{n} \, ds. \tag{2.4.8}$$

Identifying the boundary integral term to be $\mathcal{W}(\Omega)$ and $\int_\Omega \mu R dx$ to be $\mathcal{D}(\Omega)$ in (2.4.2), we postulate the constitutive class

$$R = \bar{R}(\phi, \nabla\phi, \mu), \tag{2.4.9}$$

which is restricted by the requirement of dissipation: $0 \leqslant \mathcal{D}(\Omega) = \int_\Omega \mu\bar{R}(\phi, \nabla\phi, \mu)$. Therefore, the thermodynamically consistent choice,

$$\bar{R} = m(\phi)\mu \tag{2.4.10}$$

for some function $m(\phi) \geqslant 0$ clearly satisfies the dissipation condition $\mathcal{D}(\Omega) \geqslant 0$, as

$$\int_{\Omega} \mu R \, dx = \int_{\Omega} m(\phi)\mu^2 \, dx \geqslant 0. \tag{2.4.11}$$

It can be noted here that other dependencies for the mobility, such as $m(\phi, \nabla\phi) \geqslant 0$ would also be consistent with the dissipation condition, and it is the choice of the modeller to decide which dependencies best describe their specific scenario.

Using the energy functional chosen in (2.4.6), it follows that

$$\mu = W'(\phi) - \epsilon^2 \Delta\phi, \tag{2.4.12}$$

hence the choice for $\bar{R}$ given in (2.4.10), the final Allen-Cahn equation is derived and is given as

$$\frac{\partial\phi}{\partial t} = -m(\phi)\left(W'(\phi) - \epsilon^2\Delta\phi\right). \tag{2.4.13}$$

Here, the Lapacian operator is defined as $\Delta = \nabla \cdot \nabla$.

2.4.2 Cahn-Hilliard Equation

The Cahn-Hilliard equation is conservative, and therefore its derivation starts with the general conservation equation with no source or sink term [54]:

$$\frac{\partial\phi}{\partial t} = -\nabla \cdot \mathbf{j}. \tag{2.4.14}$$

Again, substituting this into (2.4.4), we obtain

$$\frac{d}{dt}\int_{\Omega} \Psi \, dx = \int_{\Omega} -\mu\nabla \cdot \mathbf{j} \, dx + \int_{\partial\Omega} \partial_{\nabla\phi}\Psi\dot{\phi} \cdot \mathbf{n} \, ds. \tag{2.4.15}$$

Now, we postulate the constitutive class

$$\mathbf{j} = \bar{\mathbf{j}}(\phi, \nabla\phi, \mu, \nabla\mu). \tag{2.4.16}$$

Integrating by parts the first term on the right hand side, we obtain

$$\frac{d}{dt}\int_{\Omega} \Psi \, dx = \int_{\Omega} \mathbf{j} \cdot \nabla \mu \, dx + \int_{\partial\Omega} (-\mu \mathbf{j} + \partial_{\nabla\phi} \Psi \dot{\phi}) \cdot \mathbf{n} \, ds. \tag{2.4.17}$$

Again, identifying the boundary integral to be $\mathcal{W}(\Omega)$ and $-\int_{\Omega} \mathbf{j} \cdot \nabla \mu \, dx$ to be $\mathcal{D}(\Omega)$ in (2.4.2), then it is clear that a choice of

$$\bar{\mathbf{j}} = -m(\phi) \nabla \mu \tag{2.4.18}$$

for a function $m(\phi) \geqslant 0$ satisfies the energy dissipation requirement $\mathcal{D} \geqslant 0$, as

$$-\int_{\Omega} \bar{\mathbf{j}} \cdot \nabla \mu \, dx = \int_{\Omega} m(\phi) |\nabla \mu|^2 \geqslant 0. \tag{2.4.19}$$

Thus, using the energy functional (2.4.6) and the choice for $\bar{\mathbf{j}}$ made in (2.4.18), the final Cahn-Hilliard model is given by

$$\frac{\partial \phi}{\partial t} = \nabla \cdot (m(\phi) \nabla (W'(\phi) - \epsilon^2 \Delta \phi)). \tag{2.4.20}$$

The Allen-Cahn and Cahn-Hilliard models form the basis of many diffuse interface models. Non-conservative phenomena such as solidification [57] or evaporation of a liquid [58] can be modelled using Allen-Cahn type equations, whereas conservative phenomena such as the separation of mixtures via spinodal decomposition [59, 60] often take the form of the Cahn-Hilliard equation.

The above rational approach of deriving (a class of) models that are consistent with thermodynamics, in this case consistent with the free energy dissipation inequality (2.4.2), will be fully extended to the case of iso-thermal and non-isothermal solidifying thin films in Chapters 4-7.

CHAPTER 3

Numerical Methods for Phase Field Simulations

In this chapter, we investigate numerical methods for gradient flow phase-field type models. It forms a bridge to the next chapters, in which we derive families of models for thin film dynamics and the solidification of a liquid using energetic considerations from the first principles of the conservation of mass and the second law of thermodynamics. Some of the numerical methods detailed here are used in Chapter 8 to perform simulations of some of the models. This section also reviews newly developed numerical methods [61–63] that have many benefits for gradient flows.

3.1 Gradient-Flow Model

For a fixed domain Ω with boundary $\partial\Omega$, and using the standard energy functional (2.4.1), the gradient flow under consideration is the Cahn-Hilliard equation derived in the previous chapter:

$$\frac{\partial h}{\partial t} = \nabla \cdot \left[m(h) \nabla \mu \right], \tag{3.1.1}$$

$$\mu = W'(h) - \sigma^2 \Delta h, \tag{3.1.2}$$

for some quantity $h(\mathbf{x}, t)$, where $m(h) \geqslant 0$ is a positive function known as the mobility, μ is the variational derivative of the chosen energy functional $\mathcal{E}(h)$, and the Laplacian operator Δ is defined by $\Delta = \nabla \cdot \nabla$. The model is subject to the choice of boundary conditions

$$\nabla h \cdot \mathbf{n} = \nabla \mu \cdot \mathbf{n} = 0 \tag{3.1.3}$$

on $\partial\Omega$, where $\mathbf{n}$ is the outward pointing unit normal to $\partial\Omega$, and an initial condition

$$h(\mathbf{x}, 0) = h_0(\mathbf{x}) \ \forall \mathbf{x} \in \Omega. \tag{3.1.4}$$

Under these conditions, it is easy to show that

$$\begin{aligned} \frac{d}{dt}\mathcal{E}(h) =& \frac{d}{dt}\int_\Omega \left[W(h) + \frac{1}{2}\sigma^2 |\nabla h|^2 \right] \, d\mathbf{x} \\ =& \int_\Omega \left[W'(h)\frac{\partial h}{\partial t} - \sigma^2 \Delta h \frac{\partial h}{\partial t} \right] \, d\mathbf{x} \\ =& \int_\Omega \mu \nabla \cdot (m(h)\nabla \mu) \, d\mathbf{x} \\ =& -\int_\Omega m(h)|\nabla \mu|^2 \, d\mathbf{x} \leqslant 0, \end{aligned} \tag{3.1.5}$$

thus the model is energy dissipative.

3.2 Numerical Methods for Simulations

In this section, spatial and time discretisations used for simulating gradient flows are described in more detail.

3.2.1 Spatial Discretisation

A linear finite element scheme [50] can be used to discretise equations (3.1.1) and (3.1.2) in space. To do this, the equations are multiplied by a test function, integrated over the domain Ω and integrated by parts.

The weak form of the equations is then to find $h \in U$ and $\mu \in V$ such that

$$\langle h_t(t), v_1 \rangle = \int_\Omega m(h(t))\nabla\mu(t) \cdot \nabla v_1 \, dx, \tag{3.2.1}$$

$$\int_\Omega \mu(t) v_2 \, dx = \int_\Omega W'(h(t)) v_2 \, dx + \sigma^2 \int_\Omega \nabla h(t) \cdot \nabla v_2 \, dx, \tag{3.2.2}$$

$$\int_\Omega h(0) v_3 \, dx = \int_\Omega h_0 v_3 \, dx, \tag{3.2.3}$$

for all $v_1, v_2 \in H^1(\Omega), v_3 \in L^2(\Omega)$ and almost every $t \in (0, \mathcal{T}]$ where $L^2(\Omega)$ is the space of functions f over Ω such that $\int_\Omega |f|^2 \, dx$ is finite, $H^1(\Omega) := \{u : \Omega \to \mathbb{R} | u \in L^2(\Omega), \ \nabla u \in L^2(\Omega)\}$ and $\mathcal{T}$ is the end of the time interval. The solution spaces V and U are defined as $V = L^2(0, \mathcal{T}; H^1(\Omega)) := \{v(x,t) | \int_0^{\mathcal{T}} \int_\Omega (|v|^2 + |\nabla v|^2) \, dx < \infty\}$ and $U := \{u : (0, \mathcal{T}] \to \mathbb{R} | u \in L^2(0, \mathcal{T}; H^1(\Omega))$ and $u_t \in L^2(0, \mathcal{T}; H^1(\Omega)')\}$. $H^1(\Omega)'$ is the dual space of $H^1(\Omega)$. Here we have employed the boundary conditions given in (3.1.3). This problem is known to be well posed [64].

For $\Omega \in \mathbb{R}^2$, by splitting the domain into triangular elements, and defining $\varphi_i(x)$ to be the standard hat function at node i (the continuous, piecewise linear function that takes the value 1 at node i and 0 at all other nodes), the weak form can be discretised by taking the test functions v_1 and v_2 to be φ_i and approximating $h(x,t)$ and $\mu(x,t)$ by $h(x,t) \approx \sum_{j=1}^n \xi_j(t)\varphi_j(x)$ and $\mu(x,t) \approx \sum_{j=1}^n \eta_j(t)\varphi_j(x)$. This discretisation results in the system

$$\begin{cases} M\xi_t = -K_m \eta \\ M\eta = N(\xi) + \sigma^2 K \xi. \end{cases} \tag{3.2.4}$$

M and K are the mass matrix and the stiffness matrix respectively, defined such that $M_{ij} = \int_\Omega \varphi_j \varphi_i \, dV$ and $K_{ij} = \int_\Omega \nabla\varphi_j \cdot \nabla\varphi_i \, dV$, K_m is the stiffness matrix given by $K_{mij} = \int_\Omega m(h) \nabla\varphi_j \cdot \nabla\varphi_i \, dV$ and N is a vector dependent on $\xi(t)$.

3.2.2 Convex Splitting Time Discretisation

Key aspects to consider when choosing a time-stepping scheme for gradient flow are whether the scheme keeps energy dissipation, the order of its accuracy, its efficiency and how easy the scheme is to implement [65]. When choosing a time discretisation, it is desirable that the method demonstrates energy stability, that is

$$\mathcal{E}(h^{n+1}) \leqslant \mathcal{E}(h^n), \tag{3.2.5}$$

with h^i being the height function of the film at the ith time step.

A groundbreaking method to discretise in time is based on convex-splitting [46, 66], which splits the non-linear free-energy density $W(h)$ into a convex part and a concave part:

$$W(h) = W_+(h) + W_-(h), \tag{3.2.6}$$

with $W_+''(h) \geqslant 0$ and $W_-''(h) \leqslant 0$. The convex part is dealt with implicitly, and the concave part is dealt with explicitly. The mobility function $m(h)$ is also dealt with explicitly as this does not affect the energy stability, as will be shown.

The time discretisation for equations (3.1.1) and (3.1.2) is then given by

$$\frac{h^{n+1} - h^n}{\tau} = \left[\nabla \cdot m(h^n)\nabla\mu^{n+1}\right], \tag{3.2.7}$$

$$\mu^{n+1} = W_+'(h^{n+1}) + W_-'(h^n) - \sigma^2\Delta h^{n+1}, \tag{3.2.8}$$

where τ is the positive time step size. In this scenario, a constant τ is considered, however the arguments can be extended for varying time step sizes.

Arguments showing that the convex splitting method is energy stable for the Cahn-Hilliard equation ($m(h) \equiv 1$ in equation (3.1.1)) are presented in [54]. These arguments are now followed for proving the energy stability for the method when applied to equations (3.1.1), (3.1.2). In order to satisfy (3.2.5), we consider

$$\begin{aligned}\mathcal{E}(h^{n+1}) - \mathcal{E}(h^n) = \int_\Omega \Big[& W_+(h^{n+1}) + W_-(h^{n+1}) + \frac{1}{2}\sigma^2|\nabla h^{n+1}|^2 \\ & -W_+(h^n) - W_-(h^n) - \frac{1}{2}\sigma^2|\nabla h^n|^2 \Big]\, dx.\end{aligned} \tag{3.2.9}$$

Consider now the Taylor expansion of $W_+(h^n)$ about h^{n+1} with remainder term:

$$W_+(h^n) = W_+(h^{n+1}) + W_+'(h^{n+1})(h^n - h^{n+1}) + \frac{1}{2}W_+''(h^{n+\zeta_1})(h^n - h^{n+1})^2, \tag{3.2.10}$$

which can be rearranged to obtain

$$W_+(h^{n+1}) - W_+(h^n) = W_+'(h^{n+1})(h^{n+1} - h^n) - \frac{1}{2}W_+''(h^{n+\zeta_1})(h^{n+1} - h^n)^2. \tag{3.2.11}$$

Similarly, taking a Taylor expansion of $W_-(h^{n+1})$ about h^n with remainder term gives

$$W_-(h^{n+1}) - W_-(h^n) = W_-'(h^n)(h^{n+1} - h^n) + \frac{1}{2}W_-''(h^{n+\zeta_2})(h^{n+1} - h^n)^2. \tag{3.2.12}$$

In the above Taylor expansions, $\zeta_i \in (0,1)$ for $i = 1, 2$ and $h^{n+\zeta_i}$ is some value between h^n and h^{n+1}.

Substituting (3.2.11), (3.2.12) into (3.2.9) gives

$$\begin{aligned}\mathcal{E}(h^{n+1}) - \mathcal{E}(h^n) = \int_\Omega \Big[& W_+'(h^{n+1})(h^{n+1} - h^n) - \frac{1}{2}W_+''(h^{n+\zeta_1})(h^{n+1} - h^n)^2 \\ & + W_-'(h^n)(h^{n+1} - h^n) + \frac{1}{2}W_-''(h^{n+\zeta_2})(h^{n+1} - h^n)^2 \\ & + \frac{1}{2}\sigma^2\big(|\nabla h^{n+1}|^2 - |\nabla h^n|^2\big) \Big]\, dx.\end{aligned} \tag{3.2.13}$$

From (3.2.8) it can be seen that $W'_+(h^{n+1}) + W'_-(h^n) = \mu^{n+1} + \sigma^2 \Delta h^{n+1}$, and by using the convex and concave properties of $W_+(h)$ and $W_-(h)$ respectively then

$$\begin{aligned} \mathcal{E}(h^{n+1}) - \mathcal{E}(h^n) \leqslant \int_\Omega \Big[& \left(\mu^{n+1} + \sigma^2 \Delta h^{n+1}\right)\left(h^{n+1} - h^n\right) \\ & + \frac{1}{2}\sigma^2\left(|\nabla h^{n+1}|^2 - |\nabla h^n|^2\right)\Big]\, dx \end{aligned} \tag{3.2.14}$$

$$\begin{aligned} = \int_\Omega \Big[& \mu^{n+1}\left(h^{n+1} - h^n\right) + \sigma^2 \Delta h^{n+1} h^{n+1} - \sigma^2 \Delta h^{n+1} h^n \\ & + \frac{1}{2}\sigma^2\left(|\nabla h^{n+1}|^2 - |\nabla h^n|^2\right)\Big]\, dx. \end{aligned} \tag{3.2.15}$$

Integrating by parts the second and third terms and making use of the natural boundary conditions given in (3.1.3), the right hand side of the above inequality becomes

$$\int_\Omega \mu^{n+1}\left(h^{n+1} - h^n\right)\, dx - \frac{1}{2}\sigma^2 ||\nabla\left(h^{n+1} - h^n\right)||^2, \tag{3.2.16}$$

where $||\cdot||$ represents the standard L_2 norm given by $||f||^2 = \int_\Omega |f|^2 dx$. The final step is to consider the integral term in (3.2.16). Noting that

$$h^{n+1} - h^n = \tau \nabla \cdot \left[m(h^n)\nabla \mu^{n+1}\right] \tag{3.2.17}$$

from (3.2.7), the integral becomes

$$\int_\Omega \mu^{n+1}\left(h^{n+1} - h^n\right)\, dx = \tau \int_\Omega \mu^{n+1} \nabla \cdot \left[m(h^n)\nabla \mu^{n+1}\right]. \tag{3.2.18}$$

Integrating by parts the right hand side and again using the natural boundary conditions (3.1.3), the final result is obtained:

$$\int_\Omega \mu^{n+1}\left(h^{n+1} - h^n\right)\, dx = -\tau \int_\Omega m(h^n)|\nabla \mu^{n+1}|^2\, dx \leqslant 0, \tag{3.2.19}$$

recalling that $\tau > 0$ and $m(h) \geqslant 0\ \forall h$.

Combining (3.2.14), (3.2.16) and (3.2.19), the final result

$$\begin{aligned}\mathcal{E}(h^{n+1}) - \mathcal{E}(h^n) &\leqslant \int_\Omega \mu^{n+1}\left(h^{n+1} - h^n\right)\,dx - \frac{1}{2}\sigma^2||\nabla\left(h^{n+1} - h^n\right)||^2 \\ &= -\tau\int_\Omega m(h^n)|\nabla\mu^{n+1}|^2\,dx - \frac{1}{2}\sigma^2||\nabla\left(h^{n+1} - h^n\right)||^2 \\ &\leqslant 0,\end{aligned} \tag{3.2.20}$$

and so condition (3.2.5) is met, and the convex splitting scheme is unconditionally energy stable for systems of the form (3.1.1), (3.1.2). The first term on the right hand side of (3.2.20) is the physical dissipation as it is the discretised version of that found in (3.1.5). The second term is artificial dissipation.

In [54], the claim is made that, if there exists some $L_W > 0$ such that $|W''(h)| \leqslant L_W\ \forall h$ then it is possible to perform a splitting with

$$W_+(h) = \frac{L_W}{2}h^2. \tag{3.2.21}$$

This is a useful property as with this splitting, the implicitly handled terms in the scheme are linear.

3.2.3 Backwards Euler Time Discretisation

A naive alternative scheme to the Convex Splitting method for discretisation in time is the fully implicit Backwards Euler method, as it is not unconditionally stable. Here, we demonstrate that it is only conditionally energy stable. The discretisation is given by

$$\frac{h^{n+1} - h^n}{\tau} = \left[\nabla\cdot m(h^{n+1})\nabla\mu^{n+1}\right], \tag{3.2.22}$$

$$\mu^{n+1} = W'(h^{n+1}) - \sigma^2\Delta h^{n+1}. \tag{3.2.23}$$

As with the convex splitting method, we take the Taylor expansion of $W(h^n)$ about h^{n+1} and rearrange to give

$$W(h^{n+1}) - W(h^n) - W'(h^{n+1})(h^{n+1} - h^n) = -\frac{1}{2}W''(h^{n+\xi})(h^{n+1} - h^n)^2. \tag{3.2.24}$$

By insisting that $W''(\zeta) \geqslant -k_W \; \forall\zeta$ for some positive k_W, we obtain

$$W(h^{n+1}) - W(h^n) \leqslant W'(h^{n+1})(h^{n+1} - h^n) + \frac{k_W}{2}(h^{n+1} - h^n)^2. \tag{3.2.25}$$

Now, by considering the energy in a similar way to (3.2.9), we obtain

$$\begin{aligned} \mathcal{E}(h^{n+1}) - \mathcal{E}(h^n) &\leqslant \int_\Omega \Bigg[\frac{k_w}{2}(h^{n+1} - h^n)^2 + W'(h^{n+1})(h^{n+1} - h^n) \\ &\qquad + \frac{\sigma^2}{2}\left(|\nabla h^{n+1}|^2 - |\nabla h^n|^2 \right) \Bigg] dx \\ &\leqslant \int_\Omega \frac{k_w}{2}(h^{n+1} - h^n)^2 \, dx - \tau \int_\Omega m(h^{n+1})|\nabla \mu^{n+1}|^2 \, dx \\ &\qquad - \frac{\sigma^2}{2}||\nabla \left(h^{n+1} - h^n \right)||^2 \end{aligned} \tag{3.2.26}$$

by the same arguments made for convex splitting.

We now look to bound the first term. By using (3.2.22),

$$\int_\Omega (h^{n+1} - h^n)^2 \, dx = \tau \int_\Omega \nabla \cdot \left(m(h^{n+1}) \nabla \mu^{n+1} \right) (h^{n+1} - h^n) \, dx. \tag{3.2.27}$$

Integrating by parts the right hand side and applying the Cauchy-Schwarz inequality, one sees that

$$\int_\Omega (h^{n+1} - h^n)^2 \, dx \leqslant \tau ||\sqrt{m(h^{n+1})}\nabla \mu^{n+1}|| \; ||\sqrt{m(h^{n+1})}\nabla (h^{n+1} - h^n)||, \tag{3.2.28}$$

and finally, by applying Young's inequality, that

$$\begin{aligned}\int_\Omega (h^{n+1}-h^n)^2\,dx \leqslant \frac{\tau}{2\delta}\int_\Omega m(h^{n+1})|\nabla\mu^{n+1}|^2\,dx \\ +\frac{\tau\delta}{2}\int_\Omega m(h^{n+1})|\nabla(h^{n+1}-h^n)|^2\,dx,\end{aligned} \tag{3.2.29}$$

$\forall\ \delta > 0$. Substituting this into (3.2.26) and choosing $\delta = k_W/4$, it can be seen that

$$\begin{aligned}\mathcal{E}(h^{n+1})-\mathcal{E}(h^n) \leqslant & \frac{k_W^2\tau}{16}\int_\Omega m(h^{n+1})|\nabla(h^{n+1}-h^n)|^2\,dx \\ & -\frac{\sigma^2}{2}\int_\Omega |\nabla(h^{n+1}-h^n)|^2\,dx\end{aligned} \tag{3.2.30}$$

$$\leqslant \left(\frac{k_W^2\tau}{16}||m(h^{n+1})||_\infty - \frac{\sigma^2}{2}\right)||\nabla(h^{n+1}-h^n)||^2, \tag{3.2.31}$$

where $||\cdot||_\infty$ signifies the maximum value of the function over the domain Ω. From this, it can be deduced that the Backwards Euler method is energy stable if

$$\tau \leqslant \frac{8\sigma^2}{k_W^2||m(h^{n+1})||_\infty}, \tag{3.2.32}$$

and thus the scheme is only conditionally energy stable. As energy stability is key for a numerical scheme when handling phase field type models, this method can be discarded.

3.2.4 IEQ and SAV Methods

While the convex splitting method described above is unconditionally energy stable, it is only first-order, and while it is possible to construct a second-order scheme on a case-by-case basis, a general formulation of second-order convex splitting schemes is not available [63].

A much more recent approach from 2013 [67] is that of invariant energy quadratization (IEQ) which can be applied in scenarios where the free-energy density is merely bounded from below, that is $\exists\ C_0 > 0$ such that $W(h) > -C_0 \; \forall h$. One then introduces a new variable $q(t, x; h) = \sqrt{W(h) + C_0}$, and write the system of equations (3.1.1), (3.1.2) as

$$\frac{\partial h}{\partial t} = \nabla \cdot [m(h) \nabla \mu] , \tag{3.2.33}$$

$$\mu = \frac{q}{\sqrt{W(h) + C_0}} W'(h) - \sigma^2 \Delta h, \tag{3.2.34}$$

$$q_t = \frac{W'(h)}{2\sqrt{W(h) + C_0}} h_t. \tag{3.2.35}$$

This can then be time-discretised using the following first order scheme:

$$\frac{h^{n+1} - h^n}{\tau} = \nabla \cdot \left[m(h^n) \nabla \mu^{n+1} \right] , \tag{3.2.36}$$

$$\mu^{n+1} = \frac{q^{n+1}}{\sqrt{W(h^n) + C_0}} W'(h^n) - \sigma^2 \Delta h^{n+1}, \tag{3.2.37}$$

$$\frac{q^{n+1} - q^n}{\tau} = \frac{W'(h^n)}{2\sqrt{W(h^n) + C_0}} \frac{h^{n+1} - h^n}{\tau}, \tag{3.2.38}$$

which is linear and is shown to be unconditionally energy stable in [67]. An advantage of this scheme is that it can be easily extended to unconditionally energy stable second-order BDF schemes. It requires $W(h)$ to be bounded from below, which is not always the case, and it involves solving linear equations with complicated variable coefficient [63]. In addition, for a system with multiple components, the IEQ scheme leads to a coupled system.

The scalar auxiliary variable (SAV) approach [68] is obtained with a small adaption to the IEQ scheme. This scheme addresses the above discussed drawbacks of the IEQ scheme. Instead of requiring $W(h)$ is bounded from below, the scheme only requires that $E_1(h) := \int_\Omega W(h) \, dx$ is bounded from below: $E_1(h) \geqslant -C_0$. This assumption is valid for any physically sound free energy. Now a scalar auxiliary variable $r(t) = \sqrt{E_1(h) + C_0}$

is introduced, and the system can be rewritten as

$$\frac{\partial h}{\partial t} = \nabla \cdot [m(h)\nabla \mu], \tag{3.2.39}$$

$$\mu = \frac{r(t)}{\sqrt{E_1(h) + C_0}} W'(h) - \sigma^2 \Delta h, \tag{3.2.40}$$

$$r_t = \frac{1}{2\sqrt{E_1(h) + C_0}} \int_\Omega W'(h) h_t \, dx. \tag{3.2.41}$$

The first order scheme is then

$$\frac{h^{n+1} - h^n}{\tau} = \nabla \cdot \left[m(h^n)\nabla \mu^{n+1} \right], \tag{3.2.42}$$

$$\mu^{n+1} = \frac{r^{n+1}}{\sqrt{E_1(h^n) + C_0}} W'(h^n) - \sigma^2 \Delta h^{n+1}, \tag{3.2.43}$$

$$\frac{r^{n+1} - r^n}{\tau} = \frac{1}{2\sqrt{E_1(h^n) + C_0}} \int_\Omega \left(W'(h^n) \frac{h^{n+1} - h^n}{\tau} \right) dx. \tag{3.2.44}$$

Under a second-order BDF, the SAV scheme is also unconditionally energy stable [63]. For single component gradient flows, at each time step only linear equations with constant coefficients require solving, and for multi-component flows, at each time step decoupled linear equations with constant coefficients (one for each component) require solving, making the scheme very efficient [65].

In this thesis, we will primarily be using linear finite elements for the spatial discretisation and the convex splitting scheme described in Section 3.2.2 for time stepping, although the more advanced schemes are certainly applicable.

CHAPTER 4

Isothermal Thin Film Dynamics

In this Chapter we provide the rational derivation for an elementary class of thin film models. This derivation assumes an isothermal situation, and is only based on mass conservation and a free-energy dissipation inequality (hence a mechanical version of the second law of thermodynamics). [1]

Before presenting the derivation of the new models, we first present in Section 4.1 elementary models for nucleation and growth of holes in thin films, and in Section 4.2 classical PDE models for thin film dynamics based on asymptotics and gradient-flow dynamics. We present our rational framework in Section 4.3 which ends with a new class of models. It is furthermore demonstrated that the classical PDE models fit with the derived class. We also present some numerical examples for hole growth in a one and two dimensional thin film using the techniques described in Chapter 3.

---

[1] Section 4.3 is based on the publication [1], which has been slightly edited to fit in line with the notation in this thesis.

4.1 Nucleation and Growth of Holes in Thin Films

In this section we discuss the connection between the processes of hole nucleation (when holes form) and dewetting. Nucleation and growth of holes can occur in thin films as deposition techniques such as spin coating are very rarely stable, especially if prepared on non-wettable surfaces [35]. Reiter performed a series of experiments using thin polystyrene films coated on a silicon substrate to investigate the effects of film thickness on hole growth [69]. Film samples of less than 100nm were used, as it was shown in [70] that these films are unstable. The work considers different annealing times and temperatures.

Several samples of the same thickness were heated at the same temperature for different lengths of time. It was found that, as long as the holes did not coalesce, the number of defects remained constant and only the hole diameter increased. This implies that hole nucleation did not occur during the heating phase, and instead film break up (via spinodal decomposition) and hole growth occur as two separate phases. Furthermore, the experiments showed that more holes nucleate in thinner films. This is shown in Figure 4.1.

Srolovitz and Safran indicate that ways to prevent the film from dewetting include modifying the conditions so the film is thermodynamically stable, eliminating defects which lead to formation of large, substrate intersecting perturbations and decreasing the rate at which the holes grow [71]. However it is noted that these solutions are not always possible in every scenario.

4.1.1 Simple Hole Growth Models

A nice but simple model for hole growth is by Burlakov et al. [72], who derived a simple model for describing the evolution of holes in thin films over time to obtain a basic understanding of the dewetting process. The

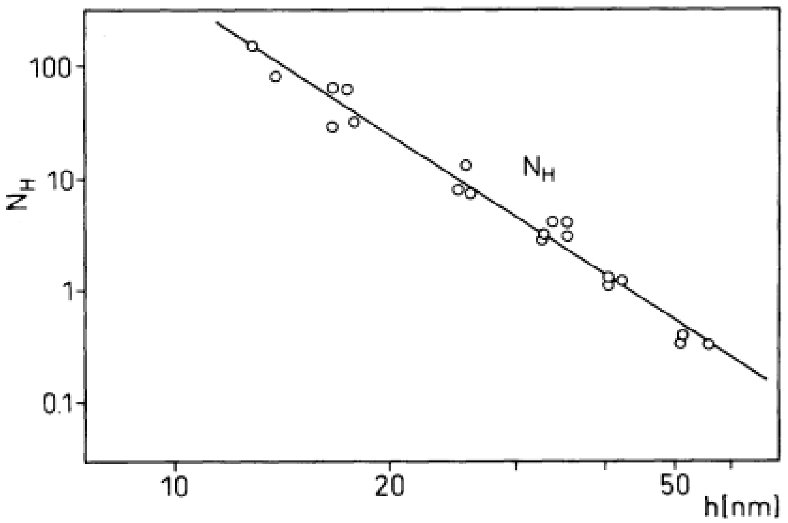

Figure 4.1: Double log plot showing the average number of initial holes per $10^4 \mu m^2$ (N_H) as a function of film thickness h, taken directly from [69].

model is derived from an energetic perspective, and is fitted to data accumulated in [14].

Srolovitz and Safran were among the first to consider the growth of holes in a thin film from this perspective [73]. They built on work by Mullins [74] in which it was shown via linear analysis that all small perturbations to film thickness will decay and the film will remain flat. They claim that this result is counter-intuitive from an energetic viewpoint as it is well documented that for a finite film the equilibrium shape is a spherical cap when the surface energy is isotropic [73]. Srolovitz and Safran explain this by claiming that substrate effects can only be studied with a nonlinear analysis, as perturbations must be large enough to rupture the film.

By considering the difference in surface energy (energy interactions between the liquid film and air, and the film and substrate), considering the small slope approximation, and minimising this energy, they deduce that there exists a threshold radius r_c for every individual scenario. Whether a hole with initial radius r_0 grows or shrinks depends on the relationship between r_0 and r_c.

Four major assumptions are made: that all holes can be considered as

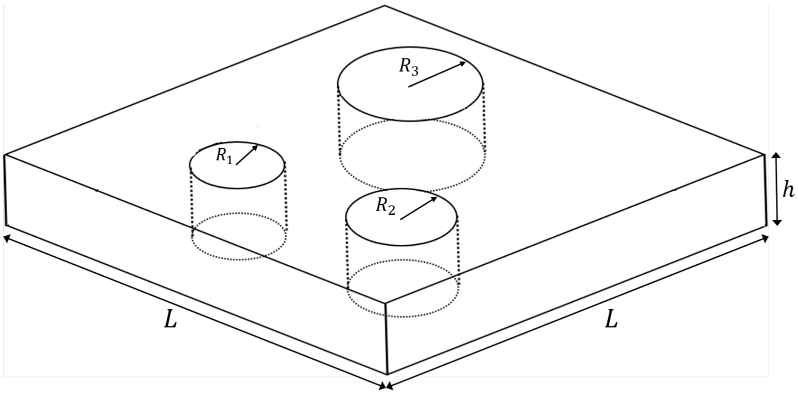

Figure 4.2: A diagram of the geometry considered in [72].

cylindrical in shape and never impinge on each other, nucleation does not take place during the hole growth phase, elastic stresses in the film are fully relaxed and all mass lost via evaporation is treated the same. The work considers a flat film with N cylindrical holes sitting on a flat solid substrate with the area $L \times L$, as shown in Figure 4.2. The surface and interface energy E is then given by

$$\begin{aligned} E(R_1, \ldots, R_N) = \gamma_F &\left(2\pi h \sum_{k=1}^{N} R_k + L^2 - \pi \sum_{k=1}^{N} R_k^2 \right) \\ &+ \gamma_I \left(L^2 - \pi \sum_{k=1}^{N} R_k^2 \right) + \gamma_S \pi \sum_{k=1}^{N} R_k^2, \end{aligned} \tag{4.1.1}$$

where h is the film thickness, γ_F, γ_S and γ_I represent the surface energies of the film, substrate and film-substrate interface respectively, and R_i is the radius of hole i. Assuming a gradient flow of energy, the time evolution of the holes' radii is given by

$$\frac{dR_i}{dt} = -\Gamma \frac{\partial E}{\partial R_i} = -2\pi\Gamma \left(\gamma_F h - R_i \left(\gamma_F + \gamma_{IS} \right) \right), \tag{4.1.2}$$

where $\gamma_{IS} = \gamma_I - \gamma_S$ and Γ is the kinetic constant. This can be rewritten as

$$\frac{dR_i}{dt} = A(R_i - R_c), \tag{4.1.3}$$

where A is a positive constant and $R_c = h/(1 + \gamma_{IS}/\gamma_F)$ is the critical

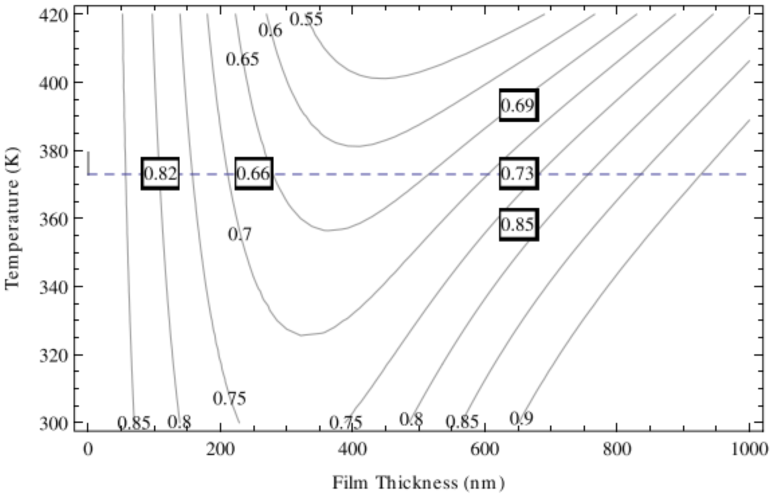

Figure 4.3: Contour plot of surface coverage as a function of initial film thickness and annealing temperature taken directly from [72]. A normal distribution was used for initial hole size. The dotted line represents $100^o C$.

radius. As predicted by [71, 73], this implies that hole growth depends on a critical radius; a hole with $R_i > R_c$ will grow while a hole with radius $R_i < R_c$ will shrink.

Given the above model of hole growth, it is possible to predict surface coverage given additional assumptions on the initial distribution of holes and the effect of evaporation. Starting with an initial Gaussian distribution of initial radii for the holes, assuming that the proportion of covered substrate to uncovered substrate is much less than 1, and calibrating the model to data collected in [14], Burlakov et al. obtained the results in Figure 4.3. The results show that for good surface coverage, very thin or very thick films must be used. However, the accuracy of the model depends on the accuracy of the experimental data.

Simple models such as those described above have many advantages: they tend to reproduce the proper qualitative behaviour, identify the important variables and indicate the manner in which these variables scale [73]. However while models such as that described in [72] may give accurate figures for the final percentage of surface covered by the film, they offer minimal insight into realistic dynamics of film morphology, and give no indication of the distribution of the uncovered areas.

4.2 PDE Models Describing the Evolution of Thin Films

In this chapter, classical approaches for deriving PDE models for describing the dynamics of a non-evaporating, dewetting thin film on a solid flat substrate are discussed. Both an asymptotic approach and an energetic approach are considered. The standard PDE model for thin films was developed by Burelbach et al. [37], and is given by

$$h_t + \left(h^{-1}h_x\right)_x + \left(h^3 h_{xxx}\right)_x = 0, \tag{4.2.1}$$

where $h(x,t)$ is the height of the film at point x at time t, and $h_x = \partial h/\partial x$. Next follows the derivation of (4.2.1).

4.2.1 Classical Thin-Film Modeling

The classical asymptotic approach to thin film modeling was reviewed by Burelbach et al. in 1988 [37]. Their model considers a thin liquid film on a flat, solid substrate with a gaseous vapour above, as depicted in Figure 4.4. It is assumed that the layer is thin enough for gravity effects to be negligible and for van der Waals forces to take effect. It is also assumed that evaporation occurs at the vapour-liquid interface $z = h(x,t)$ where h represents the thickness of the film. Mass loss, momentum transfer and energy consumption occur at this interface. The model was constructed using a single-phase approach, neglecting the dynamics of the vapour layer above the liquid film, with a long-wave approximation, and has been widely used in literature for modeling thin film evolution.

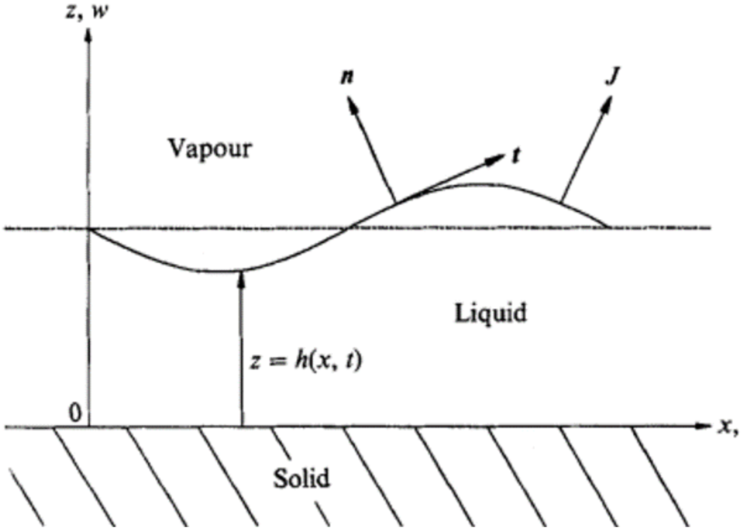

Figure 4.4: Configuration of a thin liquid film on a solid substrate in two dimensions [37]. u and w are velocities in the x and z directions respectively, $\mathbf{n}$ and $\mathbf{t}$ are the unit normal and tangent, and J is the evaporative flux across the liquid-vapour interface.

We now present the derivation of the single-phase model in (4.2.1) for the case of $d = 2$, although it should be noted that the derivation can easily be extended into higher dimensions. The derivation begins by considering the incompressible Navier-Stokes equations with an additional body force f_b to represent the van der Waals forces, along with a suitable energy equation:

$$\begin{cases} \rho(\mathbf{v}_t + \mathbf{v} \cdot \nabla \mathbf{v}) = -\nabla p + \nu \Delta \mathbf{v} - \nabla f_b \\ \nabla \cdot \mathbf{v} = 0 \\ \theta_t + \mathbf{v} \cdot \nabla \theta = \kappa \Delta \theta, \end{cases} \tag{4.2.2}$$

where $\mathbf{v} = (u, w)$ is the velocity vector in the x and z directions respectively, t is time, ρ is the density, p is pressure, ν is viscosity, T is temperature and κ is the thermal diffusivity.

At the solid-liquid interface, the no slip and no penetration conditions, $\mathbf{v}(z) = 0$ at $z = 0$, are used, and it is assumed that the liquid is heated from below, so that at this boundary there is a constant temperature $\theta =$

θ_H.

At the vapour-liquid interface five conditions are required. These are the jump mass balance,

$$J = \rho(\mathbf{v} - \mathbf{v}^I) \cdot \mathbf{n} = \rho^V(\mathbf{v}^V - \mathbf{v}^I) \cdot \mathbf{n}, \tag{4.2.3}$$

the jump energy balance,

$$J\left[L + \frac{1}{2}\left[(\mathbf{v}^V - \mathbf{v}^I) \cdot \mathbf{n}\right]^2 - \frac{1}{2}\left[(\mathbf{v}^V - \mathbf{v}^I) \cdot \mathbf{n}\right]^2\right] + k\nabla\theta \cdot \mathbf{n} - k^V\nabla\theta^V \cdot \mathbf{n} \\ + 2\nu(\boldsymbol{\tau} \cdot \mathbf{n}) \cdot (\mathbf{v} - \mathbf{v}^I) - 2\nu^V(\boldsymbol{\tau}^V \cdot \mathbf{n}) \cdot (\mathbf{v}^V - \mathbf{v}^I) = 0, \tag{4.2.4}$$

the normal stress,

$$J(\mathbf{v} - \mathbf{v}^V) \cdot \mathbf{n} - (\mathbf{T} - \mathbf{T}^V) \cdot \mathbf{n} \cdot \mathbf{n} = (\nabla \cdot \mathbf{n})\sigma(\theta), \tag{4.2.5}$$

the tangential stress,

$$J(\mathbf{v} - \mathbf{v}^V) \cdot \mathbf{t} - (\mathbf{T} - \mathbf{T}^V) \cdot \mathbf{n} \cdot \mathbf{t} = -\nabla\sigma(\theta) \cdot \mathbf{t}, \tag{4.2.6}$$

and a constitutive equation for the flux across the boundary,

$$J = \left(\frac{\alpha\rho^V L}{\theta_S^{3/2}}\right)\left(\frac{M_W}{2\pi R_g}\right)^{1/2}(\theta^I - \theta_S), \tag{4.2.7}$$

derived in [75]. J is the mass flux at the interface (due to evaporation), L is the latent heat of vaporisation, k is the thermal conductivity, $\boldsymbol{\tau}$ is the rate of deformation tensor, $\mathbf{T} = -p\mathbf{I} + 2\nu\boldsymbol{\tau}$ is the stress tensor with $\mathbf{I}$ representing the identity matrix, θ_S is a reference temperature, M_W is the molecular weight, R_g is the universal gas constant and α is the accommodation coefficient. $\sigma(\theta)$ represents surface tension and is assumed to be linear with respect to temperature. In these equations, the superscript V refers to the vapour, a superscript I refers to the interface and no superscript refers to the liquid.

The single-phase approach utilised assumes that density ρ, viscosity ν and thermal conductivity k are negligible in the vapour phase. Formally this can be written as taking the limits

$$\frac{\rho^V}{\rho}, \frac{\nu^V}{\nu}, \frac{k^V}{k} \to 0. \tag{4.2.8}$$

Finally, it is assumed that the pressure in the vapour, $p^V = 0$. Using these interface conditions and assumptions, the model can then be non-dimensionalised. Length is scaled by d_0, the initial mean film thickness, and time, velocity and pressure are scaled using viscous scales; d_0^2/ν, ν/d_0 and $\rho\nu^2/d_0^2$ respectively. The temperature difference $\theta - \theta_S$ is scaled on $\Theta = \theta_H - \theta_S$ and finally an evaporative timescale $t_E = \Theta\rho d_0^2 L/k$ is introduced.

Following non-dimensionalisation a long-wave argument is employed as detailed in [37], in which it is assumed that the gradients of h and θ are small in the areas considered. In this work, periodic long wave disturbances are considered, and a small wavenumber λ is defined. The dependent variables are expanded in λ and lubrication theory is used to truncate them to the appropriate order: u, J and $\theta = O(1)$, while $w = O(\lambda)$ as $\lambda \to 0$ to preserve continuity, and $p, f_b = O(\lambda^{-1})$ as $\lambda \to 0$ so spontaneous rupture can be examined.

Combining the resulting series of equations gives the resultant PDE to describe the evolution of an evaporating thin film:

$$\begin{aligned} h_t + E(h+K)^{-1} + S(h^3 h_{xxx})_x + \{[Ah^{-1} + E^2 D^{-1}(h+K)^{-3}h^3 \\ +KMP^{-1}(h+K)^{-2}h^2]h_x\}_x = 0. \end{aligned} \tag{4.2.9}$$

Here,

$$A = \frac{A'}{6\pi d_0 \rho \nu^2} \tag{4.2.10}$$

is a non-dimensionalised version of the dimensional Hamaker constant A',

$$P = \frac{\nu}{\kappa} \tag{4.2.11}$$

is the Prandtl number,

$$E = \frac{k\Theta}{\rho \nu L} \tag{4.2.12}$$

is the evaporation number,

$$D = \frac{3\rho^V}{2\rho} \tag{4.2.13}$$

is a parameter proportional to the ratio of vapour to liquid densities,

$$S = \frac{\sigma_0 d_0}{3\rho \nu^2} \tag{4.2.14}$$

is the non-dimensionalised surface tension, where σ_0 is the surface tension at reference temperature θ_S,

$$M = \frac{\gamma \Theta d_0}{2\rho \nu \kappa} \tag{4.2.15}$$

is the Marangoni number where $\gamma = -d\sigma/d\theta$, and

$$K = \left(\frac{k\theta_S^{3/2}}{\alpha d_0 \rho^V L^2}\right)\left(\frac{2\pi R_g}{M_W}\right)^{1/2} \tag{4.2.16}$$

is a measure of the degree of non-equilibrium at the interface.

Now, rather than having to solve a free boundary problem, one only needs to solve the PDE given in equation (4.2.9). This model includes effects from mass loss due to evaporation, vapour recoil (a force resulting from the expansion of the fluid as it changes from liquid to gas [76]), thermocapillarity, long range molecular forces, surface tension and viscous forces. To investigate the results, an isothermal case was considered

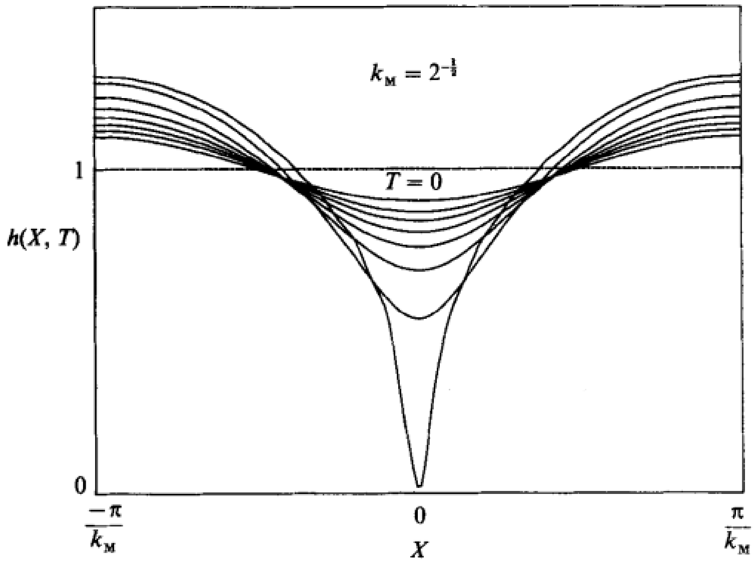

Figure 4.5: Film profiles at different times for the isothermal case $K = 0$ up to the time of film rupture using an initial condition of $h(\bar{x}, 0) = 1 + 0.1\sin(k_M\bar{x})$. Taken directly from [37].

initially, by taking $K = 0$. This reduces the model to

$$h_{\bar{t}} + (h^{-1}h_{\bar{x}})_{\bar{x}} + (h^3 h_{\bar{x}\bar{x}\bar{x}})_{\bar{x}} = 0. \tag{4.2.17}$$

by employing the scalings $\bar{x} = (A/S)^{1/2}x$ and $\bar{t} = (A^2/S)t$ and setting the remaining non-dimensional parameters to 1. A numerical solution to this model on the interval $-\pi/k_M < \bar{x} < \pi/k_M$, where k_M is the maximising wavenumber of linear theory, in this case $k_M = 2^{1/2}$, is shown in Figure 4.5. An initial condition of $h(\bar{x}, 0) = 1 + 0.1\sin(k_M\bar{x})$ was used. The rupture time calculated lines up well with the result predicted in [77].

The model proposed by Burelbach et al. has been used in many situations. Shklyaev and Fried added two terms to the model in order to account for the transport of energy along the liquid-vapour interface and the influence of effective pressure accounting for vapour recoil [78]. This is used to show that for molten metals consideration of the effective pressure substantially affects the growth rate, indicating that the effective pressure has a stabilizing effect when acting on materials with parameter values in the same range as molten metals.

Anderson and Davis [79] used lubrication theory to derive a model to simulate the spreading of volatile liquid droplets on heated surfaces. They employed the single-phase approach used by Burelbach to derive a model for continuous films, as this effectively decoupled the liquid film from the surrounding vapour. However, the model breaks down when film rupture occurs and so modifications were made to account for contact line dynamics.

The stability analysis of an evaporating or condensing film conducted in [37] plays a major role in the work by Oron et al. [80] in which macroscopic thin liquid films are studied in detail. Films acting solely under gravity, films with van der Waals forces acting upon them, films with temperature dependent properties and films on different geometries such as a thick substrate or a cylinder have been considered, among many others.

It is clear that the single-phase approach and non-dimensionalisation techniques proposed by Burelbach et al. in [37] remain key ideas in thin-film modeling. Aside from the limitations that the model breaks down as $h \to 0$ and therefore is not able to deal with film rupture and contact line dynamics, the method has been the underlying key to many models considering a continuous thin film. Further, it has provided the base for several works considering the rupture of thin films, and also films dewetting on a substrate such as in [81–83].

4.2.2 Energetic Modeling Approach in Thin Films

A different method which can be employed to model thin-film flow is a gradient flow technique, which is discussed in this section. The idea behind this technique is to consider the energy of the system, and describe its evolution by insisting the energy dissipates.

In a 2011 review, Thiele [58] builds on works in [84] and proposes that, for a standard free energy functional,

$$\Psi = \frac{\sigma^2}{2}\left(\nabla h\right)^2 + W(h), \tag{4.2.18}$$

with total energy given by

$$\mathcal{E}[h] = \int \Psi \, dA. \tag{4.2.19}$$

The equation governing the time evolution of the thickness profile $h(x, y, t)$ of a thin film acting under the sole influence of capillary and wettability is given by

$$\frac{\partial h}{\partial t} = \nabla.\left[m(h)\nabla\frac{\delta\mathcal{E}}{\delta h}\right], \tag{4.2.20}$$

where $m(h) = h^3/3\nu$ is the mobility factor assuming a Poiseuille flow [58], and $\delta\mathcal{E}/\delta h$ is the variational derivative of the free energy functional Ψ. This equation can be rewritten as

$$\frac{\partial h}{\partial t} = -\nabla.\left[\frac{h^3}{3\nu}\nabla\left(\sigma^2\Delta h - W'(h)\right)\right], \tag{4.2.21}$$

where ν is viscosity and $W(h)$ is the free energy density. Similar models have been used to simulate capillary waves [85], moving contact lines [86] and droplets and nucleation [87].

4.3 Rational Derivation of Isothermal Thin-Film Dynamics

In this section we derive a family of models describing the flow of a thin film on a flat impermeable substrate using the rational techniques described in Chapter 2. We proceed by showing that, by making specific choices within the derived family, the asymptotically derived model by Burelbach et al. [37] and the model stated by Thiele [38] both fit within this framework.

By considering the conservation of mass of a thin liquid film on a horizontal substrate $\mathfrak{D} \subset \mathbb{R}^{n-1}$ where $n = 2$ or 3, we derive an equation for the height function of the film $h(\mathbf{x}, t)$ for $\mathbf{x} \in \mathfrak{D},\ t \geq 0$.

We follow the standard argument of considering the horizontal flux $\mathbf{j}$ across an arbitrary sub-domain of the thin film, $\Omega \subset \mathfrak{D}$, such as presented in [39]. We consider the film to have constant density $\rho = 1$, and that rate of mass lost across the interface of the film (due to evaporation for example) is given by R. From the conservation of mass, we obtain

$$\frac{\partial h}{\partial t} = -\nabla \cdot \mathbf{j} - R. \tag{4.3.1}$$

We next consider the mechanical version of the second law of thermodynamics. We showed in Chapter 2 that in an isothermal case, the second law reduces to

$$\frac{d}{dt} \int_{\mathcal{B}} (\Psi + \Xi)\, dV \leqslant \mathcal{W}(\mathcal{B}), \tag{4.3.2}$$

where $\mathcal{W}(\mathcal{B})$ contains the work done on $\mathcal{B}$ and the free energy flux through the boundary $\partial\mathcal{B}$. The total energy density is given by $\mathcal{E} = \Psi + \Xi$, where Ψ is the Helmholtz free energy density of the system, and Ξ is a function encapsulating energies from other sources, including kinetic energy and energy from magnetic fields [88]. The constitutive class of Ψ, and the composition of Ξ are a choice to be made by the modeler. For a simple scenario of a static film, we take $\Xi \equiv 0$. In this case, for the subdomain Ω we write

$$\frac{d}{dt} \int_{\Omega} \Psi \, dV = \mathcal{W}(\Omega) - \mathcal{D}(\Omega) \tag{4.3.3}$$

for some function $\mathcal{D}(\Omega) \geqslant 0$, which represents the dissipation of the free energy.

4.3.1 Constitutive Dependence

We consider the Helmholtz free energy density Ψ to depend on h and its gradient, that is to say

$$\Psi = \bar{\Psi}\left(h, \nabla h\right), \tag{4.3.4}$$

and the total energy functional is given by

$$\mathcal{E}(\Omega) := \int_{\Omega} \bar{\Psi}\left(h, \nabla h\right)\, dx. \tag{4.3.5}$$

The variational derivative μ of $\mathcal{F}$ with respect to h is defined as

$$\mu = \frac{\delta \mathcal{E}}{\delta h} = \partial_h \bar{\Psi} - \nabla \cdot \left(\partial_{\nabla h} \bar{\Psi}\right). \tag{4.3.6}$$

We now define a constitutive class for $\mathbf{j}$ and R in equation (4.3.1) by postulating that these variables are dependent on h, the variational derivative μ, and the gradients of these variables. Defining $\Gamma := \{h, \nabla h, \mu, \nabla \mu\}$, this can be written

$$\mathbf{j} = \bar{\mathbf{j}}(\Gamma), \tag{4.3.7}$$

$$R = \bar{R}(\Gamma). \tag{4.3.8}$$

Having set up the constituent classes for the dependent variables in the model, we now derive constraints such that the second law of thermodynamics (4.3.3) holds.

4.3.2 Deriving Constraints

Using that $\Psi = \bar{\Psi}(h, \nabla h)$ and that Ω is not time-dependent, the left hand side of (4.3.3) equals

$$\frac{d}{dt}\int_\Omega \bar{\Psi}\,(h, \nabla h)\,dV = \int_\Omega \left(\partial_h \bar{\Psi}\dot{h} + \partial_{\nabla h}\bar{\Psi}\cdot(\dot{\nabla h})\right) dV, \tag{4.3.9}$$

where ∂_h is the partial derivative with respect to h and $\dot{h}$ is the time derivative of h. Switching the time and space derivatives in the last term of (4.3.9) results in

$$\frac{d}{dt}\int_\Omega \bar{\Psi}\,(h, \nabla h)\;dV = \int_\Omega \left(\partial_h \bar{\Psi}\dot{h} + \partial_{\nabla h}\bar{\Psi}\cdot\nabla\dot{h}\right) dV, \tag{4.3.10}$$

which when integrating the second term on the right hand side by parts gives

$$\frac{d}{dt}\int_\Omega \bar{\Psi}\,(h, \nabla h)\,dV = \int_\Omega \partial_h \bar{\Psi}\dot{h}\,dV - \int_\Omega \dot{h}\nabla\cdot(\partial_{\nabla h}\bar{\Psi})\,dV + \int_{\partial\Omega} \partial_{\nabla h}\bar{\Psi}\dot{h}\cdot\mathbf{n}\,ds. \tag{4.3.11}$$

Combining the integrals over Ω and using (4.3.6) results in

$$\frac{d}{dt}\int_\Omega \bar{\Psi}\,(h, \nabla h)\,dV = \int_\Omega \dot{h}\mu\,dV + \int_{\partial\Omega} \partial_{\nabla h}\bar{\Psi}\dot{h}\cdot\mathbf{n}\,ds. \tag{4.3.12}$$

We can now substitute (4.3.1) into (4.3.12) to give

$$\frac{d}{dt}\int_\Omega \bar{\Psi}\,(h, \nabla h)\,dV = \int_\Omega (-\nabla\cdot\mathbf{j} - R)\mu\,dV + \int_{\partial\Omega} \partial_{\nabla h}\bar{\Psi}\dot{h}\cdot\mathbf{n}\,ds, \tag{4.3.13}$$

and integrating by parts the term involving $\mu\nabla\cdot\mathbf{j}$ results in

$$\frac{d}{dt}\int_\Omega \bar{\Psi}\,dV = -\int_\Omega \left(\mu R - \mathbf{j}\cdot\nabla\mu\right)\;dV + \int_{\partial\Omega} \left(-\mu\mathbf{j} + \partial_{\nabla h}\bar{\Psi}\dot{h}\right)\cdot\mathbf{n}\,ds. \tag{4.3.14}$$

Comparing (4.3.14) to (4.3.3), we identify the domain integral to be the dissipation $\mathcal{D}(\Omega)$ and the boundary integral to be $\mathcal{W}(\Omega)$, which are natural identifications, similar to the choices made in earlier works [89].

Thus, a family of models that suitably describes the evolution of a thin film on a solid substrate while ensuring energy dissipation is given by

$$\frac{\partial h}{\partial t} + \nabla \cdot \bar{\mathbf{j}} = -\bar{R}, \tag{4.3.15}$$

where $\bar{\mathbf{j}}$ and $\bar{R}$ are chosen to be as in (4.3.7) and (4.3.8) and

$$\mu \bar{R} - \bar{\mathbf{j}} \cdot \nabla \mu \geqslant 0, \tag{4.3.16}$$

with $\mu = \partial_h \bar{\Psi} - \nabla \cdot (\partial_{\nabla h} \bar{\Psi})$.

4.3.3 Choices

Having derived a constraint on $\bar{\mathbf{j}}$ and $\bar{R}$ we can make choices that satisfy the constituent classes which ensure the restrictions are met. We make the choices such that the constraint is satisfied term-wise. It is apparent that making the choices

$$\bar{R} = k_1(\Gamma)\mu, \tag{4.3.17}$$

and

$$\bar{\mathbf{j}} = -k_2(\Gamma)\nabla \mu, \tag{4.3.18}$$

with $k_1,\ k_2 \geqslant 0$ for all realistic scenarios satisfies (4.3.16). This can be confirmed by substituting these choices into (4.3.16) to give

$$k_1(\Gamma)\mu^2 + k_2(\Gamma)|\nabla \mu|^2 \geqslant 0. \tag{4.3.19}$$

A classical choice for the free energy density $\bar{\Psi}$ which applies in this scenario is

$$\bar{\Psi}(h, \nabla h) = W(h) + \frac{\sigma^2}{2}\left|\nabla h\right|^2, \tag{4.3.20}$$

with corresponding variational derivative

$$\mu = W'(h) - \sigma^2 \Delta h, \tag{4.3.21}$$

where $W(h)$ is a free energy function depending only on the height h, and the second term represents energy due to variations in height, with σ being the surface tension. Having made these choices, the final model to describe the evolution of a thin liquid film on a solid substrate is given by

$$\frac{\partial h}{\partial t} = \nabla \cdot [k_2(\Gamma)\nabla\mu] - k_1(\Gamma)\mu, \tag{4.3.22}$$

$$\mu = W'(h) - \sigma^2\Delta h. \tag{4.3.23}$$

4.3.4 Connections

In this section, we show that the family of models described above is consistent with existing models for thin film evolution when the modeler makes particular choices for $k_1(\Gamma)$, $k_2(\Gamma)$ and $W(h)$.

Thiele's model [38] for a non-volatile case is given by

$$\frac{\partial h}{\partial t} = \nabla \cdot \left[M_c(h)\nabla\frac{\delta\mathcal{E}}{\delta h}\right], \tag{4.3.24}$$

where $M_c(h) \geqslant 0$ is the mobility function for the thin film and $\delta\mathcal{E}/\delta h$ is given in (4.3.6), with $\mathcal{E}$ given in (4.3.5). It is clear that this model fits into the framework (4.3.22-4.3.23) with $k_1(\Gamma) = 0$ and $k_2(\Gamma) = M_c(h)$, and with these choices it is also clear that constraint (4.3.16) is satisfied, implying the dissipation

$$\mathcal{D}(\Omega) = \int_\Omega M_c(h)|\nabla\mu|^2 \geqslant 0. \tag{4.3.25}$$

We now show that the model derived using asymptotic approaches by Burelbach et al. [37] also satisfies these requirements. The equation for a non-volatile case ($k_1(\Gamma) = 0$) given in [37] is

$$\frac{\partial h}{\partial t} + S\nabla \cdot \left(h^3\nabla\Delta h\right) + \nabla \cdot \left(\left[Ah^{-1}\right]\nabla h\right) = 0, \tag{4.3.26}$$

where $A \geqslant 0$ is a non-dimensionalised version of the Hamaker constant and $S \geqslant 0$ is the non-dimensionalised surface tension. This can be rewritten

$$\frac{\partial h}{\partial t} = -\nabla \cdot \left[\frac{Sh^3}{\sigma^2} \sigma^2 \nabla \Delta h + \frac{A}{h} \nabla h \right]. \tag{4.3.27}$$

Factoring out Sh^3/σ^2 results in

$$\frac{\partial h}{\partial t} = -\nabla \cdot \left[\frac{Sh^3}{\sigma^2} \left(\sigma^2 \nabla \Delta h + \frac{A\sigma^2}{Sh^4} \nabla h \right) \right]. \tag{4.3.28}$$

Noting that for some function $f(h)$ the chain rule gives $\nabla f(h) = f'(h) \nabla h$ then we can write

$$\frac{A\sigma^2}{Sh^4} \nabla h = \nabla \left(-\frac{A\sigma^2}{3Sh^3} \right), \tag{4.3.29}$$

which can be substituted back into (4.3.28) to give

$$\frac{\partial h}{\partial t} = \nabla \cdot \left[\frac{Sh^3}{\sigma^2} \nabla \left(\frac{A\sigma^2}{3Sh^3} - \sigma^2 \Delta h \right) \right]. \tag{4.3.30}$$

It can be seen that by choosing

$$W(h) = -\frac{A\sigma^2}{6Sh^2}, \tag{4.3.31}$$

in (4.3.23), and

$$k_2(\Gamma) = \frac{Sh^3}{\sigma^2} \tag{4.3.32}$$

in (4.3.22), noting that as $h > 0$ for all realistic situations then $k_2(\Gamma) \geqslant 0$ also, the model derived asymptotically by Burelbach et al. fits within the framework derived from first principles, with $k_1(\Gamma) = 0$.

With these choices along with (4.3.17) and (4.3.18), the dissipation given by

$$\mathcal{D}(\Omega) = \int_\Omega \mu \bar{R} - \bar{\mathbf{j}} \cdot \nabla \mu \, dV \tag{4.3.33}$$

is given by

$$\mathcal{D}(\Omega) = \int_\Omega \frac{Sh^3}{\sigma^2} \left| \nabla \mu \right|^2 \, dV \geqslant 0, \tag{4.3.34}$$

for any realistic situation, and so the model is thermodynamically consistent.

A point of interest here is that the so-called disjoining pressure $\Pi(h)$ chosen in the derivation of the model (4.3.26) is given by $\Pi(h) = -kW'(h) = Ah^{-3}$ for constant $k = \frac{3S}{\sigma^2}$, and so is directly proportional to $-W'(h)$, see also [58].

4.3.5 Regularisation of the Asymptotic Model

A characteristic of model (4.3.26) is that it breaks down as the film ruptures since $h^{-1} \to \infty$. In typical numerical simulations this breakdown is observed by h becoming negative. To enable simulations to continue past the point of rupture one can regularise the bulk free energy $W(h)$ and the mobility function $m(h) = Sh^3\sigma^{-2}$ as follows.

The dotted lines in Figure 4.6 show the non-regularised $m(h)$ and $W(h)$. To regularise the mobility, we force $m(h) = 0$ for $h \leq 0$ as depicted in the top panel of Figure 4.6. To handle $W(h)$, we choose a small $\epsilon > 0$ and construct $W(h)$ to be quadratic for $h < \epsilon$, and remain defined as in (4.3.31) for $h \geq \epsilon$. We require the minimum of $W(h)$ to be at $h = 0$ and for the function to be continuous with a continuous derivative. The regularised function is given by

$$W(h) = \begin{cases} \dfrac{1}{6\epsilon^4}h^2 - \dfrac{1}{3\epsilon^2} & \text{if } h < \epsilon, \\[2ex] -\dfrac{1}{6}h^{-2} & \text{if } h \geq \epsilon. \end{cases} \tag{4.3.35}$$

and is shown in the bottom panel of Figure 4.6.

To perform numerical simulations we use a linear finite element discretisation in space for h and μ in (4.3.22) and (4.3.23) having set $k_1(\Gamma) = 0$ in the former, employing homogeneous Neumann boundary conditions and triangular elements for the case of $n = 3$. For the time discretisation we use a convex splitting method in which the non-linear term is split as $W(h) = W_+(h) + W_-(h)$ with $W_+(h)$ being convex and $W_-(h)$ being concave. It is shown in Chapter 3 that if $W_+(h)$ is treated implicitly and $W_-(h)$ explicitly then the method is energy stable. In addition, it is claimed in [54] that if $\exists\ L_W > 0$ such that $|W''(h)| \leq L_W\ \forall h$ then there exists a convex split with $W_+(h) = L_W h^2/2$. This is a useful property as it results in the implicit terms being linear, removing the need to use a non-linear solver. Also, we use a semi-implicit treatment of the mobility term $m(h)$.

Figure 4.7 shows examples of numerical solutions for $d = 2$ (top panel) and $d = 3$ (bottom panel). σ, S and A are taken to be 1. For $n = 2$, $\epsilon = 0.1$ and $\Delta t = 0.00032$, with an initial condition of $h(x,0) = 1 - 0.1\cos(x/\sqrt{2})$. For $n = 3$, $\epsilon = 0.5$, $\Delta t = 0.025$ and $h(x,y,0) = 1 - 0.05(\cos(x/\sqrt{2}) + \cos(y/\sqrt{2}))$. The chosen initial conditions represent a small perturbation in a flat film.

It should be noted here that this figure is a visual representation of the physical effects of film rupture and dewetting, and the time taken for the film to undergo this evolution is not intended to be realistic. Due to the different choices made between the $n = 2$ and $n = 3$ cases (in particular ϵ), the two graphs should not be directly compared in terms of timescale. However, it is clear that in both cases the small perturbation in the film grows until the film ruptures, at which point a hole forms and grows via dewetting.

4.3.6 Conclusion

In this work a family of thermomechanically consistent models for predicting the evolution of a non-volatile thin liquid film on a flat substrate was derived from mass conservation laws and the second law of thermodynamics, and it was shown that existing models fit within this family.

In particular, this allowed for a simple regularisation that can be applied to modeling choices to better handle film rupture and investigate dewetting of the film.

In [38, 58] more complex thin-film processes are described that require a change in the energy functional $W(h)$, but the general form of the equation remains unchanged. Similarly, Lyushnin et al. [90] postulate a different choice of $W(h)$ to simulate fingering instabilities. Further, it can be shown that other existing models, such as those developed in [91, 92] fit the framework, covering a wide range of applications from introducing a regime to account for slip to the growth of dry regions.

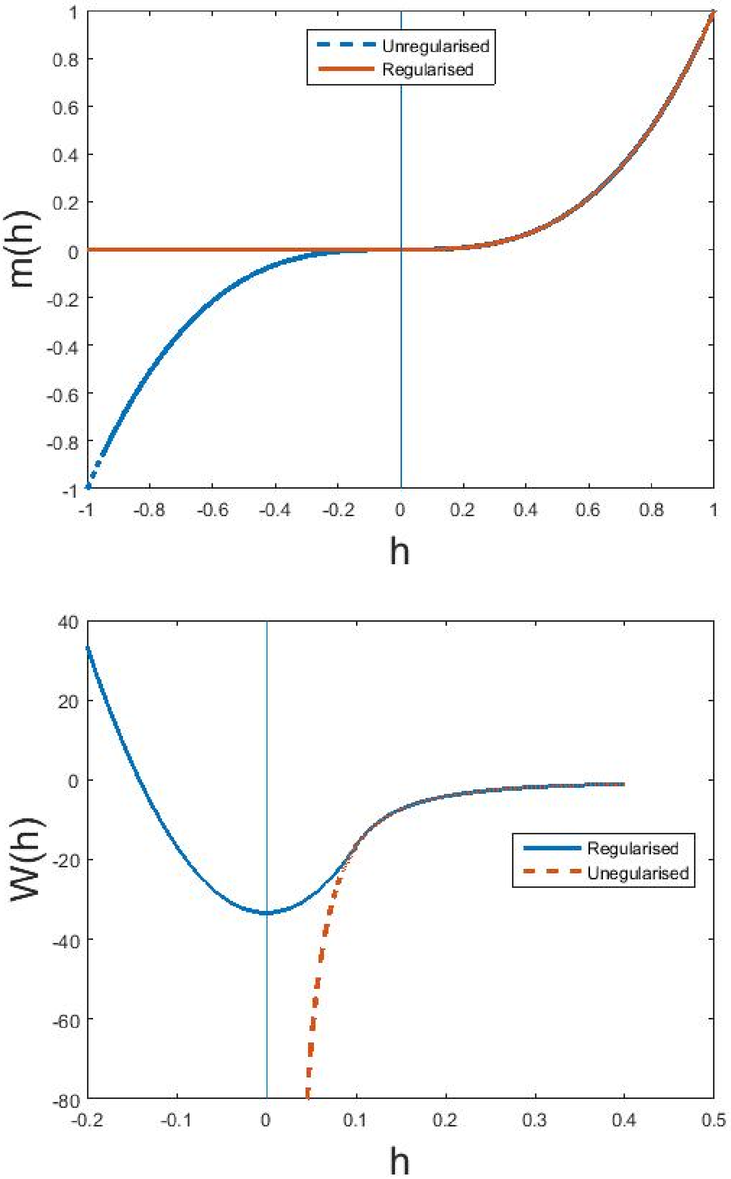

Figure 4.6: Graphs of the original mobility $m(h)$ (top) and free energy $W(h)$ (bottom), along with the regularised versions of these functions, with $\epsilon = 0.1$ in the regularised graph of $W(h)$.

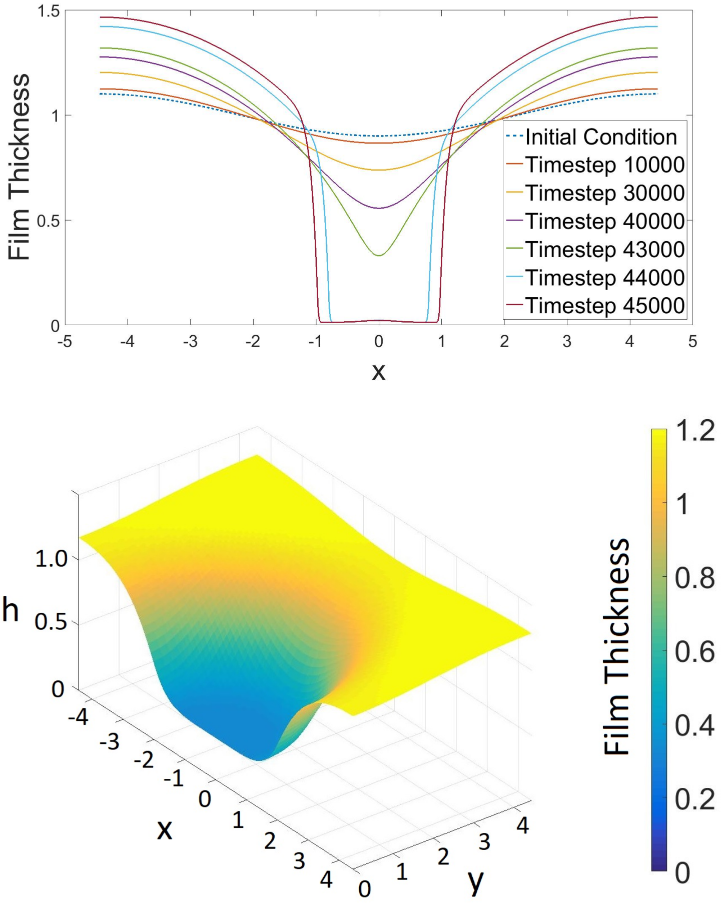

Figure 4.7: Top: Simulation with $n = 2$ of the regularised asymptotic model showing film rupture in the domain $\mathfrak{D} = [-\pi\sqrt{2}, \pi\sqrt{2}]$. Here, $\Delta t = 0.00032$ and $\epsilon = 0.1$. **Bottom:** Simulation with $n = 3$ showing how a small perturbation in a flat thin film can result in a hole forming. Only half the domain $\mathfrak{D} = [-\pi\sqrt{2}, \pi\sqrt{2}] \times [0, \pi\sqrt{2}]$ is shown to visualise the dewetted area and the final time of $t = 6.25$. Here, $\Delta t = 0.025$ and $\epsilon = 0.5$.

CHAPTER 5

Solidification in a Bulk Fluid

The change of phase from a liquid to a solid is a complex problem to model, but which has many important practical applications. An understanding of the solidification process helps to understand dendrite formation during the solidification of a metal from its melt, and microsegregation during fusion welding of alloys. In addition, the rate at which an evolving body solidifies has a large effect on its final morphology.

This chapter investigates the modelling of solidification in a bulk fluid. A review of previous studies into this phenomenon is presented, before a phase-field model for describing solidification is rigorously derived using the principles of rational continuum mechanics presented in Chapter 2. Finally, connections are made between this derived model and models that already exist in the literature.

This chapter forms a basis for Chapter 7, in which the rational framework derived in this chapter is extended to thin films.

5.1 Existing Work

Early models for solidification relied on a sharp boundary between the solid and liquid phases of the material, with differential equations describing the diffusion of heat within the individual phases, with boundary conditions applied to the moving interface [93]. This posed major issues, as the interface itself was unknown, resulting in models that are very computationally expensive to simulate. The development of phase-field modelling led to a change in focus for modelling solidification, as this technique does not require the moving boundary to be tracked. In this section we present the derivation of the sharp interface model, and discuss in more detail the development and refinement of the diffuse interface models commonly used in the literature.

5.1.1 Sharp Interface Model

The conventional sharp interface model for a pure substance solidifying from its melt is driven by the diffusion of latent heat away from the interface [94, 95]. Defining the thermal diffusion field to be

$$u = \frac{\theta - \theta_M}{k}, \tag{5.1.1}$$

where θ is the temperature, θ_M is the melting temperature of the material, and k is the ratio of the latent heat to the specific heat capacity, the diffusion of the latent heat can be written

$$\frac{\partial u}{\partial t} = D\Delta u, \tag{5.1.2}$$

for some diffusion coefficient D. The first boundary condition, relating to heat conservation, states that the normal growth velocity v_n can be written

$$v_n = -\left[D\nabla u \cdot n\right], \tag{5.1.3}$$

where n is the unit normal pointing outwards from the solid phase and the square brackets represent the discontinuity across the boundary. The second boundary condition states that the equilibrium temperature u_s at the interface can be written

$$u_s = -d\kappa - \beta(v_n). \tag{5.1.4}$$

Here d is proportional to the surface tension, κ is the sum of the principle curvatures of the interface and the term $\beta(v_n)$ accounts for deviation from the local equilibrium due to the movement of the interface. This is often written as

$$v_n = \beta^{-1}(-d\kappa - u_s). \tag{5.1.5}$$

The model, now completed, can theoretically be solved numerically. However, as Langer points out [96], the computational expense of solving such a system is very large, particularly considering that β^{-1} can be highly non linear in the majority of real cases. Langer proceeds to provide the derivation of a phase field model of which the previously-described sharp interface model is a limiting case. The model is an adaption of Halperin, Hohenberg and Ma's 'model C' [97], and the derivation is summarised below.

5.1.2 Phase-Field Modelling

Let $\phi(\mathbf{x}, t)$ be the phase-field, and define its equation of motion to be

$$\frac{\partial \phi}{\partial t} = -\Gamma \frac{\delta F}{\delta \phi} \tag{5.1.6}$$

for kinetic coefficient Γ and free energy F defined as

$$F[\phi] = \int \left[\frac{K}{2} |\nabla \phi|^2 + f(\phi) - \alpha u \phi \right], \tag{5.1.7}$$

where $f(\phi)$ is a double well function with minima at the equilibrium values of ϕ and gradient-energy coefficient K. The coupling coefficient α can be calculated by considering the thermodynamic equilibrium. The temperature equation is just given as heat conservation.

Penrose and Fife [47] investigated the method applied in Halerpin et al, and concluded that the treatment of the temperature variable was ad hoc. Specifically, the phase-change equation was derived as if in an isothermal setting, with the equation for the change of temperature being derived using other methods, such as by Fick's law [48]. This results in a model that is not strictly relaxational, and thus the model derived may be considered to be thermodynamically inconsistent. The proposed solution was, instead of initially stating the free energy functional Ψ, to define an entropy functional to be used as a starting point.

To achieve this, Penrose and Fife start with the Legendre transform equations

$$f(\theta,\phi) = \inf_e \left[e - \theta\eta(e,\phi) \right], \tag{5.1.8}$$

and

$$\eta(e,\phi) = \inf_\theta \left[\frac{e}{\theta} - \frac{f(\theta,\phi)}{\theta} \right]. \tag{5.1.9}$$

Differentiating the latter of these equations with respect to ϕ, we can write the energy density in the form

$$e = \frac{\partial(f(\theta,\phi)/\theta)}{\partial(1/\theta)}. \tag{5.1.10}$$

Considering the standard form of the energy functional,

$$F = \int_\Omega f(\theta,\phi) + \frac{1}{2}\kappa|\nabla\phi|^2 \, dx \tag{5.1.11}$$

$$= \int_\Omega \left(\inf_e \left[e - \theta\eta(e,\phi) \right] + \frac{1}{2}\kappa|\nabla\phi|^2 \right) \, dx \tag{5.1.12}$$

$$= \inf_e \int_\Omega \left(e - \theta\eta(e,\phi) + \frac{1}{2}\kappa|\nabla\phi|^2 \right) \, dx \tag{5.1.13}$$

$$= \inf_e \left(E\left[e\right] - \theta S\left[e,\phi\right] \right), \tag{5.1.14}$$

where the internal energy functional is given by

$$E[e] = \int_{\Omega} e \, dx, \tag{5.1.15}$$

and the entropy functional is given by

$$S[e, \phi] = \int_{\Omega} \eta - \frac{\kappa}{2\theta} |\nabla \phi|^2 \, dx. \tag{5.1.16}$$

By making the assumption that κ/θ is constant, and differentiating (5.1.16) with respect to time it can be seen that the variational derivatives of $S[e, \phi]$ are given by

$$\frac{\delta S}{\delta e} = \frac{\partial \eta}{\partial e} = \frac{1}{\theta} \tag{5.1.17}$$

and

$$\frac{\delta S}{\delta \phi} = \frac{\partial \eta}{\partial \phi} + \frac{\kappa}{\theta} \Delta \phi = \frac{1}{\theta} \left(-\frac{\partial f}{\partial \phi} + \kappa \Delta \phi \right). \tag{5.1.18}$$

For conserved order parameters, one can now write

$$\frac{\partial \phi}{\partial t} = -\nabla \cdot \left(M \theta \nabla \left[\frac{\delta S}{\delta \phi} \right] \right), \tag{5.1.19}$$

and for a non conserved parameter we write

$$\frac{\partial \phi}{\partial t} = K \theta \frac{\delta S}{\delta \phi}. \tag{5.1.20}$$

It is postulated that the energy density can be written in the form

$$e = u(\theta) v(\phi) + w(\phi), \tag{5.1.21}$$

with $u(\theta)$ strictly increasing. Combining this with (5.1.10) and integrating with respect to $1/\theta$ one obtains the kinetic equation for ϕ to be

$$\frac{\partial \phi}{\partial t} = K \theta \left(-\frac{u_1(\theta)}{\theta} v'(\theta) - \frac{w'(\phi)}{\theta} + s_0'(\phi) + \kappa_1 \Delta \phi \right), \tag{5.1.22}$$

where

$$u_1(\theta) = \theta \int_\Omega u(\theta) d(1/\theta), \tag{5.1.23}$$

and $s_0(\phi)$ is an as yet undefined function arising from the integration. The equation for e is given by

$$\frac{\partial e}{\partial t} = -\nabla \cdot \left(M \nabla \frac{1}{\theta} \right), \tag{5.1.24}$$

which can be combined with (5.1.21) to give

$$v(\phi) \frac{\partial u}{\partial t} - \left[u(\theta) v'(\phi) + w'(\phi) \right] \frac{\partial \phi}{\partial t} = -\nabla \cdot \left(M \nabla \frac{1}{\theta} \right). \tag{5.1.25}$$

The term in the square brackets is considered to represent the latent heat of the phase transition. Through making the choices $u(\theta) = -1/\theta, v(\phi) = 1, w(\phi) = -\lambda\phi$ for λ constant, and $M = 1$, these equations reduce to the model formed by Halperin, confirming that this system of equations is indeed thermodynamically consistent. The method of deriving a model starting from the entropy functional as opposed to the free energy functional has been used in many works. Notably, Wang et al. [57] used this method to investigate the crystalisation of a pure substance from its melt.

5.1.3 Adaptions to the Phase-Field Model

Fabrizio et al. [43] made two significant adaptions to this method. Firstly, based off recommendations from [98, 99] for non-isothermal conditions, the free energy functional should be multiplied through by a factor of $1/\theta$. Secondly, in the second law of thermodynamics, an additional term is considered in the entropy flux to give

$$\frac{d}{dt} \int_\Omega \rho\eta \, dv \geqslant -\int_\Omega \nabla \cdot \left(\frac{\mathbf{q}}{\theta} + \mathbf{k} \right) dv + \int_\Omega \frac{r}{\theta} \, dv. \tag{5.1.26}$$

The new **k** term accounts for entropy fluxes on the diffuse boundary between the solid and the liquid phases.

One issue with both the Halperin model and the Penrose and Fife model is that they rely on knowing either the free energy functional or the entropy functional before the modelling process starts. In the next section, we use the axioms from rational continuum mechanics from an unspecified free energy functional. We then propose constituent classes for the variables and employ the Coleman-Noll procedure to reduce the system to a thermodynamically consistent class of models for the solidification of a liquid.

5.2 Rational Derivation of a Model

In this section, we derive a family of thermodynamically consistent models for describing the solidification of a liquid in a non-isothermal bulk setting from first principles, using the key laws detailed in Chapter 2. We then make specific choices to reduce this family of models to the specific cases derived by Halerpin and Penrose and Fife.

For a body of material $\mathcal{B} \subset \mathbb{R}^d$, we consider an arbitrary subset of the material $\mathcal{P} \subset \mathcal{B}$, and introduce a phase-field parameter $\phi(\mathbf{x}, t)$, which takes the value of 1 if the material at $\mathbf{x} \subset \mathcal{P}$ is purely liquid, 0 if it is purely solid, and has a smooth transition between the values on the boundary between the phases. We assume the density of the body is constant in both liquid and solid phases with $\rho = 1$.

5.2.1 Deriving Constraints

For this scenario we require the first and second laws of thermodynamics, given in general form in (2.2.31) and (5.1.26). We consider a fixed body, and so $\mathcal{P}_t = \mathcal{P}\ \forall t$. As the volume being integrated over is not time dependent, the time derivative can be moved inside the integral, and by applying the divergence theorem on the boundary term, we obtain

$$\int_{\mathcal{P}} \frac{\partial e}{\partial t}\, dV = -\int_{\mathcal{P}} \nabla \cdot \mathbf{q}\, dV + \int_{\mathcal{P}} r\, dv. \tag{5.2.1}$$

where $e(\mathbf{x}, t)$, $\mathbf{q}(\mathbf{x}, t)$ and $r(\mathbf{x}, t)$ are the the energy density, heat flux and a source term respectively at point $\mathbf{x}$ at time t. Noting that $\mathcal{P}$ was chosen arbitrarily, the equation for the change in internal energy of the material is given by

$$\dot{e} = -\nabla \cdot \mathbf{q} + r. \tag{5.2.2}$$

Here, $\dot{e}$ represents the material derivative of e, which in this case is equivalent to the time derivative as the body is fixed. Similarly for the second law of thermodynamics, we move the time derivative inside the integral, use the divergence theorem on the boundary term and use the arbitrary choice of $\mathcal{P}$ to obtain the inequality

$$\dot{\eta} \geqslant -\nabla \cdot \left(\frac{\mathbf{q}}{\theta} + \mathbf{k}\right) + \frac{r}{\theta}, \tag{5.2.3}$$

where $\eta(\mathbf{x}, t)$ is the entropy density, $\mathbf{k}(\mathbf{x}, t)$ is a term related to the entropy on the boundary and $\theta(\mathbf{x}, t)$ is the temperature at point $\mathbf{x}$ at time t. We define the phase change equation to be

$$\dot{\phi} = \gamma, \tag{5.2.4}$$

where γ has a form yet to be decided. We now construct the Helmholtz free energy at point $\mathbf{x}$ at time t, $\Psi(\mathbf{x}, t)$, to connect the energy and entropy densities. We define

$$\Psi = e - \theta\eta. \tag{5.2.5}$$

Taking the time derivative of both sides results in

$$\dot{\Psi} = \dot{e} - \theta\dot{\eta} - \eta\dot{\theta}. \tag{5.2.6}$$

Rearranging this to leave it in terms of $\dot{\eta}$ gives

$$\dot{\eta} = \frac{1}{\theta}\left(\dot{e} - \eta\dot{\theta} - \dot{\Psi}\right). \tag{5.2.7}$$

We now combine (5.2.7) with (5.2.3) to obtain the following inequality

$$\frac{1}{\theta}\left(\dot{e} - \eta\dot{\theta} - \dot{\Psi}\right) \geqslant -\nabla \cdot \left(\frac{\mathbf{q}}{\theta} + \mathbf{k}\right) + \frac{r}{\theta}, \tag{5.2.8}$$

and substituting in (5.2.2) results in

$$\frac{1}{\theta}\left(-\nabla \cdot \mathbf{q} + r - \eta\dot{\theta} - \dot{\Psi}\right) \geqslant -\nabla \cdot \left(\frac{\mathbf{q}}{\theta} + \mathbf{k}\right) + \frac{r}{\theta}. \tag{5.2.9}$$

Finally, expanding the divergence term using the divergence term on the right hand side, we obtain

$$-\frac{1}{\theta}\nabla \cdot \mathbf{q} + \frac{1}{\theta^2}\mathbf{q} \cdot \nabla\theta - \nabla \cdot \mathbf{k} + \frac{r}{\theta} - \frac{1}{\theta}\left(-\nabla \cdot \mathbf{q} + r - \eta\dot{\theta} - \dot{\Psi}\right) \leqslant 0, \tag{5.2.10}$$

which, when multiplying through by θ, reduces to

$$\dot{\Psi} + \eta\dot{\theta} - \theta\nabla \cdot \mathbf{k} + \frac{1}{\theta}\mathbf{q} \cdot \nabla\theta \leqslant 0. \tag{5.2.11}$$

Any choices that are made for any of the dependant variables must satisfy this constraint for any realistic scenario for a model to maintain thermo-dynamic consistency.

5.2.2 Choices of Constituent Classes

We now look to define a constituent class for $\Psi, \eta, \mathbf{k}, \mathbf{q}$ and γ. The constituent choices for these variables are $\{\theta, \phi, \nabla\theta, \nabla\phi, \Delta\theta, \Delta\phi\}$. We then define

$$\Gamma = \{\theta, \phi, \nabla\theta, \nabla\phi, \Delta\theta, \Delta\phi\}, \tag{5.2.12}$$

and choose the constituent class

$$\Psi = \bar{\Psi}(\Gamma). \tag{5.2.13}$$

We follow the work of [43] for solidification in a non-isothermal case, and define μ to be the variational derivative of $\bar{\Psi}/\theta$ with respect to ϕ, given by

$$\mu = \frac{\delta}{\delta\phi}\left(\frac{\bar{\Psi}}{\theta}\right) = \frac{\partial_\phi \hat{\Psi}}{\theta} - \nabla \cdot \left(\frac{\partial_{\nabla\phi}\bar{\Psi}}{\theta}\right). \tag{5.2.14}$$

We then pose the constitutive classes for the remaining variables:

$$\eta = \bar{\eta}(\Gamma, \mu, \nabla\mu), \tag{5.2.15}$$

$$\mathbf{k} = \bar{\mathbf{k}}(\Gamma, \mu, \nabla\mu), \tag{5.2.16}$$

$$\mathbf{q} = \bar{\mathbf{q}}(\Gamma, \mu, \nabla\mu), \tag{5.2.17}$$

and

$$\gamma = \bar{\gamma}(\Gamma, \mu, \nabla\mu). \tag{5.2.18}$$

These dependencies are new in the context of solidification, however it has recently been proposed to be natural for Phase-field models [54].

Theorem 1. *Given* (5.2.11)*, the constitutive class of* Ψ *can be reduced to* $\Psi = \bar{\Psi}(\theta, \phi, \nabla\phi)$*. In addition,* $\bar{\eta}(\Gamma, \mu, \nabla\mu) = -\partial_\theta \bar{\Psi}$*. With these enforced choices, the constraint to be satisfied becomes*

$$\partial_\phi \bar{\Psi}\dot{\phi} + \partial_{\nabla\phi}\bar{\Psi}(\dot{\nabla\phi}) - \theta\nabla \cdot \mathbf{k} + \frac{1}{\theta}\mathbf{q} \cdot \nabla\theta \leqslant 0. \tag{5.2.19}$$

Proof. Taking the time derivative of $\hat{\Psi}$ results in

$$\dot{\bar{\Psi}} = \partial_\theta \bar{\Psi}\dot{\theta} + \partial_\phi \bar{\Psi}\dot{\phi} + \partial_{\nabla\theta}\bar{\Psi}(\dot{\nabla\theta}) + \partial_{\nabla\phi}\bar{\Psi}(\dot{\nabla\phi}) + \partial_{\Delta\theta}\bar{\Psi}(\dot{\Delta\theta}) + \partial_{\Delta\phi}\bar{\Psi}(\dot{\Delta\phi}). \tag{5.2.20}$$

Substituting this back into (5.2.11) and recalling that $\dot{\phi} = \gamma$ results in

$$\begin{aligned}&(\partial_\theta \bar{\Psi} + \eta)\dot{\theta} + \partial_\phi \bar{\Psi}\bar{\gamma} + \partial_{\nabla\theta}\bar{\Psi}(\dot{\nabla\theta}) + \partial_{\nabla\phi}\bar{\Psi}(\dot{\nabla\phi}) + \partial_{\Delta\theta}\bar{\Psi}(\dot{\Delta\theta}) +\\ &\partial_{\Delta\phi}\bar{\Psi}(\dot{\Delta\phi}) - \theta\nabla\cdot\mathbf{k} + \frac{1}{\theta}\mathbf{q}\cdot\nabla\theta \leqslant 0.\end{aligned} \tag{5.2.21}$$

We now proceed with the Coleman-Noll procedure. Given the constitutive choices made, and using the fact that this inequality must hold in all scenarios, we fix all variables with the exception of $(\dot{\Delta\phi})$. There are no restrictions on the size of the value of $(\dot{\Delta\phi})$, the restriction can only hold if the coefficient of $(\dot{\Delta\phi})$ is zero. The same method can be applied to $\dot{\theta}$, $(\dot{\nabla\theta})$, $(\dot{\nabla\phi})$ and $(\dot{\Delta\theta})$ to result in $(\partial_\theta\bar{\Psi} + \bar{\eta}) = 0$, $\partial_{\nabla\theta}\bar{\Psi} = 0$, $\partial_{\nabla\phi}\bar{\Psi} = 0$, $\partial_{\Delta\theta}\bar{\Psi} = 0$ and $\partial_\Delta\Phi\Psi = 0$. Thus we conclude that

$$\Psi = \bar{\Psi}(\theta, \phi, \nabla\phi) \tag{5.2.22}$$

and

$$\bar{\eta} = -\partial_\theta\Psi. \tag{5.2.23}$$

Having found this reduced choice of constituent class for Ψ, we can substitute (5.2.22) and 5.2.23 into (5.2.11) to result in

$$\partial_\phi\bar{\Psi}\dot{\phi} + \partial_{\nabla\phi}\bar{\Psi}(\dot{\nabla\phi}) - \theta\nabla\cdot\mathbf{k} + \frac{1}{\theta}\mathbf{q}\cdot\nabla\theta \leqslant 0 \tag{5.2.24}$$

as required. ∎

It can be noted that this definition for the entropy density found in (5.2.23) is commonly found in literature, for example in [54]. (5.2.24) can be made into

$$\gamma\mu + \gamma\nabla\cdot\left(\frac{\partial_{\nabla\phi}\bar{\Psi}}{\theta}\right) + \frac{1}{\theta}\partial_{\nabla\phi}\bar{\Psi}(\dot{\nabla\phi}) - \nabla\cdot\mathbf{k} + \frac{1}{\theta^2}\mathbf{q}\cdot\nabla\theta \leqslant 0 \tag{5.2.25}$$

by dividing through by θ and using (5.2.4) and (5.2.14). Noting that

$(\dot{\nabla\phi}) = \nabla\dot{\phi} = \nabla\gamma$ the final constraint can be rearranged as

$$\gamma\mu + \nabla \cdot \left(\frac{\partial_{\nabla\phi}\bar{\Psi}}{\theta}\gamma - \mathbf{k} \right) + \frac{1}{\theta^2}\mathbf{q} \cdot \nabla\theta \leqslant 0. \tag{5.2.26}$$

One method to ensure that (5.2.26) is met is to ensure that each individual term adheres to the inequality withing the bounds of the chosen constituent classes. Thus, a clear choice for $\bar{\gamma}$ is

$$\bar{\gamma} = -k_1(\Gamma)\mu, \tag{5.2.27}$$

for some $k_1(\Gamma) \geqslant 0$. We also make the choice of

$$\bar{\mathbf{q}} = -k_2(\Gamma)\nabla\theta, \tag{5.2.28}$$

for some $k_2(\Gamma) \geqslant 0$. It should be noted that in some literature, such as [29], $\bar{\mathbf{q}}$ is chosen as $k_2'(\Gamma)\nabla(1/\theta)$. Performing the chain rule on this gradient term results in $\bar{\mathbf{q}} = -\left(k_2'(\Gamma)/\theta^2\right)\nabla\theta$, so this choice is equivalent to (5.2.28) with $k_2(\Gamma) = k_2'(\Gamma)/\theta^2$. The final choice we make is to pick

$$\bar{\mathbf{k}} = -k_1(\Gamma)\mu\frac{\partial_{\nabla\varphi}\hat{\Psi}}{\theta}. \tag{5.2.29}$$

With these definitions, (5.2.26) becomes

$$-k_1(\Gamma)\mu^2 - \frac{k_2(\Gamma)}{\theta^2}|\nabla\theta|^2 \leqslant 0, \tag{5.2.30}$$

and so will hold for all energy functionals $\bar{\Psi}$ within the constituent class (5.2.22), which is still to be defined.

5.2.3 The Free Energy Functional

Recalling (5.2.5) and (5.2.23), we can write

$$\bar{e} = \bar{\Psi} - \theta \partial_\theta \bar{\Psi} = -\theta^2 \frac{\partial}{\partial \theta} \left(\frac{\bar{\Psi}}{\theta} \right), \tag{5.2.31}$$

and so we can define the free energy by choosing a suitable form for the internal energy density. We use for the internal energy function the same form as used in the literature:

$$e = u(\theta) v(\phi) + w(\phi). \tag{5.2.32}$$

For temperatures greater than around 100K it is well established that the internal energy has a linear dependence on the temperature [100] and so we set $u(\theta) = c\theta$ for some constant c and $v(\phi) = 1$. Initially we postulate a linear dependence on the phase by setting $w(\phi) = \lambda\phi$ for a constant λ, however towards the end of this chapter we suggest an alteration to make this dependence non linear. With these modelling decisions, we write

$$\bar{e} = c\theta + \lambda\phi. \tag{5.2.33}$$

Using (5.2.31), rearranging and integrating with respect to θ we obtain the expression for $\bar{\Psi}$:

$$\bar{\Psi} = -c\theta \ln \left(\frac{\theta}{\theta_0} \right) + \left(1 - \frac{\theta}{\theta_0} \right) \lambda\phi + \frac{\theta}{\theta_0} W(\phi) + \frac{\sigma^2}{2\theta_0} \theta |\nabla\phi|^2, \tag{5.2.34}$$

where θ_0 is the melting point of the material. In commonly used phase field models, $W(\phi)$ is given as a double well function with minima at 0 and 1. The term containing σ is a common inclusion in free energies for solidification models and represents the free energy on the diffuse boundary between the two phases [29]. Finally, the term containing λ can be thought of as the latent heat of phase change, that is the energy that is either gained or lost during the change of phase without having an effect on the temperature. The coefficient of the latent heat of $(1 - \theta/\theta_0)$ ensures that if the temperature of the substance is below its melting point ($\theta/\theta_0 < 1$) then the film is transitioning from the liquid phase into a solid phase, and so energy is given out, as the latent heat contribution is positive. On the other hand, a solid film absorbs heat when it melts, and so when $\theta/\theta_0 > 1$ the contribution of latent heat to the free energy is negative.

Returning to equations (5.2.2) and (5.2.4) we can now derive the final system of equations for describing the solidification of a bulk material. Differentiating (5.2.33) with respect to time and combining this with (5.2.2) results in

$$c\dot{\theta} + \lambda\dot{\phi} = k_2\Delta\theta + r. \tag{5.2.35}$$

It can be noted that for a material not undergoing a phase change, that is when $\dot{\phi} = 0$, this equation reduces to the standard heat equation. We employ the non-dimensionalisation $\bar{\theta} = \theta/\theta_0$. Then the variational derivative for our choice of $\bar{\Psi}$ is given by

$$\mu = \frac{\lambda}{\theta_0}\frac{(1-\bar{\theta})}{\bar{\theta}} + \frac{1}{\theta_0}W'(\phi) - \frac{1}{\theta_0}\sigma^2\Delta\phi. \tag{5.2.36}$$

Thus, the final system of equations is given by

$$\bar{c}\dot{\bar{\theta}} = -\lambda\dot{\phi} + \bar{k_2}\Delta\bar{\theta} + r, \tag{5.2.37}$$

$$\dot{\phi} = -\bar{k_1}\left[\frac{(1-\bar{\theta})}{\bar{\theta}}\lambda + W'(\phi) - \sigma^2\Delta\phi\right], \tag{5.2.38}$$

where $\bar{c} = c\theta_0$, $\bar{k_1} = k_1/\theta_0$ and $\bar{k_2} = k_2\theta_0$. This is equivalent to the model derived by Langer [96].

A potential improvement to this model is to allow the internal energy density to depend on the phase in a non-linear way, by setting $w(\phi)$ to be non constant. We write

$$\bar{e} = c\theta + w(\phi). \tag{5.2.39}$$

This choice results in a free energy density functional of

$$\bar{\Psi} = -c\theta \ln\left(\frac{\theta}{\theta_0}\right) + \left(1 - \frac{\theta}{\theta_0}\right) w(\phi) + \frac{\theta}{\theta_0} W(\phi) + \frac{\sigma^2}{2\theta_0}\theta|\nabla\phi|^2, \tag{5.2.40}$$

which, following the same non-dimensionalisation of $\bar{\theta} = \theta/\theta_0$ leads to the final system of equations

$$\bar{c}\dot{\bar{\theta}} = -w'(\phi)\dot{\phi} + \bar{k_2}\Delta\bar{\theta} + r, \tag{5.2.41}$$

$$\dot{\phi} = -\bar{k_1}\left[\frac{(1-\bar{\theta})}{\bar{\theta}} w'(\phi) + W'(\phi) - \sigma\Delta\phi\right]. \tag{5.2.42}$$

Choosing $w'(\phi)$ to be a quadratic function by setting

$$w'(\phi) = -a\phi^2 + b\phi + c, \tag{5.2.43}$$

and describing the potential $W(\phi)$ as a double well function, for example

$$W(\phi) = \phi^2(\phi - 1)^2, \tag{5.2.44}$$

results in the model derived by Penrose and Fife [47].

5.3 Conclusions

In this chapter, a family of thermodynamically consistent models to describe the solidification of a pure material from its melt has been derived from the key axioms from rational continuum mechanics. We have shown that by making certain choices, existing models that are commonly used in the literature fit within this framework. However, as we have left the choosing of the energy function until last, the model derived in this section can be easily adapted to describe a range of scenarios.

Langer suggests that in order to capture the growth of dendrites often seen during crystallisation, one can add higher derivatives into the free energy. However, one must be cautious that, if the constitutive class of the free energy Ψ is changed, the model remains thermodynamically consistent.

In the coming chapters, we employ the theories described here for bulk solidification in conjunction with the methods used to describe thin film flow to derive a system of equations for prediction the evolution of a solidifying thin film.

CHAPTER 6

Thin Film Heat Equation

In this chapter we derive a new class of models for the diffusion of heat in a rigid thin film in d-dimensions. We introduce the concept of vertically averaging key variables to reduce the problem from a d-dimensional to a $(d-1)$-dimensional problem. In doing so, a closure problem arises when accounting for fluctuations in the vertical direction. Lastly, we make constitutive choices to result in a final model.

6.1 Geometry

As in Chapter 4, we consider a d-dimensional thin film on a flat solid substrate $\mathcal{D} \subset \mathbb{R}^{d-1}$. We consider a fixed arbitrary region $\Omega \subset \mathcal{D}$, and define the height of the film above the substrate at point $\mathbf{x} \in \Omega$ to be $h(\mathbf{x}, t)$. For the purpose of this chapter, we assume the height function to be non time dependent, and so write $h(\mathbf{x}, t) = h_0(\mathbf{x})\ \forall\ t$. Then we define the region

$$\mathcal{P} := \bigcup_{\mathbf{x}\in\Omega} \{(\mathbf{x}, z) | z \in [0, h_0(\mathbf{x})]\} \tag{6.1.1}$$

for $\mathbf{x} \in \mathbb{R}^{d-1}$ and $z \in \mathbb{R}$ to be a fixed arbitrary region of the film bound by Ω, the top surface of the film and vertical sides. Denote by $\partial\mathcal{P}$ the boundary of $\mathcal{P}$, and note that this can be written as the union of three surfaces: the bottom

$$B := \Omega \times \{0\}, \tag{6.1.2}$$

the vertical sides

$$S := \bigcup_{\mathbf{x} \in \partial\Omega} \{\mathbf{x}\} \times [0, h_0(\mathbf{x})], \tag{6.1.3}$$

where $\partial\Omega$ is the boundary of Ω, and the top surface of the film

$$T := \bigcup_{\mathbf{x} \in \Omega} \{\mathbf{x}\} \times \{h_0(\mathbf{x})\}. \tag{6.1.4}$$

A depiction of this geometry for the case $d = 2$ is shown in Figure 6.1.

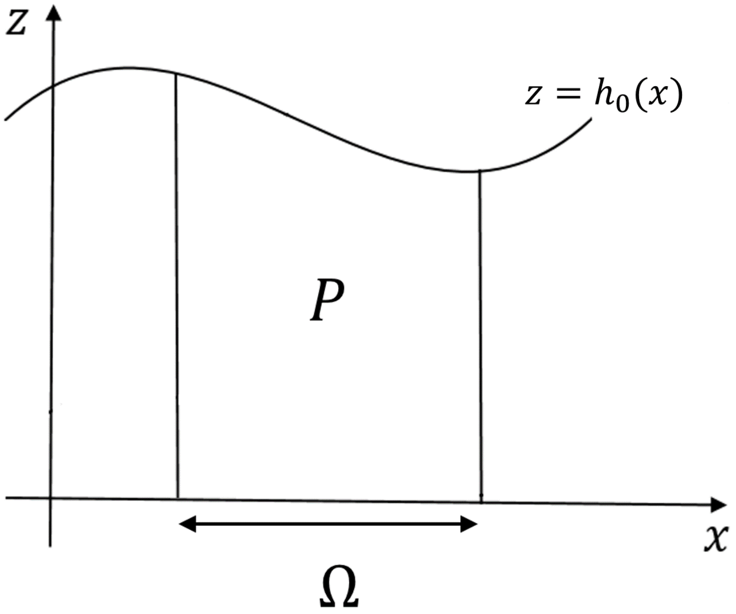

Figure 6.1: The geometry of a thin film on a solid substrate for the case of $d = 2$. $\mathcal{P}$ is an arbitrary fixed subset of the film with Ω as its base, $h_0(x)$ as the top surface and vertical sides.

We begin this section with a key result that will play a vital role in the remaining chapters of this work. Given some surface Σ_M which can be projected onto another surface Σ using the transformation M, for some quantity ζ on Σ_M

$$\int_{\Sigma_M} \zeta \, d\Sigma_M = \int_{\Sigma} (\zeta \circ M) \, F \, d\Sigma, \tag{6.1.5}$$

where

$$F := J_M | \left(\nabla M\right)^{-T} \mathbf{n}|, \tag{6.1.6}$$

with $\nabla \mathbf{M}^{-T}$ representing the inverse of the transpose of the matrix ∇M, and

$$J_M := \det \nabla M. \tag{6.1.7}$$

Here, $\mathbf{n}$ is the outward pointing unit normal to Σ. Proof for this result can be found in [101]. The result given in equations (6.1.5)-(6.1.7) can be applied to the top boundary T. Choose Σ to be Ω and Σ_M to be T, and define the map M such that

$$M : \begin{pmatrix} \mathbf{x} \\ z \end{pmatrix} \to \begin{pmatrix} \mathbf{x} \\ z + h_0(\mathbf{x}) \end{pmatrix}. \tag{6.1.8}$$

Then, by defining the operator $\nabla_{\mathbf{x}} = (\partial/\partial x_1, \partial/\partial x_2, \ldots, \partial/\partial x_{d-1})$ we see that

$$\nabla M = \begin{pmatrix} \mathbf{I} & \mathbf{0} \\ (\nabla_{\mathbf{x}} h_0)^T & 1 \end{pmatrix}, \tag{6.1.9}$$

where $\mathbf{I}$ is the $d-1$ dimensional identity matrix and $\mathbf{0}$ is the $(d-1) \times 1$ vector with every entry 0. From this we obtain

$$J_M = 1. \tag{6.1.10}$$

For the choice of $\Sigma = \Omega$, the outward pointing unit normal $\mathbf{n}$ is given by

$$\mathbf{n} = \begin{pmatrix} \mathbf{0} \\ -1 \end{pmatrix}. \tag{6.1.11}$$

Then F can be calculated as

$$F = \sqrt{|\nabla_{\mathbf{x}} h_0|^2 + 1}. \tag{6.1.12}$$

In this scenario, F is the arclength of $h_0(x)$. From this result it can be seen that for any quantity Q on the top boundary T, it stands that

$$\int_T Q\,dT = \int_\Omega Q\sqrt{|\nabla_{\mathbf{x}} h_0|^2 + 1}\,d\Omega = \int_\Omega QF\,d\Omega. \tag{6.1.13}$$

6.2 Vertical Averaging

A key operator in this chapter is taking the vertical average. For a quantity $\hat{Q}(\mathbf{x}, z)$ defined for all $z \in [0, h_0]$, the vertically averaged quantity $Q(\mathbf{x})$ is taken to be

$$Q(\mathbf{x}) = \frac{1}{h_0(\mathbf{x})}\int_0^{h_0(\mathbf{x})} \hat{Q}(\mathbf{x}, z)\,dz. \tag{6.2.1}$$

We now apply this vertical averaging operator to the laws of thermodynamics described in Chapter 2.

6.2.1 Conservation of Energy

First, we consider the first law of thermodynamics, given in (2.2.31). Let $\hat{e}(\mathbf{x}, z, t)$, $\hat{\mathbf{q}}(\mathbf{x}, z, t)$ and $\hat{r}(\mathbf{x}, z, t)$ be the energy density, heat flux and heat source at point $(\mathbf{x}, z)$ at time t respectively. Then

$$\frac{d}{dt}\int_{\mathcal{P}} \hat{e}\,dV = -\int_{\partial\mathcal{P}} \hat{\mathbf{q}}\cdot\mathbf{n}\,ds + \int_{\mathcal{P}} \hat{r}\,dV. \tag{6.2.2}$$

where $\mathbf{n}$ is the outward pointing normal to $\partial\mathcal{P}$. Splitting the integral over $\partial\mathcal{P}$ into integrals over the three separate boundaries T, B and S we can write

$$\int_{\partial\mathcal{P}} \hat{\mathbf{q}}\cdot\mathbf{n}\,ds = \int_T \hat{\mathbf{q}}\cdot\mathbf{n}_T\,ds + \int_B \hat{\mathbf{q}}\cdot\mathbf{n}_B\,ds + \int_S \hat{\mathbf{q}}\cdot\mathbf{n}_S\,ds, \tag{6.2.3}$$

where $\mathbf{n}_i$ represents the unit normal to surface i. Defining

$$\mathbf{e}_d = \begin{pmatrix} \mathbf{0} \\ 1 \end{pmatrix} \tag{6.2.4}$$

as the unit normal perpendicular to Ω, we obtain

$$\begin{aligned} \int_\Omega \frac{d}{dt} \int_0^{h_0} \hat{e}\, dz\, dA = &- \int_{\partial\Omega} \left(\int_0^{h_0} \hat{\mathbf{q}}\, dz \right) \cdot \mathbf{n}_\Omega\, ds \\ &- \int_\Omega \hat{\mathbf{q}}(\mathbf{x}, h(\mathbf{x}, t), t) \cdot \mathbf{e}_d F\, dA \\ &- \int_\Omega \hat{\mathbf{q}}(\mathbf{x}, 0, t) \cdot (-\mathbf{e}_d)\, dA + \int_\Omega \int_0^{h_0} \hat{r}\, dz\, dA, \end{aligned} \tag{6.2.5}$$

where $\mathbf{n}_\Omega$ is the outward pointing unit normal to $\partial\Omega$. Applying the vertical average operator to the internal energy density, energy flux and energy source, we obtain

$$e = \frac{1}{h_0} \int_0^{h_0} \hat{e}\, dz, \tag{6.2.6}$$

$$\mathbf{q} = \frac{1}{h_0} \int_0^{h_0} \hat{\mathbf{q}}\, dz, \tag{6.2.7}$$

$$r = \frac{1}{h_0} \int_0^{h_0} \hat{r}\, dz \tag{6.2.8}$$

respectively, and further defining

$$q_T = \hat{\mathbf{q}}(\mathbf{x}, h_0, t) \cdot \mathbf{e}_d, \tag{6.2.9}$$

$$q_B = \hat{\mathbf{q}}(\mathbf{x}, 0, t) \cdot \mathbf{e}_d, \tag{6.2.10}$$

and noting that Ω was chosen arbitrarily, the final conservation of energy equation is obtained:

$$\frac{d}{dt}(h_0 e) = -\nabla_{\mathbf{x}} \cdot (h_0 \mathbf{q}) - q_T F + q_B + h_0 r. \tag{6.2.11}$$

6.2.2 Entropy Inequality

Next, we consider the second law of thermodynamics. Let $\hat{\Phi}(\mathbf{x}, z, t)$ be the entropy flux of the film and $\hat{H}(\mathbf{x}, z, t)$ be an entropy source. Then by (2.2.38)

$$\frac{d}{dt}\int_{\mathcal{P}} \hat{\eta}\, dV \geqslant -\int_{\partial\mathcal{P}} \hat{\Phi}\cdot\mathbf{n}\, ds + \int_{\mathcal{P}} \hat{H}\, dV, \tag{6.2.12}$$

where $\hat{\eta} = \hat{\eta}(\mathbf{x}, z, t)$ represents the entropy density at position $(\mathbf{x}, z)$ at time t. As with the bulk equations, we define

$$\hat{\Phi} = \frac{\hat{\mathbf{q}}}{\hat{\theta}} + \hat{\mathbf{k}}, \tag{6.2.13}$$

and

$$\hat{H} = \frac{\hat{r}}{\hat{\theta}}, \tag{6.2.14}$$

where $\hat{\theta}(\mathbf{x}, z, t)$ is the temperature at position $(\mathbf{x}, z)$ at time t, and $\hat{\mathbf{k}}$ represents an entropy flux related to the diffuse boundaries between the different phases of solidification in the film. In this case, where there is only one phase, $\hat{\mathbf{k}} \equiv 0$. Again splitting the boundary integral and applying (6.1.13) results in

$$\begin{aligned}\int_{\Omega}\frac{d}{dt}\int_0^{h_0}\hat{\eta}\, dz\, dA \geqslant{}& -\int_{\partial\Omega}\left(\int_0^{h_0}\frac{\hat{\mathbf{q}}}{\hat{\theta}}\, dz\right)\cdot\mathbf{n}_{\Omega}\, ds \\ -\int_{\Omega}\frac{\hat{\mathbf{q}}(\mathbf{x}, h_0, t)}{\hat{\theta}(\mathbf{x}, h_0, t), t)}\cdot\mathbf{e}_d F\, dA &- \int_{\Omega}\frac{\hat{\mathbf{q}}(\mathbf{x}, 0, t)}{\hat{\theta}(\mathbf{x}, 0, t)}\cdot(-\mathbf{e}_d)\, dA \\ &+ \int_{\Omega}\int_0^{h_0}\frac{\hat{r}}{\hat{\theta}}\, dz\, dA.\end{aligned} \tag{6.2.15}$$

Taking the vertical average of the entropy density gives

$$\eta = \frac{1}{h_0}\int_0^{h_0}\hat{\eta}\, dz, \tag{6.2.16}$$

and defining the temperature at the top and bottom boundaries to be

$$\theta_T = \hat{\theta}(\mathbf{x}, h_0, t) \tag{6.2.17}$$

and

$$\theta_B = \hat{\theta}(\mathbf{x}, 0, t), \tag{6.2.18}$$

respectively, the final entropy inequality becomes

$$\frac{d}{dt}(h\eta) \geqslant -\nabla_{\mathbf{x}} \cdot \left(\int_0^{h_0} \frac{\hat{\mathbf{q}}}{\hat{\theta}}\, dz \right) - \frac{q_T F}{\theta_T} + \frac{q_B}{\theta_B} + \int_0^{h_0} \frac{\hat{r}}{\hat{\theta}}\, dz. \tag{6.2.19}$$

With the key laws vertically averaged, we now define a free energy Ψ and choose the dependent variables to ensure that the model is thermodynamically consistent.

6.2.3 Applying Laws of Thermodynamics

We now look to combine the first and second laws of thermodynamics Define a free energy functional $\Psi(\mathbf{x}, t)$ such that

$$h_0\Psi = h_0 e - \theta h_0 \eta, \tag{6.2.20}$$

where $\theta(\mathbf{x}, t)$ is defined such that

$$\frac{1}{\theta} = \frac{1}{h_0} \int_0^{h_0} \frac{1}{\hat{\theta}}\, dz. \tag{6.2.21}$$

Taking the time derivative of this equation and rearranging results in

$$(\dot{h_0\eta}) = \frac{1}{\theta}\left[(\dot{h_0 e}) - h_0\eta\dot{\theta} - (\dot{h_0\Psi}) \right]. \tag{6.2.22}$$

As $h_0(\mathbf{x})$ is not time dependent, $(\dot{h_0\Psi}) = h_0\dot{\Psi}$, and so combining (6.2.22) with (6.2.11) and (6.2.19) we obtain

$$\begin{aligned} &\frac{1}{\theta}\left[-\nabla_{\mathbf{x}} \cdot (h_0\mathbf{q}) - q_T F + q_B + h_0 r - h_0\eta\dot{\theta} - h_0\dot{\Psi} \right] \\ &\quad \geqslant -\nabla_{\mathbf{x}} \cdot \left(\int_0^{h_0} \frac{\hat{\mathbf{q}}}{\hat{\theta}}\, dz \right) - \frac{q_T F}{\theta_T} + \frac{q_B}{\theta_B} + \int_0^{h_0} \frac{\hat{r}}{\hat{\theta}}\, dz. \end{aligned} \tag{6.2.23}$$

This constraint must hold in all physical scenarios for all energy functionals Ψ. In the next section we pick a constituent classes for the variables that relate specifically to the transfer of heat within a rigid thin film.

6.3 Free Energy Functional

We look to postulate a constitutive class for the free energy Ψ, and we choose the dependent variables suitable within this class. The constituent properties for a material in this scenario are $\theta, \nabla\theta$ and $\Delta\theta$. Therefore we define $\Gamma = \{\theta, \nabla\theta, \Delta\theta\}$ and postulate the constitutive classes of Ψ and η to be

$$\Psi = \Psi(\Gamma), \tag{6.3.1}$$

and

$$\eta = \eta(\Gamma). \tag{6.3.2}$$

Theorem 2. *Given* (6.2.23)*, the constituent class of* Ψ *reduces to* $\Psi = \Psi(\theta)$*. In addition,* $\eta = -\partial_\theta \Psi$*. With these enforced choices, the constraint to be satisfied becomes*

$$\frac{1}{\theta^2} h_0 \mathbf{q} \cdot \nabla_{\mathbf{x}} \theta + \nabla_{\mathbf{x}} \cdot \left(\frac{1}{\theta} h_0 \mathbf{q} \right) - \nabla_{\mathbf{x}} \cdot \left(\int_0^{h_0} \frac{\hat{\mathbf{q}}}{\hat{\theta}} \, dz \right) + \frac{q_T F}{\theta} - \frac{q_T F}{\theta_T} - \frac{q_B}{\theta} + \frac{q_B}{\theta_B} \\ - \frac{h_0 r}{\theta} + \int_0^{h_0} \frac{\hat{r}}{\hat{\theta}} \, dz \leqslant 0. \tag{6.3.3}$$

Proof. By the chain rule, the time differential of $\Psi(\theta, \nabla\theta, \Delta\theta)$ is given by

$$\dot{\Psi} = \partial_\theta \Psi \dot{\theta} + \partial_{\nabla\theta} \Psi (\dot{\nabla\theta}) + \partial_{\Delta\theta} \Psi (\dot{\Delta\theta}). \tag{6.3.4}$$

Substituting this into (6.2.23) results in

$$\begin{aligned}\frac{1}{\theta}\big[-\nabla_{\mathbf{x}}\cdot(h_0\mathbf{q}) - q_T F + q_B + h_0 r - h_0\eta\dot{\theta} - h_0\partial_\theta\Psi\dot{\theta}\\ -h_0\partial_{\nabla\theta}\Psi(\dot{\nabla\theta}) - h_0\partial_{\Delta\theta}\Psi(\dot{\Delta\theta}) \geqslant -\nabla_{\mathbf{x}}\cdot\left(\int_0^{h_0}\frac{\hat{\mathbf{q}}}{\hat{\theta}}\,dz\right)\\ -\frac{q_T F}{\theta_T} + \frac{q_B}{\theta_B} + \int_0^{h_0}\frac{\hat{r}}{\hat{\theta}}\,dz.\end{aligned} \tag{6.3.5}$$

which can be rearranged to give

$$\begin{aligned}\frac{1}{\theta^2}h_0\mathbf{q}\cdot\nabla_{\mathbf{x}}\theta + \nabla_{\mathbf{x}}\cdot\left(\frac{1}{\theta}h_0\mathbf{q}\right) - \nabla_{\mathbf{x}}\cdot\left(\int_0^{h_0}\frac{\hat{\mathbf{q}}}{\hat{\theta}}\,dz\right) + \frac{q_T F}{\theta} - \frac{q_T F}{\theta_T} - \frac{q_B}{\theta} + \frac{q_B}{\theta_B}\\ -\frac{h_0 r}{\theta} + \int_0^{h_0}\frac{\hat{r}}{\hat{\theta}}\,dz + \frac{1}{\theta}h_0(\partial_\theta\Psi + \eta)\dot{\theta} + \frac{1}{\theta}h_0\partial_{\nabla\theta}\Psi(\dot{\nabla\theta}) + \frac{1}{\theta}h_0\partial_{\Delta\theta}\Psi(\dot{\Delta\theta}) \leqslant 0.\end{aligned} \tag{6.3.6}$$

We now apply the Coleman-Noll argument to (6.3.6). The constraint must hold in all situations. By fixing $\theta, \nabla\theta, \Delta\theta, (\dot{\nabla\theta})$ and $(\dot{\Delta\theta})$, it is always possible to pick a $\dot{\theta}$ to break the constraint. Therefore, the coefficient of $\dot{\theta}$ must be 0. Similar arguments can be applied to $(\dot{\nabla\theta})$ and $(\dot{\Delta\theta})$, resulting in the conclusion that $\partial_\theta\Psi + \eta = 0$, $\partial_{\nabla\theta}\Psi = 0$ and $\partial_{\Delta\theta}\Psi = 0$. Therefore for a model to be thermodynamically consistent,

$$\Psi = \Psi(\theta) \tag{6.3.7}$$

and

$$\eta = -\partial_\theta\Psi. \tag{6.3.8}$$

With these choices, (6.3.6) becomes

$$\begin{aligned}\frac{1}{\theta^2}h_0\mathbf{q}\cdot\nabla_{\mathbf{x}}\theta + \nabla_{\mathbf{x}}\cdot\left(\frac{1}{\theta}h_0\mathbf{q}\right) - \nabla_{\mathbf{x}}\cdot\left(\int_0^{h_0}\frac{\hat{\mathbf{q}}}{\hat{\theta}}\,dz\right) + \frac{q_T F}{\theta} - \frac{q_T F}{\theta_T} - \frac{q_B}{\theta} + \frac{q_B}{\theta_B}\\ -\frac{h_0 r}{\theta} + \int_0^{h_0}\frac{\hat{r}}{\hat{\theta}}\,dz \leqslant 0\end{aligned} \tag{6.3.9}$$

as required. ■

It is noted that the result for the entropy η is consistent with the choice of entropy made for solidification in a bulk system in Chapter 5 as well as in many cases in the literature.

6.3.1 Defining the Dependent Variables

We now choose the remaining variables such that the constraint (6.3.9) holds. Whereas it was a necessity within the chosen constituent class for (6.3.8) to hold, there may be multiple viable options for the variables defined in this section. We therefore try to select the option within the framework derived that best describes the physical situation.

Source Terms

We firstly turn our attention to the energy source $\hat{r}$, we argue that this is known, and that it is equal to the vertically averaged energy source, $\hat{r} = r$. Then we have

$$\int_0^{h_0} \frac{\hat{r}}{\hat{\theta}}\, dz - \frac{h_0 r}{\theta} = \int_0^{h_0} \frac{r}{\hat{\theta}}\, dz - r \int_0^{h_0} \frac{1}{\hat{\theta}}\, dz. \tag{6.3.10}$$

However, r is not dependent on z and can be taken out of the integral, resulting in

$$\int_0^{h_0} \frac{\hat{r}}{\hat{\theta}}\, dz - \frac{h_0 r}{\theta} = 0. \tag{6.3.11}$$

Heat Flux Terms

Now it remains to ensure that

$$\begin{aligned} \frac{1}{\theta^2} h_0 \mathbf{q} \cdot \nabla_{\mathbf{x}} \theta + \nabla_{\mathbf{x}} \cdot \left(\frac{1}{\theta} h_0 \mathbf{q} \right) - \nabla_{\mathbf{x}} \cdot \left(\int_0^{h_0} \frac{\hat{\mathbf{q}}}{\hat{\theta}}\, dz \right) \\ + q_T F \left(\frac{1}{\theta} - \frac{1}{\theta_T} \right) - q_B \left(\frac{1}{\theta} - \frac{1}{\theta_B} \right) \leqslant 0. \end{aligned} \tag{6.3.12}$$

First, consider the terms within the divergence:

$$\frac{1}{\theta}h_0\mathbf{q} - \int_0^{h_0} \frac{\hat{\mathbf{q}}}{\hat{\theta}}\,dz = -h_0\left(\frac{1}{h_0}\int_0^{h_0} \frac{\hat{\mathbf{q}}}{\hat{\theta}}\,dz - \frac{1}{\theta}\mathbf{q}\right). \tag{6.3.13}$$

Define $\mathbf{K}(\mathbf{x})$ to be the difference between the quotient of the vertically averaged quantities $\mathbf{q}$ and θ and the vertical averaging of the quotient of $\hat{\mathbf{q}}$ and $\hat{\theta}$:

$$\mathbf{K} = \frac{1}{h_0}\int_0^{h_0} \frac{\hat{\mathbf{q}}}{\hat{\theta}}\,dz - \frac{1}{\theta}\mathbf{q}. \tag{6.3.14}$$

Note that the term with the vertical integral of the quotient is still in terms of non-averaged quantities, and hence this is a closure problem. We proceed with an approach for this closure problem by considering fluctuations of the quantities from the vertical average. We can write

$$\hat{\mathbf{q}}(\mathbf{x},z) = \mathbf{q}(\mathbf{x}) + \tilde{\mathbf{q}}(\mathbf{x},z), \tag{6.3.15}$$

where $\tilde{\mathbf{q}}$ represents the deviation of the heat flux at point $(\mathbf{x},z)$ from the vertically averaged heat flux at $\mathbf{x}$. Similarly, we define $\tilde{\theta}^{-1}$ such that

$$\hat{\theta}^{-1}(\mathbf{x},z) = \theta^{-1}(\mathbf{x}) + \tilde{\theta}^{-1}(\mathbf{x},z), \tag{6.3.16}$$

with $\tilde{\theta}^{-1}$ representing the deviation of θ^{-1} from the vertically averaged value. By definition,

$$\frac{1}{h_0}\int_0^{h_0} \tilde{\mathbf{q}}\,dz = \frac{1}{h_0}\int_0^{h_0} \tilde{\theta}^{-1}\,dz = 0. \tag{6.3.17}$$

Taking the product of $\hat{\mathbf{q}}$ and $\hat{\theta}^{-1}$ results in

$$\hat{\mathbf{q}}\hat{\theta}^{-1} = \mathbf{q}\theta^{-1} + \mathbf{q}\tilde{\theta}^{-1} + \tilde{\mathbf{q}}\theta^{-1} + \tilde{\mathbf{q}}\tilde{\theta}^{-1}. \tag{6.3.18}$$

Applying the vertical averaging operator to both sides results in

$$\begin{aligned}\frac{1}{h_0}\int_0^{h_0}\hat{\mathbf{q}}\hat{\theta}^{-1}\,dz =& \frac{1}{h_0}\int_0^{h_0}\mathbf{q}\theta^{-1}\,dz + \frac{1}{h_0}\int_0^{h_0}\mathbf{q}\tilde{\theta}^{-1}\,dz \\ &+ \frac{1}{h_0}\int_0^{h_0}\tilde{\mathbf{q}}\theta^{-1}\,dz + \frac{1}{h_0}\int_0^{h_0}\tilde{\mathbf{q}}\tilde{\theta}^{-1}\,dz.\end{aligned} \tag{6.3.19}$$

The vertically averaged quantities can be pulled outside of the integral as they are not dependent on z, and so the right hand side becomes

$$\begin{aligned}\mathbf{q}\theta^{-1}\frac{1}{h_0}\int_0^{h_0}\,dz + \mathbf{q}\frac{1}{h_0}\int_0^{h_0}\tilde{\theta}^{-1}\,dz + \theta^{-1}\frac{1}{h_0}\int_0^{h_0}\tilde{\mathbf{q}}\,dz \\ + \frac{1}{h_0}\int_0^{h_0}\tilde{\mathbf{q}}\tilde{\theta}^{-1}\,dz = \mathbf{q}\theta^{-1} + \frac{1}{h_0}\int_0^{h_0}\tilde{\mathbf{q}}\tilde{\theta}^{-1}\,dz\end{aligned} \tag{6.3.20}$$

by applying (6.3.17). Thus, by substituting this into (6.3.14) we obtain

$$\mathbf{K} = \frac{1}{h_0}\int_0^{h_0}\tilde{\mathbf{q}}\tilde{\theta}^{-1}\,dz, \tag{6.3.21}$$

and can rewrite (6.3.12) as

$$\frac{1}{\theta^2}h_0\mathbf{q}\cdot\nabla_{\mathbf{x}}\theta - \nabla_{\mathbf{x}}\cdot(h_0\mathbf{K}) + q_T F\left(\frac{1}{\theta} - \frac{1}{\theta_T}\right) - q_B\left(\frac{1}{\theta} - \frac{1}{\theta_B}\right) \leqslant 0. \tag{6.3.22}$$

Now we are required to model the form of $\mathbf{K}$. We make the assumption that if the temperature at the top of the film θ_T is the same as the temperature at the bottom of the film θ_B, the temperature is constant in the z direction. We also note that when $\nabla_{\mathbf{x}}(\theta_T - \theta_B)$ is nonzero, one may expect fluctuations to appear in z-direction. We therefore postulate that $\mathbf{K}$ takes the form

$$\mathbf{K} = \mathbf{q}'(\nabla_{\mathbf{x}}(\theta_T - \theta_B))\,(\theta_T - \theta_B) \tag{6.3.23}$$

for some function $\mathbf{q}'$. With this form, we have that if $\theta_T = \theta_B$ then $\mathbf{K} = 0$. Taking the divergence of this term now results in

$$\begin{aligned} \nabla_{\mathbf{x}} \cdot (h_0 \mathbf{K}) &= (\theta_T - \theta_B) \nabla_{\mathbf{x}} \cdot (h_0 \mathbf{q}') + h_0 \mathbf{q}' \cdot \nabla_{\mathbf{x}} (\theta_T - \theta_B) \\ &= (\theta_T - \theta_B) \nabla_{\mathbf{x}} \cdot (h_0 \mathbf{q}') + h_0 \mathbf{q}' \cdot (\nabla_{\mathbf{x}} \theta_T - \nabla_{\mathbf{x}} \theta_B) . \end{aligned} \tag{6.3.24}$$

Substituting this back into (6.3.22) gives the requirement

$$\begin{aligned} &\frac{1}{\theta^2} h_0 \mathbf{q} \cdot \nabla_{\mathbf{x}} \theta - (\theta_T - \theta_B) \nabla_{\mathbf{x}} \cdot (h_0 \mathbf{q}') - h_0 \mathbf{q}' \cdot \nabla_{\mathbf{x}} (\theta_T - \theta_B) \\ &\qquad + q_T F \left(\frac{1}{\theta} - \frac{1}{\theta_T} \right) - q_B \left(\frac{1}{\theta} - \frac{1}{\theta_B} \right) \leqslant 0, \end{aligned} \tag{6.3.25}$$

where now we are required to choose $\mathbf{q}, \mathbf{q}', q_T$ and q_B. We have already specified the constituent class of $\mathbf{q}'$ in (6.3.23); we now propose the following constituent classes for the remaining variables:

$$\mathbf{q} = \mathbf{q}(\nabla_{\mathbf{x}} \theta), \tag{6.3.26}$$

$$q_T = q_T \left(h_0, \nabla_{\mathbf{x}} h_0, \theta, \theta_T, \nabla_{\mathbf{x}} (\theta_T - \theta_B), \Delta_{\mathbf{x}} (\theta_T - \theta_B) \right), \tag{6.3.27}$$

$$q_B = q_B \left(h_0, \nabla_{\mathbf{x}} h_0, \theta, \theta_B, \nabla_{\mathbf{x}} (\theta_T - \theta_B), \Delta_{\mathbf{x}} (\theta_T - \theta_B) \right). \tag{6.3.28}$$

We make the choice of

$$\mathbf{q} = -k_2 \nabla_{\mathbf{x}} \theta, \tag{6.3.29}$$

which is consistent with the choice made for the heat flux in the bulk situation, shown in Chapter 5. In order to ensure that the third term in (6.3.25) is negative, we choose

$$\mathbf{q}' = k_4 \nabla_{\mathbf{x}} (\theta_T - \theta_B) \tag{6.3.30}$$

for some function $k_4 \geqslant 0$, leaving the requirement to be

$$- (\theta_T - \theta_B) \nabla_{\mathbf{x}} \cdot (h_0 k_4 \nabla_{\mathbf{x}} (\theta_T - \theta_B)) + q_T F \left(\frac{1}{\theta} - \frac{1}{\theta_T} \right) - q_B \left(\frac{1}{\theta} - \frac{1}{\theta_B} \right) \leqslant 0. \tag{6.3.31}$$

We rearrange the terms containing q_T and q_B to result in

$$-\left(\theta_T-\theta_B\right)\nabla_{\mathbf{x}}\cdot\left(h_0k_4\nabla_{\mathbf{x}}\left(\theta_T-\theta_B\right)\right)+\frac{q_TF}{\theta\theta_T}\left(\theta_T-\theta\right)-\frac{q_B}{\theta\theta_B}\left(\theta_B-\theta\right)\leqslant 0, \tag{6.3.32}$$

and write the first term on the left hand side as

$$-\left(\theta_T-\theta+\theta-\theta_B\right)\nabla_{\mathbf{x}}\cdot\left(h_0k_4\nabla_{\mathbf{x}}\left(\theta_T-\theta_B\right)\right). \tag{6.3.33}$$

The constraint can now naturally be split into two separate constraints; the first relating to the heat flux across the top boundary

$$-\left(\theta_T-\theta\right)\nabla_{\mathbf{x}}\cdot\left(h_0k_4\nabla_{\mathbf{x}}\left(\theta_T-\theta_B\right)\right)+\frac{q_TF}{\theta\theta_T}\left(\theta_T-\theta\right)\leqslant 0, \tag{6.3.34}$$

and the second relating to the heat flux across the bottom boundary

$$-\left(\theta-\theta_B\right)\nabla_{\mathbf{x}}\cdot\left(h_0k_4\nabla_{\mathbf{x}}\left(\theta_T-\theta_B\right)\right)-\frac{q_B}{\theta\theta_B}\left(\theta_B-\theta\right)\leqslant 0. \tag{6.3.35}$$

We make the choice of

$$q_T=\frac{\theta\theta_T}{F}\nabla_{\mathbf{x}}\cdot\left(h_0k_4\nabla_{\mathbf{x}}(\theta_T-\theta_B)\right)-k_5\left(\theta_T-\theta\right). \tag{6.3.36}$$

We verify that this is an acceptable choice by substituting it into (6.3.34) to give

$$\begin{aligned}&-\left(\theta_T-\theta\right)\nabla_{\mathbf{x}}\cdot\left(h_0k_4\nabla_{\mathbf{x}}\left(\theta_T-\theta_B\right)\right)+\\&\left[\nabla_{\mathbf{x}}\cdot\left(h_0k_4\nabla_{\mathbf{x}}(\theta_T-\theta_B)\right)-\frac{k_5F}{\theta\theta_T}\left(\theta_T-\theta\right)\right]\left(\theta_T-\theta\right)\\&=-\left(\theta_T-\theta\right)\nabla_{\mathbf{x}}\cdot\left(h_0k_4\nabla_{\mathbf{x}}\left(\theta_T-\theta_B\right)\right)+\left(\theta_T-\theta\right)\nabla_{\mathbf{x}}\cdot\left(h_0k_4\nabla_{\mathbf{x}}\left(\theta_T-\theta_B\right)\right)\\&-\frac{k_5F}{\theta\theta_T}\left(\theta_T-\theta\right)\left(\theta_T-\theta\right)=-\frac{k_5F}{\theta\theta_T}\left(\theta_T-\theta\right)^2\leqslant 0.\end{aligned} \tag{6.3.37}$$

Similarly, we make the choice of

$$q_B = \theta\theta_B \nabla_{\mathbf{x}} \cdot \left(h_0 k_4 \nabla_{\mathbf{x}} \left(\theta_T - \theta_B\right)\right) + k_6 \left(\theta_B - \theta\right) \tag{6.3.38}$$

to satisfy (6.3.35), which reduces to

$$-\frac{k_6}{\theta\theta_B} \left(\theta_B - \theta\right)^2 \leqslant 0. \tag{6.3.39}$$

These choices for the boundary heat fluxes are consistent with the findings in [102].

6.3.2 Final Equation

All the choices in this section can be combined and substituted back into the original equation for the internal energy density, equation (6.2.11), to result in

$$\begin{aligned}\frac{d}{dt}(h_0 e) = \nabla_{\mathbf{x}} \cdot h_0 k_2 \nabla_{\mathbf{x}} \theta - (\theta_T - \theta_B)\theta \left[\nabla_{\mathbf{x}} \cdot \left(h_0 k_4 \nabla_{\mathbf{x}} (\theta_T - \theta_B)\right)\right] \\ + k_5 F \left(\theta_T - \theta\right) + k_6 \left(\theta_B - \theta\right) + h_0 r.\end{aligned} \tag{6.3.40}$$

As in Chapter 5, we use that the internal energy depends linearly on the temperature, $e = c\theta$ for some constant c, which can be multiplied through by h_0 to give

$$h_0 e = c h_0 \theta. \tag{6.3.41}$$

Taking the time derivative of this results in the final thin film heat equation

$$\begin{aligned}c h_0 \dot{\theta} = \nabla_{\mathbf{x}} \cdot h_0 k_2 \nabla_{\mathbf{x}} \theta - (\theta_T - \theta_B)\theta \left[\nabla_{\mathbf{x}} \cdot \left(h_0 k_4 \nabla_{\mathbf{x}} (\theta_T - \theta_B)\right)\right] \\ + k_5 F \left(\theta_T - \theta\right) + k_6 \left(\theta_B - \theta\right) + h_0 r.\end{aligned} \tag{6.3.42}$$

CHAPTER 7

Thin Film Solidification

In this chapter, we combine the procedures used in the previous chapters in order to create a thermodynamically consistent class of models for describing the evolution of a solidifying thin film.

As in Chapter 4, consider a d-dimensional thin film on a flat solid substrate $\mathfrak{D} \subset \mathbb{R}^{d-1}$. Consider a fixed yet arbitrary region $\Omega \subset \mathfrak{D}$ on the substrate and define by the function $h(\mathbf{x}, t) : \Omega \times [0, \infty) \to [0, \infty)$ the height above the substrate of the surface of the film at time $t \in [0, \infty)$. Finally define a region

$$\mathcal{P}_t := \bigcup_{\mathbf{x} \in \Omega} \{(\mathbf{x}, z) \,|z \in [0, h(\mathbf{x}, t)]\} \tag{7.0.1}$$

to be an arbitrary subset of the film bounded by Ω, vertical sides, and the time dependent top of the film. This can be seen in Figure 7.1. Note that $\mathbf{x} \subset \mathbb{R}^{d-1}$ and $z \subset \mathbb{R}$.

As in the case of the thin film heat equation, the boundary of $\mathcal{P}_t$, denoted $\partial\mathcal{P}_t$, can be split into three separate components: the bottom surface

$$B := \Omega \times \{0\}, \tag{7.0.2}$$

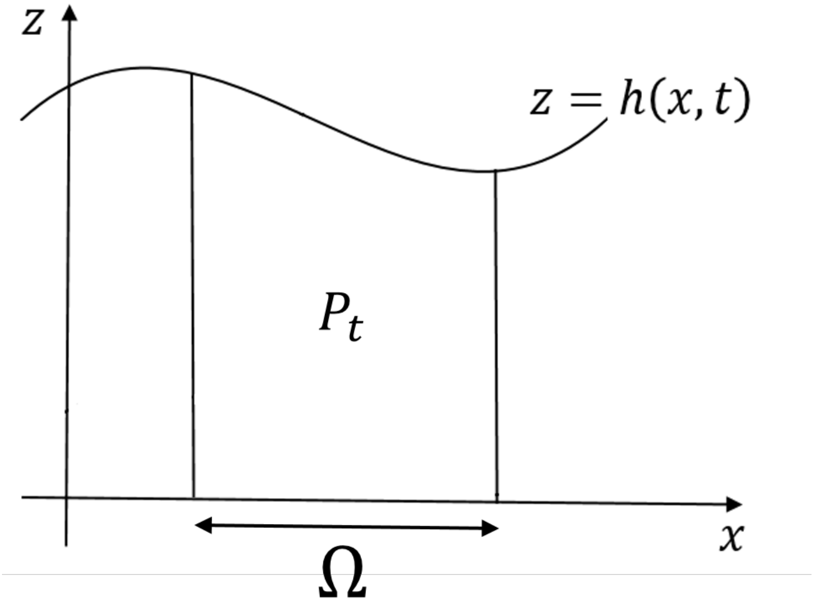

Figure 7.1: The geometry of a thin film on a solid substrate for the case of $d = 2$. $\mathcal{P}_t$ is an arbitrary subset of the film with Ω as its base, $h(x, t)$ as the top surface and vertical sides.

the vertical sides

$$S_t := \bigcup_{\mathbf{x} \in \partial\Omega} \{\mathbf{x}\} \times [0, h(\mathbf{x}, t)], \tag{7.0.3}$$

where $\partial\Omega$ is the boundary of Ω, and the top surface of the film

$$T_t := \bigcup_{\mathbf{x} \in \Omega} \{\mathbf{x}\} \times \{h(\mathbf{x}, t)\}. \tag{7.0.4}$$

It can be noted that, unlike in the case of the thin film heat equation, S_t and T_t are time dependent, although B remains non time dependent.

7.1 Axiomatic Laws for a Solidifying Thin Film

7.1.1 Conservation of Mass

Let $\hat{\rho}(\mathbf{x}, z, t)$ be the density of the film at point $(\mathbf{x}, z)$ at time t. For this section we assume $\hat{\rho}(\mathbf{x}, z, t) = \hat{\rho_0}$ is constant in both the solid and liquid phases of the film. The total mass enclosed by $\mathcal{P}_t$ is given by

$$\int_{\mathcal{P}_t} \hat{\rho_0}\, dV. \tag{7.1.1}$$

Therefore, the conservation of mass results in

$$\frac{d}{dt}\int_{\mathcal{P}_t} \hat{\rho_0}\, dV = -\int_{\partial\mathcal{P}_t} \hat{\rho_0}\hat{\mathbf{j}}\cdot\mathbf{n}\, ds + \int_{\mathcal{P}_t} R\, dV, \tag{7.1.2}$$

where $\partial\mathcal{P}_t$ is the boundary of volume $\mathcal{P}_t$, $\hat{\mathbf{j}}(\mathbf{x},z,t)$ is the flux of the film at point $(\mathbf{x},z)$ at time t, $\mathbf{n}(\mathbf{x},z)$ is the outward pointing unit normal to $\mathcal{P}_t$ at $(\mathbf{x},z)$ and R represents a source term for the film within $\mathcal{P}_t$. It is assumed that there is no source or sink term, and so $R \equiv 0$.

Equation (7.1.2) can be written

$$\frac{d}{dt}\int_{\mathcal{P}_t} \hat{\rho_0}\, dV = -\int_{S} \hat{\rho_0}\hat{\mathbf{j}}\cdot\mathbf{n}_S\, ds - \int_{B} \hat{\rho_0}\hat{\mathbf{j}}\cdot\mathbf{n}_B\, ds - \int_{T} \hat{\rho_0}\hat{\mathbf{j}}\cdot\mathbf{n}_T\, ds, \tag{7.1.3}$$

where $\mathbf{n}_i$ represents the unit normal to surface i. Define

$$\mathbf{e}_d = \begin{pmatrix} \mathbf{0} \\ 1 \end{pmatrix} \tag{7.1.4}$$

as the unit normal perpendicular to Ω.

Equations (7.0.2)-(7.0.4), (7.1.3), (7.1.4) and result (6.1.13) can be combined to give

$$\begin{aligned} \frac{d}{dt}\int_{\Omega}\int_0^{h(\mathbf{x},t)} \hat{\rho_0}\, dz\, dA = &-\int_{\partial\Omega}\left(\int_0^{h(\mathbf{x},t)} \hat{\rho_0}\hat{\mathbf{j}}(\mathbf{x},z,t)\, dz\right)\cdot\mathbf{n}_\Omega\, ds \\ &-\int_{\Omega}\hat{\rho_0}\hat{\mathbf{j}}(\mathbf{x},0,t)\cdot(-\mathbf{e}_d)\, dA - \int_{\Omega}\hat{\rho_0}\hat{\mathbf{j}}(\mathbf{x},h(\mathbf{x},t),t)\cdot\mathbf{e}_d F\, dA. \end{aligned} \tag{7.1.5}$$

As the region Ω is not time dependent, the time differential can be moved inside the integral over Ω. Note that in the first term on the right hand side of (7.1.5), the normal to Ω, $\mathbf{n}_\Omega$, can be taken out of the integral in the vertical direction as it is independent of z $\forall\mathbf{x} \in \partial\Omega$. We now define the vertically averaged mass flux

$$\mathbf{j} = \frac{1}{h}\int_0^{h(\mathbf{x},t)} \hat{\mathbf{j}}(\mathbf{x},z,t)\,dz, \tag{7.1.6}$$

$$j_B = \hat{\mathbf{j}}(\mathbf{x},0,t)\cdot\mathbf{e}_d, \tag{7.1.7}$$

and

$$j_T = \hat{\mathbf{j}}(\mathbf{x},h(\mathbf{x},t),t)\cdot\mathbf{e}_d. \tag{7.1.8}$$

By employing the divergence theorem to the boundary integral in (7.1.5) we obtain

$$\begin{aligned}\int_\Omega \frac{d}{dt}\int_0^{h(\mathbf{x},t)} \hat{\rho_0}\,dz\,dA = &-\int_\Omega \nabla_{\mathbf{x}}\cdot\left(\int_0^{h(\mathbf{x},t)} \hat{\rho_0}\hat{\mathbf{j}}(\mathbf{x},z,t)\,dz\right)\,dA \\ &-\int_\Omega \hat{\rho_0}\hat{\mathbf{j}}(\mathbf{x},0,t)\cdot(-\mathbf{e}_d)\,dA - \int_\Omega \hat{\rho_0}\hat{\mathbf{j}}(\mathbf{x},h(\mathbf{x},t),t)\cdot\mathbf{e}_d F\,dA,\end{aligned} \tag{7.1.9}$$

where $\nabla_{\mathbf{x}}$ represents the $d-1$ dimensional gradient given by $(\partial/\partial x_1, \partial/\partial x_2, \ldots, \partial/\partial x_{d-1})^T$. Noting that Ω was chosen arbitrarily, we can rewrite this as

$$\frac{d}{dt}\int_0^{h(\mathbf{x},t)} \hat{\rho_0}\,dz = -\nabla_{\mathbf{x}}\cdot(\hat{\rho_0}h\mathbf{j}) - \hat{\rho_0}j_T F + \hat{\rho_0}j_B. \tag{7.1.10}$$

Finally, by recalling that $\hat{\rho_0}$ is constant, the equation of the rate of change in the height of the film is obtained:

$$\frac{dh}{dt} = -\nabla_{\mathbf{x}}\cdot(h\mathbf{j}) - j_T F + j_B. \tag{7.1.11}$$

7.1.2 Conservation of Energy

As in the case of a rigid film described in Section 6.2, the change of energy in a given region of the film is affected by the flux of energy across the boundary and internal sources or sinks. Let $\hat{e}(\mathbf{x},z,t)$, $\hat{\mathbf{q}}(\mathbf{x},z,t)$ and $\hat{r}(\mathbf{x},z,t)$ be the energy density, heat flux and heat source at point $(\mathbf{x},z)$ at time t respectively. Then from the first law of thermodynamics,

$$\frac{d}{dt}\int_{\mathcal{P}_t} \hat{e}\, dV = -\int_{\partial\mathcal{P}_t} \hat{\mathbf{q}}\cdot\mathbf{n}\, ds + \int_{\mathcal{P}_t} \hat{r}\, dV. \tag{7.1.12}$$

Defining sets as in (7.0.2), (7.0.3) and (7.0.4), and following the same process as for the conservation of mass, this can be written as

$$\begin{aligned}\int_\Omega \frac{d}{dt}\int_0^{h(\mathbf{x},t)} \hat{e}\, dz\, dA = &-\int_{\partial\Omega}\left(\int_0^{h(\mathbf{x},t)} \hat{\mathbf{q}}\, dz\right)\cdot\mathbf{n}_\Omega\, ds \\ &-\int_\Omega \hat{\mathbf{q}}(\mathbf{x},h(\mathbf{x},t),t)\cdot\mathbf{e}_d F\, dA \\ -\int_\Omega \hat{\mathbf{q}}(\mathbf{x},0,t)\cdot(-\mathbf{e}_d)\, dA &+ \int_\Omega\int_0^{h(\mathbf{x},t)} \hat{r}\, dz\, dA\end{aligned} \tag{7.1.13}$$

Define the vertically averaged internal energy density, energy flux and energy source to be

$$e = \frac{1}{h}\int_0^{h(\mathbf{x},t)} \hat{e}\, dz, \tag{7.1.14}$$

$$\mathbf{q} = \frac{1}{h}\int_0^{h(\mathbf{x},t)} \hat{\mathbf{q}}\, dz, \tag{7.1.15}$$

$$r = \frac{1}{h}\int_0^{h(\mathbf{x},t)} \hat{r}\, dz \tag{7.1.16}$$

respectively. Further defining

$$q_T = \hat{\mathbf{q}}(\mathbf{x},h(\mathbf{x},t),t)\cdot\mathbf{e}_d, \tag{7.1.17}$$

$$q_B = \hat{\mathbf{q}}(\mathbf{x},0,t)\cdot\mathbf{e}_d, \tag{7.1.18}$$

and again noting that Ω is arbitrary, the final conservation of energy equation is obtained:

$$\frac{d}{dt}(he) = -\nabla_{\mathbf{x}}\cdot(h\mathbf{q}) - q_T F + q_B + hr. \tag{7.1.19}$$

7.1.3 Entropy Inequality

Let $\hat{\Phi}(\mathbf{x}, z, t)$ be the entropy flux of the film and $\hat{H}(\mathbf{x}, z, t)$ be an entropy source. As in Section 6.2, by the second law of thermodynamics, entropy must be non-decreasing, and so

$$\frac{d}{dt}\int_{\mathcal{P}_t} \hat{\eta}\, dV \geqslant -\int_{\partial\mathcal{P}_t} \hat{\Phi}\cdot\mathbf{n}\, ds + \int_{\mathcal{P}_t} \hat{H}\, dV, \tag{7.1.20}$$

where $\hat{\eta} = \hat{\eta}(\mathbf{x}, z, t)$ represents the entropy density at position $(\mathbf{x}, z)$ at time t. As in the bulk equations, we define

$$\hat{\Phi} = \frac{\hat{\mathbf{q}}}{\hat{\theta}} + \hat{\mathbf{k}}, \tag{7.1.21}$$

for some $\hat{\mathbf{k}}$ which represents an entropy flux related to the diffuse boundaries involved in the problem, and

$$\hat{H} = \frac{\hat{r}}{\hat{\theta}}, \tag{7.1.22}$$

where $\hat{\theta}(\mathbf{x}, z, t)$ is the temperature at position $(\mathbf{x}, z)$ at time t. Again splitting the boundary integral into integrals of the sets (7.0.2), (7.0.3) and (7.0.4) results in

$$\begin{aligned}
&\int_{\Omega}\frac{d}{dt}\int_0^{h(\mathbf{x},t)} \hat{\eta}\, dz\, dA \geqslant \\
&-\int_{\partial\Omega}\left(\int_0^{h(\mathbf{x},t)}\frac{\hat{\mathbf{q}}}{\hat{\theta}}\, dz\right)\cdot\mathbf{n}_{\Omega}\, ds - \int_{\partial\Omega}\left(\int_0^{h(\mathbf{x},t)}\hat{\mathbf{k}}\, dz\right)\cdot\mathbf{n}_{\Omega}\, ds \\
&-\int_{\Omega}\frac{\hat{\mathbf{q}}(\mathbf{x}, h(\mathbf{x},t), t)}{\hat{\theta}(\mathbf{x}, h(\mathbf{x},t), t)}\cdot\mathbf{e}_d F\, dA - \int_{\Omega}\frac{\hat{\mathbf{q}}(\mathbf{x}, 0, t)}{\hat{\theta}(\mathbf{x}, 0, t)}\cdot(-\mathbf{e}_d)\, dA \\
&-\int_{\Omega}\hat{\mathbf{k}}(\mathbf{x}, h(\mathbf{x},t), t)\cdot\mathbf{e}_d F\, dA - \int_{\Omega}\hat{\mathbf{k}}(\mathbf{x}, 0, t)\cdot(-\mathbf{e}_d)\, dA \\
&+\int_{\Omega}\int_0^{h(\mathbf{x},t)}\frac{\hat{r}}{\hat{\theta}}\, dz\, dA.
\end{aligned} \tag{7.1.23}$$

We define

$$\eta = \frac{1}{h}\int_0^{h(\mathbf{x},t)} \hat{\eta}\, dz, \tag{7.1.24}$$

and

$$\mathbf{k} = \frac{1}{h}\int_0^{h(\mathbf{x},t)} \hat{\mathbf{k}}\, dz, \tag{7.1.25}$$

to be the vertically averaged entropy density and non-thermal entropy flux at position **x** and time *t* respectively. Further, we define

$$\theta_T = \hat{\theta}(\mathbf{x}, h(\mathbf{x},t), t) \tag{7.1.26}$$

and

$$\theta_B = \hat{\theta}(\mathbf{x}, 0, t) \tag{7.1.27}$$

to be the temperature at the top surface and the bottom surface of the film respectively. In addition, as the top and bottom surfaces of the film are sharp interfaces, the term relating to entropy within a diffuse boundary can be set as

$$\hat{\mathbf{k}}(\mathbf{x}, h(\mathbf{x},t), t) \cdot \mathbf{e}_d = \hat{\mathbf{k}}(\mathbf{x}, 0, t) \cdot \mathbf{e}_d = 0. \tag{7.1.28}$$

With these definitions, employing the divergence theorem on the boundary integrals, and using that Ω is arbitrary, the final entropy inequality becomes

$$\frac{d}{dt}(h\eta) \geqslant -\nabla_{\mathbf{x}} \cdot \left(\int_0^{h(\mathbf{x},t)} \frac{\hat{\mathbf{q}}}{\hat{\theta}}\, dz \right) - \nabla_{\mathbf{x}} \cdot (h\mathbf{k}) - \frac{q_T F}{\theta_T} + \frac{q_B}{\theta_B} + \int_0^{h(\mathbf{x},t)} \frac{\hat{r}}{\hat{\theta}}\, dz. \tag{7.1.29}$$

7.1.4 Solidification

We define a phase parameter $\phi(\mathbf{x}, t)$ for $\mathbf{x} \in \Omega$ such that $\phi(\mathbf{x}, t) = 0$ if the vertical strip of film at point **x** is solid at time *t*, and $\phi(\mathbf{x}, t) = 1$ if it is a liquid. Consider a mass conservation argument for the arbitrary area Ω:

$$\frac{d}{dt}\int_\Omega \phi\, ds = \int_\Omega \gamma\, ds, \tag{7.1.30}$$

where γ is the rate of the phase change from liquid to solid and has a form yet to be defined. Then given that Ω is arbitrary and not dependent on time, the equation describing the evolution of ϕ in time is given by

$$\frac{d\phi}{dt} = \gamma. \tag{7.1.31}$$

It can be noted that $0 < \phi < 1$ describes a diffuse interface between the two phases.

7.1.5 The Reduced Dissipation Inequality

We introduce an averaged temperature parameter, $\theta(\mathbf{x}, t)$, defined such that

$$\frac{1}{\theta} = \frac{1}{h}\int_0^{h(\mathbf{x},t)} \frac{1}{\hat{\theta}}\, dz. \tag{7.1.32}$$

Using this definition, we construct a Helmholtz free energy $\Psi(\mathbf{x}, t)$ given by

$$h\Psi = he - \theta h\eta. \tag{7.1.33}$$

Differentiating with respect to time results in

$$(\dot{h\eta}) = \frac{1}{\theta}\left[(\dot{h\epsilon}) - \dot{\theta}h\eta - (\dot{h\Psi})\right]. \tag{7.1.34}$$

Substituting this and (7.1.19) into inequality (7.1.29) and noting that $(\dot{h\Psi}) = \dot{h}\Psi + h\dot{\Psi}$ gives

$$\begin{gathered}-\nabla_{\mathbf{x}} \cdot \left(\int_0^{h(\mathbf{x},t)} \frac{\hat{\mathbf{q}}}{\hat{\theta}}\, dz\right) - \nabla_{\mathbf{x}} \cdot (h\mathbf{k}) - \frac{q_T F}{\theta_T} + \frac{q_B}{\theta_B} + \int_0^{h(\mathbf{x},t)} \frac{\hat{r}}{\hat{\theta}}\, dz \leqslant \\ \frac{1}{\theta}\left[-\nabla_{\mathbf{x}} \cdot (h\mathbf{q}) - q_T F + q_B + hr - \dot{\theta}h\eta - h\dot{\Psi} - \dot{h}\Psi\right].\end{gathered} \tag{7.1.35}$$

Using the result that for a scalar x and vector $\mathbf{v}$,

$$\nabla_{\mathbf{x}} \cdot (x\mathbf{v}) = x\nabla_{\mathbf{x}} \cdot \mathbf{v} + \mathbf{v} \cdot \nabla_{\mathbf{x}} x, \tag{7.1.36}$$

we obtain

$$
\begin{aligned}
&-\nabla_{\mathbf{x}}\cdot\left(\int_0^{h(\mathbf{x},t)}\frac{\hat{\mathbf{q}}}{\hat{\theta}}\,dz\right)-\nabla_{\mathbf{x}}\cdot(h\mathbf{k})+\nabla_{\mathbf{x}}\cdot\left(\frac{1}{\theta}h\mathbf{q}\right)+\frac{1}{\theta^2}(h\mathbf{q})\cdot\nabla_{\mathbf{x}}\theta\\
&+\frac{1}{\theta}h\dot{\Psi}+\frac{1}{\theta}\dot{h}\Psi-\frac{q_TF}{\theta_T}+\frac{q_B}{\theta_B}+\int_0^{h(\mathbf{x},t)}\frac{\hat{r}}{\hat{\theta}}\,dz+\frac{1}{\theta}q_TF-\frac{1}{\theta}q_B-\frac{1}{\theta}hr\\
&+\frac{1}{\theta}\dot{\theta}h\eta\leqslant 0.
\end{aligned}
\tag{7.1.37}
$$

For a model to be thermo-mechanically consistent, equation (7.1.37) must hold in all realistic situations.

7.2 Choices of Constituent Classes and Dependent Variables

Having found a constraint to ensure that the family of models is thermo-mechanically consistent, choices must now be made for the constituent classes for the dependent variables. From these classes, specific choices are either forced or made to result in an individual model which can then be used to simulate the evolution of a solidifying thin film over time.

7.2.1 Free Energy Functional

The initial decision is to choose a constitutive class for the free energy functional Ψ. The constitutive properties related to this problem are the height of the film, the phase of solidification and the temperature. We define $\Gamma=\{\theta,\nabla\theta,\Delta\theta,\phi,\nabla\phi,\Delta\phi,h,\nabla h,\Delta h\}$ and define the constituent classes

$$\Psi=\Psi\left(\Gamma\right) \tag{7.2.1}$$

and

$$\eta=\eta(\Gamma). \tag{7.2.2}$$

Theorem 3. *Given* (7.1.37)*, the constituent class of* Ψ *reduces to* $\Psi = \Psi(\theta, \phi, \nabla_{\mathbf{x}}\phi, h, \nabla_{\mathbf{x}}h)$*. In addition,* $\eta = -\partial_\theta\Psi$*. With these choices, the constraint* (7.1.37) *becomes*

$$
\begin{aligned}
&-\nabla_{\mathbf{x}}\cdot\left(\int_0^{h(\mathbf{x},t)}\frac{\hat{\mathbf{q}}}{\hat{\theta}}\,dz\right)-\nabla_{\mathbf{x}}\cdot(h\mathbf{k})+\nabla_{\mathbf{x}}\cdot\left(\frac{1}{\theta}h\mathbf{q}\right)+\frac{1}{\theta^2}(h\mathbf{q})\cdot\nabla_{\mathbf{x}}\theta\\
&-\frac{q_T F}{\theta_T}+\frac{q_B}{\theta_B}+\int_0^{h(\mathbf{x},t)}\frac{\hat{r}}{\hat{\theta}}\,dz+\frac{1}{\theta}q_T F-\frac{1}{\theta}q_B-\frac{1}{\theta}hr+\frac{1}{\theta}\dot{h}\Psi\\
&+\frac{1}{\theta}h\partial_h\Psi\dot{h}+\frac{1}{\theta}h\partial_{\nabla_{\mathbf{x}}h}\Psi(\dot{\nabla_{\mathbf{x}}h})+\frac{1}{\theta}h\partial_\phi\Psi\dot{\phi}+\frac{1}{\theta}h\partial_{\nabla_{\mathbf{x}}\phi}\Psi(\dot{\nabla_{\mathbf{x}}\phi})\leqslant 0.
\end{aligned}
\tag{7.2.3}
$$

Proof. Employing the chain rule to (7.2.1) it can be seen that

$$
\begin{aligned}
\dot{\Psi} =&\partial_\theta\Psi\dot{\theta}+\partial_{\nabla_{\mathbf{x}}\theta}\Psi(\dot{\nabla_{\mathbf{x}}\theta})+\partial_{\Delta_{\mathbf{x}}\theta}\Psi(\dot{\Delta_{\mathbf{x}}\theta})+\partial_h\Psi\dot{h}+\partial_{\nabla_{\mathbf{x}}h}\Psi(\dot{\nabla_{\mathbf{x}}h})\\
&+\partial_{\Delta_{\mathbf{x}}h}\Psi(\dot{\Delta_{\mathbf{x}}h})+\partial_\phi\Psi\dot{\phi}+\partial_{\nabla_{\mathbf{x}}\phi}\Psi(\dot{\nabla_{\mathbf{x}}\phi})+\partial_{\Delta_{\mathbf{x}}\phi}\Psi(\dot{\Delta_{\mathbf{x}}\phi}),
\end{aligned}
\tag{7.2.4}
$$

where $\partial_x y$ represents the partial derivative of x with respect to y. Substituting this into (7.1.37) results in

$$
\begin{aligned}
&-\nabla_{\mathbf{x}}\cdot\left(\int_0^{h(\mathbf{x},t)}\frac{\hat{\mathbf{q}}}{\hat{\theta}}\,dz\right)-\nabla_{\mathbf{x}}\cdot(h\mathbf{k})+\nabla_{\mathbf{x}}\cdot\left(\frac{1}{\theta}h\mathbf{q}\right)+\frac{1}{\theta^2}(h\mathbf{q})\cdot\nabla_{\mathbf{x}}\theta\\
&-\frac{q_T F}{\theta_T}+\frac{q_B}{\theta_B}+\int_0^{h(\mathbf{x},t)}\frac{\hat{r}}{\hat{\theta}}\,dz+\frac{1}{\theta}q_T F-\frac{1}{\theta}q_B-\frac{1}{\theta}hr+\frac{1}{\theta}\dot{h}\Psi+\frac{1}{\theta}h(\partial_\theta\Psi+\eta)\dot{\theta}\\
&+\frac{1}{\theta}h\partial_{\nabla_{\mathbf{x}}\theta}\Psi(\dot{\nabla_{\mathbf{x}}\theta})+\frac{1}{\theta}h\partial_{\Delta_{\mathbf{x}}\theta}\Psi(\dot{\Delta_{\mathbf{x}}\theta})+\frac{1}{\theta}h\partial_h\Psi\dot{h}+\frac{1}{\theta}h\partial_{\nabla_{\mathbf{x}}h}\Psi(\dot{\nabla_{\mathbf{x}}h})\\
&+\frac{1}{\theta}h\partial_{\Delta_{\mathbf{x}}h}\Psi(\dot{\Delta_{\mathbf{x}}h})+\frac{1}{\theta}h\partial_\phi\Psi\dot{\phi}+\frac{1}{\theta}h\partial_{\nabla_{\mathbf{x}}\phi}\Psi(\dot{\nabla_{\mathbf{x}}\phi})+\frac{1}{\theta}h\partial_{\Delta_{\mathbf{x}}\phi}\Psi(\dot{\Delta_{\mathbf{x}}\phi})\leqslant 0.
\end{aligned}
\tag{7.2.5}
$$

We substitute in (7.1.11) and (7.1.31) employ the Coleman-Noll procedure. As the constraint must hold for all values, we fix all variables $\{\Gamma\}\backslash\Delta_{\mathbf{x}}\theta$. $\Delta_{\mathbf{x}}\theta$ is linear in the inequality, and therefore it will be always be possible to break the constraint by picking the right value of $\Delta_{\mathbf{x}}\theta$, unless the coefficient of $\Delta_{\mathbf{x}}\theta$ is zero. Using the same arguments for the other variables linear in the inequality, we can conclude that $\partial_{\nabla_{\mathbf{x}}\theta}\Psi = 0$, $\partial_{\Delta_{\mathbf{x}}\theta}\Psi = 0$, $\partial_{\Delta_{\mathbf{x}}\phi}\Psi = 0$, $\partial_{\Delta_{\mathbf{x}}h}\Psi = 0$ and $(\eta + \partial_\theta\Psi) = 0$. Therefore we conclude that the constituent class of Ψ reduces to

$$\Psi = \Psi(\theta, \phi, \nabla_{\mathbf{x}}\phi, h, \nabla_{\mathbf{x}}h), \tag{7.2.6}$$

and

$$\eta = -\partial_\theta \Psi. \tag{7.2.7}$$

Now substituting (7.2.6) and (7.2.7) into (7.1.37) results in the final constraint:

$$\begin{aligned}
&-\nabla_{\mathbf{x}} \cdot \left(\int_0^{h(\mathbf{x},t)} \frac{\hat{\mathbf{q}}}{\hat{\theta}}\, dz \right) - \nabla_{\mathbf{x}} \cdot (h\mathbf{k}) + \nabla_{\mathbf{x}} \cdot \left(\frac{1}{\theta} h\mathbf{q} \right) + \frac{1}{\theta^2}(h\mathbf{q}) \cdot \nabla_{\mathbf{x}}\theta \\
&- \frac{q_T F}{\theta_T} + \frac{q_B}{\theta_B} + \int_0^{h(\mathbf{x},t)} \frac{\hat{r}}{\hat{\theta}}\, dz + \frac{1}{\theta} q_T F - \frac{1}{\theta} q_B - \frac{1}{\theta} hr + \frac{1}{\theta}\dot{h}\Psi \\
&+ \frac{1}{\theta} h\partial_h \Psi \dot{h} + \frac{1}{\theta} h\partial_{\nabla_{\mathbf{x}}h}\Psi(\overset{\cdot}{\nabla_{\mathbf{x}}h}) + \frac{1}{\theta} h\partial_\phi \Psi \dot{\phi} + \frac{1}{\theta} h\partial_{\nabla_{\mathbf{x}}\phi}\Psi(\overset{\cdot}{\nabla_{\mathbf{x}}\phi}) \leqslant 0,
\end{aligned} \tag{7.2.8}$$

as required. ■

Define the chemical potentials of ϕ and h as

$$\mu_\phi = h\frac{\partial_\phi \Psi}{\theta} - \nabla_{\mathbf{x}} \cdot \left(h\frac{\partial_{\nabla_{\mathbf{x}}\phi}\Psi}{\theta} \right) \tag{7.2.9}$$

and

$$\mu_h = \frac{1}{\theta}\Psi + h\frac{\partial_h \Psi}{\theta} - \nabla_{\mathbf{x}} \cdot \left(h\frac{\partial_{\nabla_{\mathbf{x}}h}\Psi}{\theta} \right) \tag{7.2.10}$$

respectively. We now use (7.2.8) and employ the same methods as described in Chapter 5 to rewrite the constraint as

$$\begin{aligned}
&-\nabla_{\mathbf{x}}\cdot\left(\int_0^{h(\mathbf{x},t)}\frac{\hat{\mathbf{q}}}{\hat{\theta}}\,dz\right)-\nabla_{\mathbf{x}}\cdot(h\mathbf{k})+\nabla_{\mathbf{x}}\cdot\left(\frac{1}{\theta}h\mathbf{q}\right)+\frac{1}{\theta}\Psi\dot{h}\\
&+\frac{1}{\theta^2}(h\mathbf{q})\cdot\nabla_{\mathbf{x}}\theta+\frac{1}{\theta}q_TF-\frac{1}{\theta}q_B-\frac{1}{\theta}hr-\frac{q_TF}{\theta_T}+\frac{q_B}{\theta_B}+\int_0^{h(\mathbf{x},t)}\frac{\hat{r}}{\hat{\theta}}\,dz\\
&+h\frac{\partial_h\Psi}{\theta}\dot{h}-\nabla_{\mathbf{x}}\cdot\left(h\frac{\partial_{\nabla_{\mathbf{x}}h}\Psi}{\theta}\right)\dot{h}+\nabla_{\mathbf{x}}\cdot\left(h\frac{\partial_{\nabla_{\mathbf{x}}h}\Psi}{\theta}\right)\dot{h}+h\frac{\partial_{\nabla_{\mathbf{x}}h}\Psi}{\theta}\dot{(\nabla_{\mathbf{x}}h)}\\
&+h\frac{\partial_\phi\Psi}{\theta}\dot{\phi}-\nabla_{\mathbf{x}}\cdot\left(h\frac{\partial_{\nabla_{\mathbf{x}}\phi}\Psi}{\theta}\right)\dot{\phi}+\nabla_{\mathbf{x}}\cdot\left(h\frac{\partial_{\nabla_{\mathbf{x}}\phi}\Psi}{\theta}\right)\dot{\phi}+h\frac{\partial_{\nabla_{\mathbf{x}}\phi}\Psi}{\theta}\dot{(\nabla_{\mathbf{x}}\phi)}\\
&\leqslant 0.
\end{aligned}\tag{7.2.11}$$

Noting that for some Y, $\dot{(\nabla_{\mathbf{x}}Y)}=\nabla_{\mathbf{x}}\dot{Y}$ we can use the definitions of the chemical potentials (7.2.9) and (7.2.10) to rewrite (7.2.11) as

$$\begin{aligned}
&-\nabla_{\mathbf{x}}\cdot\left(\int_0^{h(\mathbf{x},t)}\frac{\hat{\mathbf{q}}}{\hat{\theta}}\,dz\right)-\nabla_{\mathbf{x}}\cdot(h\mathbf{k})+\nabla_{\mathbf{x}}\cdot\left(\frac{1}{\theta}h\mathbf{q}\right)\\
&+\frac{1}{\theta^2}(h\mathbf{q})\cdot\nabla_{\mathbf{x}}\theta+\frac{1}{\theta}q_TF-\frac{1}{\theta}q_B-\frac{1}{\theta}hr-\frac{q_TF}{\theta_T}+\frac{q_B}{\theta_B}+\int_0^{h(\mathbf{x},t)}\frac{\hat{r}}{\hat{\theta}}\,dz\\
&+\mu_h\dot{h}+\nabla_{\mathbf{x}}\cdot\left(h\frac{\partial_{\nabla_{\mathbf{x}}h}\Psi}{\theta}\dot{h}\right)+\mu_\phi\dot{\phi}+\nabla_{\mathbf{x}}\cdot\left(h\frac{\partial_{\nabla_{\mathbf{x}}\phi}\Psi}{\theta}\dot{\phi}\right)\leqslant 0.
\end{aligned}\tag{7.2.12}$$

We integrate (7.2.12) over the domain Ω and substitute in (7.1.11). The term containing $\dot{h}\mu_h$ becomes

$$\int_\Omega \dot{h}\mu_h\,dA=\int_\Omega\left(-\nabla_{\mathbf{x}}\cdot(h\mathbf{j})-j_TF+j_B\right)\mu_h\,dA. \tag{7.2.13}$$

Integrate by parts the first term, and using the homogenous boundary conditions $\mu_h\cdot\mathbf{n}_\Omega=0$ on $\partial\Omega$, it is found that

$$\int_\Omega \dot{h}\mu_h\,dA=\int_\Omega\left(\nabla_{\mathbf{x}}\mu_h\cdot(h\mathbf{j})-j_TF\mu_h+j_B\mu_h\right)\,dA. \tag{7.2.14}$$

Removing the integrals and substituting in (7.1.31) results in the final constraint for the constituent class of Ψ chosen in (7.2.1)

$$\begin{aligned}
&-\nabla_{\mathbf{x}}\cdot\left(\int_0^{h(\mathbf{x},t)}\frac{\hat{\mathbf{q}}}{\hat{\theta}}\,dz\right)-\nabla_{\mathbf{x}}\cdot(h\mathbf{k})+\nabla_{\mathbf{x}}\cdot\left(\frac{1}{\theta}h\mathbf{q}\right)\\
&+\frac{1}{\theta^2}(h\mathbf{q})\cdot\nabla_{\mathbf{x}}\theta+\frac{1}{\theta}q_TF-\frac{1}{\theta}q_B-\frac{1}{\theta}hr-\frac{q_TF}{\theta_T}+\frac{q_B}{\theta_B}+\int_0^{h(\mathbf{x},t)}\frac{\hat{r}}{\hat{\theta}}\,dz\\
&+\nabla_{\mathbf{x}}\mu_h\cdot(h\mathbf{j})-j_TF\mu_h+j_B\mu_h+\mu_\phi\gamma\\
&+\nabla_{\mathbf{x}}\cdot\left(h\frac{\partial_{\nabla_{\mathbf{x}}h}\Psi}{\theta}\dot{h}\right)+\nabla_{\mathbf{x}}\cdot\left(h\frac{\partial_{\nabla_{\mathbf{x}}\phi}\Psi}{\theta}\dot{\phi}\right)\leqslant 0.
\end{aligned} \tag{7.2.15}$$

Having defined the chemical potentials and found a constraint that must hold for any choice of dependent variables for the choice of constituent class made in (7.2.6), we are able to postulate constituent classes for these variables to give a thermodynamically consistent model that fits within this framework.

7.2.2 Choices of Dependent Variables

In this section we break (7.2.15) into groups of terms, and ensure that each group piecewise satisfies the constraint. From this section onwards, as we have reduced the problem to a $(d-1)$-dimensional problem, we drop the $\mathbf{x}$ subscript from the gradient, thus $\nabla = (\partial/\partial x_1, \ldots, \partial/\partial x_{d-1})^T$.

Energy Source Terms

We first turn our attention to the energy source terms. The energy source is a known input, and so it is possible to calculate the vertically averaged source. Therefore, we choose $\hat{r}$ to be a vertically averaged heat source, thus making it independent of z. The terms containing the energy source in (7.2.15) are

$$\int_0^{h(\mathbf{x},t)}\frac{\hat{r}}{\hat{\theta}}\,dz-\frac{1}{\theta}hr \tag{7.2.16}$$

which, by using the definition of r given in (7.1.16) and the definition of θ given in (7.1.32), can be written

$$\int_0^{h(\mathbf{x},t)} \frac{\hat{r}}{\hat{\theta}}\, dz - \frac{1}{h}\int_0^{h(\mathbf{x},t)} \frac{1}{\hat{\theta}}\, dz \int_0^{h(\mathbf{x},t)} \hat{r}\, dz. \tag{7.2.17}$$

As $\hat{r}$ does not depend on z, the right hand side can be rearranged to give

$$\int_0^{h(\mathbf{x},t)} \frac{\hat{r}}{\hat{\theta}}\, dz - \frac{1}{\theta}hr = \int_0^{h(\mathbf{x},t)} \frac{\hat{r}}{\hat{\theta}}\, dz - \frac{1}{h}\int_0^{h(\mathbf{x},t)} \frac{\hat{r}}{\hat{\theta}}\, dz\, h = 0, \tag{7.2.18}$$

and so (7.2.15) is satisfied for the energy source terms.

Mass Flux and Solidification Terms

The next group of terms to define relate to the movement of mass and the changing of the phase of solidification. It requires that the following constraint holds:

$$\nabla\mu_h \cdot (h\mathbf{j}) - j_T F\mu_h + j_B\mu_h + \mu_\phi\gamma \leqslant 0. \tag{7.2.19}$$

Almost universally in energetically derived solidification models, the change of phase is driven by the chemical potential of the energy functional with respect to the phase. Therefore, as in Chapter 5 we postulate the constitutive class of

$$\gamma = \gamma(\mu_\phi). \tag{7.2.20}$$

From Chapter 4, evaporation of the material is driven by the chemical potential relating to the height of the film, while the flow of the material is driven by the gradient of this property and the height of the film. In addition, it is obvious that the phase of solidification has an impact on the movement of mass of the film. We postulate the classes

$$\mathbf{j} = \mathbf{j}(h, \phi, \nabla\mu_h), \tag{7.2.21}$$

$$j_T = j_T(\phi, \mu_h) \tag{7.2.22}$$

and

$$j_B = j_B(\phi, \mu_h). \tag{7.2.23}$$

With these constituent classes defined, we pick

$$\gamma = -k_1 \mu_\phi \tag{7.2.24}$$

for a positive constant $k_1 \geqslant 0$,

$$\mathbf{j} = -m_1(h, \phi)\nabla \mu_h, \tag{7.2.25}$$

$$j_T = m_2(\phi)\mu_h, \tag{7.2.26}$$

and

$$j_B = -m_3(\phi)\mu_h \tag{7.2.27}$$

for mobility functions $m_i(\theta, \phi) \geqslant 0$ for $i = 1, 2, 3$. The choice for $\mathbf{j}$ is consistent with the form derived in Chapter 4 which is equivalent to both energetically derived models as well as asymptotically derived models [37, 38] from literature. The terms for mass flux across the boundary, j_T and j_B represent evaporation of the film. In the case of a non-volatile film such as that used in the previous chapters, $m_2 = m_3 = 0$. The form of j_T is consistent with that postulated by Thiele [58] for a volatile liquid film. However the evaporative terms in the model by Burelbach et al. were not derived with energetic considerations in mind, and we have been unable to prove that they are consistent with the second law of thermodynamics, and therefore comparisons here are not made.

From these choices, it can be seen that the evolution of the film exhibits Cahn-Hilliard like properties, while evaporation acts like the Allen-Cahn equation derived in Chapter 2

Recalling that $\phi(\mathbf{x})$ is defined as 1 if the film is liquid at point $\mathbf{x}$ and 0 if the film is solid, with a smooth transition between the phases, a clear choice for the form of m_1 would be

$$m_1(h, \phi) = \phi m_1'(h) \tag{7.2.28}$$

for a function $m_1' \geqslant 0$. This dependence on ϕ ensures that if the film is solid, the mass does not move and evaporation does not occur. In addition, as the film transitions from a liquid into a solid, the mobility decreases.

Heat Flux Terms

Next we turn attention to the terms containing the flux of heat both within the main body of the material $\mathbf{q}$ and across the top and bottom boundaries q_T and q_B. Our choices are required to satisfy

$$\begin{aligned} &-\nabla \cdot \left(\int_0^{h(\mathbf{x},t)} \frac{\hat{\mathbf{q}}}{\hat{\theta}} \, dz \right) + \nabla \cdot \left(\frac{1}{\theta} h \mathbf{q} \right) + \frac{1}{\theta^2} h \mathbf{q} \cdot \nabla \theta \\ &+ \frac{1}{\theta} q_T F - \frac{1}{\theta} q_B - \frac{q_T F}{\theta_T} + \frac{q_B}{\theta_B} \leqslant 0. \end{aligned} \tag{7.2.29}$$

Initially we consider the difference between the vertically averaged heat flux term and the un-averaged term,

$$-\nabla \cdot \left(\int_0^{h(\mathbf{x},t)} \frac{\hat{\mathbf{q}}}{\hat{\theta}} \, dz \right) + \nabla \cdot \left(\frac{1}{\theta} h \mathbf{q} \right), \tag{7.2.30}$$

which can be written

$$-\nabla \cdot \left[h \left(\frac{1}{h} \int_0^{h(\mathbf{x},t)} \frac{\hat{\mathbf{q}}}{\hat{\theta}} \, dz - \frac{1}{\theta} \mathbf{q} \right) \right]. \tag{7.2.31}$$

The vertical integral contains non-averaged terms, and so this is a similar closure problem to that described in Chapter 6. The term in the round brackets is the difference between the vertical average of a product of two variables and the product of the vertical average of the product. We call this difference **K**, so that

$$\mathbf{K} = \frac{1}{h}\int_0^{h(\mathbf{x},t)} \frac{\hat{\mathbf{q}}}{\hat{\theta}}\, dz - \frac{1}{\theta}\mathbf{q}. \tag{7.2.32}$$

We note that **K** is a vertically averaged quantity which accounts for fluctuations in $\hat{\mathbf{q}}$ and $\hat{\theta}$ in the z-direction, and is itself not dependent on z. As in Chapter 6, we write

$$\hat{\mathbf{q}}(\mathbf{x}, z) = \mathbf{q}(\mathbf{x}) + \tilde{\mathbf{q}}(\mathbf{x}, z) \tag{7.2.33}$$

and

$$\hat{\theta}^{-1}(\mathbf{x}, z) = \theta^{-1}(\mathbf{x}) + \tilde{\theta}^{-1}(\mathbf{x}, z). \tag{7.2.34}$$

where a tilde represents the deviation in the z-direction from the vertically averaged value. From these definitions it is clear that

$$\frac{1}{h}\int_0^{h(\mathbf{x},t)} \tilde{\mathbf{q}}\, dz = \frac{1}{h}\int_0^{h(\mathbf{x},t)} \tilde{\theta}^{-1}\, dz = 0. \tag{7.2.35}$$

Taking the product of (7.2.33) and (7.2.34), integrating over the interval $[0, h(\mathbf{x}, t)]$ and substituting the result into (7.2.32) results in

$$\mathbf{K} = \frac{1}{h}\int_0^{h(\mathbf{x},t)} \tilde{\mathbf{q}}\tilde{\theta}^{-1}\, dz. \tag{7.2.36}$$

This results now in only the single term **K** needing to be modelled. We can write (7.2.29) as

$$-\nabla\cdot(h\mathbf{K}) + \frac{1}{\theta^2}h\mathbf{q}\cdot\nabla\theta + \frac{1}{\theta}q_T F - \frac{1}{\theta}q_B - \frac{q_T F}{\theta_T} + \frac{q_B}{\theta_B} \leqslant 0. \tag{7.2.37}$$

We now postulate that the heat flux within the material is dependent on the temperature gradient, and state that

$$\mathbf{q} = \mathbf{q}(\nabla\theta). \tag{7.2.38}$$

Within this constituent class we make the choice of

$$\mathbf{q} = -k_2 \nabla \theta \tag{7.2.39}$$

for a positive constant $k_2 > 0$. This choice of $\mathbf{q}$ is consistent with the choice (5.2.28) made in the case of bulk solidification. This also corresponds with many other works in the literature, [29, 43].

As in Chapter 6, we assume that if $\theta_T(\mathbf{x}) = \theta_B(\mathbf{x})$ then the temperature does not vary in the z-direction. We therefore postulate that $h\mathbf{K}$ takes the form

$$\mathbf{K} = \mathbf{q}'(\theta_T - \theta_B) \tag{7.2.40}$$

for some function $\mathbf{q}'$. As in Chapter 6, if the gradient of the difference of the boundary temperatures is nonzero, one would expect to see temperature fluctuations in the z-direction, and so we pose the constitutive class

$$\mathbf{q}' = \mathbf{q}'(\nabla(\theta_T - \theta_B)). \tag{7.2.41}$$

With these choices, we can write

$$\nabla \cdot (h\mathbf{K}) = (\theta_T - \theta_B)\nabla(h\mathbf{q}') + h\mathbf{q}' \cdot \nabla(\theta_T - \theta_B). \tag{7.2.42}$$

Substituting this into (7.2.37) gives

$$-(\theta_T - \theta_B)\nabla(h\mathbf{q}') - h\mathbf{q}' \cdot \nabla(\theta_T - \theta_B) + \frac{1}{\theta} q_T F - \frac{1}{\theta} q_B - \frac{q_T F}{\theta_T} + \frac{q_B}{\theta_B} \leqslant 0. \tag{7.2.43}$$

Note we have omitted the term containing $h\mathbf{q}$ as $\mathbf{q}$ has already been chosen to satisfy the constraint. Factorising the terms relating to q_T and q_B

results in

$$\begin{aligned}&-(\theta_T-\theta_B)\nabla(h\mathbf{q}')-h\mathbf{q}'\cdot\nabla(\theta_T-\theta_B)+q_TF\left(\frac{1}{\theta}-\frac{1}{\theta_T}\right)-q_B\left(\frac{1}{\theta}-\frac{1}{\theta_B}\right)\\&=-(\theta_T-\theta_B)\nabla(h\mathbf{q}')-h\mathbf{q}'\cdot\nabla(\theta_T-\theta_B)+\frac{q_TF}{\theta\theta_T}(\theta_T-\theta)-\frac{q_B}{\theta\theta_B}(\theta_B-\theta)\\&\leqslant 0.\end{aligned} \tag{7.2.44}$$

Recalling constitutive class (7.2.41), we pick

$$\mathbf{q}'=k_4\nabla(\theta_T-\theta_B) \tag{7.2.45}$$

for some function $k_4\geqslant 0$ to ensure the second term in this equation is always non-negative. It remains to define q_T and q_B such that the constraint always holds. We postulate constitutive classes of

$$q_T=q_T\left(h,\nabla h,\theta,\theta_T,\nabla(\theta_T-\theta_B),\Delta(\theta_T-\theta_B)\right) \tag{7.2.46}$$

and

$$q_B=q_B\left(h,\nabla h,\theta,\theta_B,\nabla(\theta_T-\theta_B),\Delta(\theta_T-\theta_B)\right). \tag{7.2.47}$$

The first term of (7.2.44) can be split to give

$$(\theta_T-\theta_B)\nabla(h\mathbf{q}')=(\theta_T-\theta+\theta-\theta_B)\nabla(h\mathbf{q}'), \tag{7.2.48}$$

which enables the constraint to be split into two separate constraints; one handling the heat flux over the top boundary and the other handling the heat flux over the bottom boundary:

$$-(\theta_T-\theta)\nabla\cdot[hk_4\nabla(\theta_T-\theta_B)]+\frac{q_TF}{\theta\theta_T}(\theta_T-\theta)\leqslant 0, \tag{7.2.49}$$

and

$$-(\theta-\theta_B)\nabla\cdot\left[hk_4\nabla(\theta_T-\theta_B)\right]-\frac{q_B}{\theta\theta_B}\left(\theta_B-\theta\right)\leqslant 0. \tag{7.2.50}$$

From these constraints, we define

$$q_T=\frac{\theta\theta_T}{F}\left[\nabla\cdot\left(hk_4\nabla_{\mathbf{x}}(\theta_T-\theta_B)\right]-k_5(\theta_T-\theta)\right. \tag{7.2.51}$$

and

$$q_B=\theta\theta_B\left[\nabla\cdot\left(hk_4\nabla_{\mathbf{x}}(\theta_T-\theta_B)\right]+k_6(\theta_B-\theta)\right. \tag{7.2.52}$$

for functions $k_5\geqslant 0$ and $k_6\geqslant 0$.

These choices align with the choices made in Chapter 6, along with the claims made in [102]. With the choices made in this section, constraint (7.2.29) reduces to

$$-k_5F(\theta_T-\theta)^2-k_6(\theta_B-\theta)^2-\frac{1}{\theta^2}k_2h|\nabla\theta|^2\leqslant 0. \tag{7.2.53}$$

Entropy on the Diffuse Boundary

Finally, we consider the entropy on the diffuse boundary, **k**. As previously discussed, this term is related to uncertainties on the diffuse boundary, and accounts for the variations averaged out in the vertical direction. The part of (7.2.15) relating to these terms is

$$-\nabla\cdot(h\mathbf{k})+\nabla\cdot\left(h\frac{\partial_{\nabla\phi}\Psi}{\theta}\dot{\phi}\right)+\nabla\cdot\left(h\frac{\partial_{\nabla h}\Psi}{\theta}\dot{h}\right)\leqslant 0. \tag{7.2.54}$$

We postulate a constituent class

$$\mathbf{k}=\mathbf{k}(\Gamma,\mu_h,\nabla\mu_h,\mu_\phi,\nabla\mu_\phi), \tag{7.2.55}$$

and make the choice of

$$\mathbf{k} = \frac{\partial_{\nabla\phi}\Psi}{\theta}\dot{\phi} + \frac{\partial_{\nabla h}\Psi}{\theta}\dot{h}. \tag{7.2.56}$$

With this choice, (7.2.54) becomes

$$\nabla \cdot \left[-h\left(\frac{\partial_{\nabla\phi}\Psi}{\theta}\dot{\phi} + \frac{\partial_{\nabla h}\Psi}{\theta}\dot{h}\right) + h\frac{\partial_{\nabla\phi}\Psi}{\theta}\dot{\phi} + h\frac{\partial_{\nabla h}\Psi}{\theta}\dot{h}\right] = 0. \tag{7.2.57}$$

Having now chosen a constitutive class for Ψ and defined all parameters such that (7.2.15) holds for this constituent class, we now proceed to pick a specific Ψ and finalise the model.

7.3 Internal Energy and the Free Energy

As in previous chapters, we state that the internal energy of the film can be written as a function of ϕ and θ in the form

$$e = u(\theta)v(\phi) + w(\phi). \tag{7.3.1}$$

We once again make the assumption that $v(\phi) = 1$ and that the energy relating to varies linearly in all non-extreme cases and so write

$$e = c\theta + w(\phi). \tag{7.3.2}$$

In this expression, $c\theta$ represents the energy in the system due to the internal heat. $w(\phi)$ represents the latent heat of phase change, defined to be the amount of energy gained or lost during the change of phase of a material without the temperature.

Multiplying through by h and differentiating the result with respect to time we obtain

$$(\dot{he}) = ch\dot{\theta} + c\dot{h}\theta + hw'(\phi)\dot{\phi} + \dot{h}w(\phi). \tag{7.3.3}$$

Using (7.1.19) along with (7.2.39), (7.2.51) and (7.2.52) we obtain the heat transfer equation

$$\begin{aligned}c h\dot{\theta} =& -c\dot{h}\theta - hw'(\phi)\dot{\phi} - \dot{h}w(\phi) + \nabla\cdot hk_2\nabla\theta - \\ &(\theta_T-\theta_B)\theta\left[\nabla\cdot(hk_4\nabla(\theta_T-\theta_B))\right] + k_5F(\theta_T-\theta) + k_6(\theta_B-\theta) + hr.\end{aligned} \tag{7.3.4}$$

The final two terms in (7.3.4) suggest that if the average temperature inside the material, θ, is greater than the external temperature on one of the boundaries, θ_T or θ_B, energy is lost through this surface. Conversely, if θ is lower than the boundary temperature θ_T, energy is absorbed through the boundary.

The temperature equation combined with (7.1.11) and (7.1.31) give the final system of equations for describing the evolution of a solidifying thin film:

$$\begin{aligned}c h\dot{\theta} =& -c\dot{h}\theta - hw'(\phi)\dot{\phi} - \dot{h}w(\phi) + \nabla\cdot hk_2\nabla\theta - \\ &(\theta_T-\theta_B)\theta\left[\nabla\cdot(hk_4\nabla(\theta_T-\theta_B))\right] + k_5F(\theta_T-\theta) + k_6(\theta_B-\theta) + hr,\end{aligned} \tag{7.3.5}$$

$$\dot{h} = \nabla\cdot hm_1\nabla\mu_h - (m_2F + m_3)\mu_h, \tag{7.3.6}$$

$$\dot{\phi} = -k_1\mu_\phi, \tag{7.3.7}$$

where

$$\mu_h = \frac{\Psi}{\theta} + h\frac{\partial_h\Psi}{\theta} - \nabla\cdot\left(h\frac{\partial_{\nabla h}\Psi}{\theta}\right), \tag{7.3.8}$$

and

$$\mu_\phi = h\frac{\partial_\phi\Psi}{\theta} - \nabla\cdot\left(h\frac{\partial_{\nabla\phi}\Psi}{\theta}\right). \tag{7.3.9}$$

It now remains to define a free energy. Recall that $\Psi = e - \theta\eta$, and also that $\eta = -\partial_\theta\Psi$. Therefore

$$e = -\theta^2\frac{\partial}{\partial\theta}\left(\frac{\Psi}{\theta}\right), \tag{7.3.10}$$

which by substituting in e can be written

$$c\theta + w(\phi) = -\theta^2 \frac{\partial}{\partial \theta}\left(\frac{\Psi}{\theta}\right). \tag{7.3.11}$$

Also recalling that the constituent class of $\Psi = \Psi(\theta, \phi, h, \nabla\phi, \nabla h)$, then by dividing through by $-\theta^2$ and integrating with respect to θ we obtain the form of the free energy to be

$$\frac{\Psi}{\theta} = -c \ln\theta + \frac{w(\phi)}{\theta} + G(\phi, \nabla\phi, h, \nabla h), \tag{7.3.12}$$

where $G(\phi, \nabla\phi, h, \nabla h)$ is still to be picked. In the next two sections we propose two different models based on differing choices for Ψ. As both models are chosen within the constituent class of Ψ, they are both thermodynamically consistent.

7.4 Specific Models

In this section we present two thermodynamically consistent models that fit within the framework derived in the previous sections of this chapter. We start by identifying a function for the latent heat $w'(\phi)$ which is used in both models. The final models are then presented.

7.4.1 Latent Heat

To model the latent heat of phase change, we are required to define a function that is 0 in the pure phases, and so we define $w(\phi)$ such that

$$w'(0) = w'(1) = 0. \tag{7.4.1}$$

We follow similar methods to those used by Penrose and Fife [47] and take the latent heat function to be quadratic, and therefore $w(\phi)$ to be cubic, by defining

$$w(\phi) = \lambda_0(-4\phi^3 + 6\phi^2 - 1) \tag{7.4.2}$$

for some constant $\lambda_0 > 0$, the magnitude of which describes the amount of energy that is released during the liquid-to-solid phase transition. The reason behind picking $w(\phi)$ to be cubic is for numerical purposes and is made clear in Chapter 8.

7.4.2 Model A

For the first model, we make the choice of

$$\begin{aligned}\frac{\Psi}{\theta} = -c\ln\left(\frac{\theta}{\theta_0}\right) + \frac{1}{\theta}\left(1 - \frac{\theta}{\theta_0}\right)w(\phi) + \frac{W_1(\phi)}{\theta_0} + \frac{\sigma_1^2}{2\theta_0}|\nabla\phi|^2 \\ + \frac{W_2(h)}{\theta_0} + \frac{\sigma_2^2}{2\theta_0}|\nabla h|^2,\end{aligned} \tag{7.4.3}$$

where θ_0 is the melting point of the material. The $1 - \theta/\theta_0$ dictates whether latent heat is added or taken away during phase transition. If the average temperature of the material is lower than its melting point, $\theta/\theta_0 < 1$, then the energy contribution is positive; this is equivalent to energy being released during solidification. If the temperature is higher than the melting point, $\theta/\theta_0 > 1$, this term is negative, suggesting energy is absorbed during melting.

As in previous chapters, $W_1(\phi)$ and $W_2(h)$ are the free energy potentials relating to the phase and height functions respectively. $W_1(\phi)$ has minima at $\phi = 0$ and $\phi = 1$ and $W_2(h)$ has a minimum point at $h = 0$. The term containing σ_1 represents the contribution to the free energy on the diffuse interface between the pure phases, and the term containing σ_2 represents surface tension.

As in Chapter 5, we non-dimensionalise the temperature parameter by defining $\bar{\theta} = \theta/\theta_0$, and so the chemical potentials for this choice of free energy are given by

$$\mu_\phi = \frac{1}{\theta_0}\left(h\frac{(1-\bar{\theta})}{\bar{\theta}}w'(\phi) + hW_1'(\phi) - \nabla\cdot\left(h\sigma_1^2\nabla\phi\right)\right), \tag{7.4.4}$$

and

$$\mu_h = \frac{1}{\theta_0}\left(\frac{\Psi}{\bar{\theta}} + hW_2'(h) - \nabla\cdot\left(\sigma_2^2 h\nabla h\right)\right). \tag{7.4.5}$$

Applying a similar non-dimensionalisation of $\bar{\theta}_T = \theta_T/\theta_0$ and $\bar{\theta}_B = \theta_B/\theta_0$ to the boundary temperatures, the final system of equations describing the evolution of a thin film undergoing solidification is given by

$$\begin{aligned}\bar{c}h\dot{\bar{\theta}} =& -\bar{c}\dot{h}\bar{\theta} - hw'(\phi)\dot{\phi} - \dot{h}w(\phi) + \nabla\cdot\left(h\bar{k}_2\nabla\bar{\theta}\right) - \\ &(\bar{\theta}_T - \bar{\theta}_B)\bar{\theta}\left[\nabla\cdot\left(h\bar{k}_4\nabla(\bar{\theta}_T - \bar{\theta}_B)\right)\right] + \bar{k}_5F(\bar{\theta}_T - \bar{\theta}) + \bar{k}_6(\bar{\theta}_B - \bar{\theta}) + hr,\end{aligned} \tag{7.4.6}$$

$$\dot{h} = \nabla\cdot\left(h\bar{m}_1\nabla\mu_h\right) - (\bar{m}_2F + \bar{m}_3)\mu_h, \tag{7.4.7}$$

$$\dot{\phi} = -\bar{k}_1\mu_\phi, \tag{7.4.8}$$

with

$$\mu_h = \frac{\Psi}{\bar{\theta}} + hW_2'(h) - \nabla\cdot\left(\sigma_2^2 h\nabla h\right), \tag{7.4.9}$$

and

$$\mu_\phi = h\frac{(1-\bar{\theta})}{\bar{\theta}}w'(\phi) + hW_1'(\phi) - \nabla\cdot\left(h\sigma_1^2\nabla\phi\right), \tag{7.4.10}$$

where $\bar{c} = c\theta_0$, $\bar{k}_1 = k_1/\theta_0$, $\bar{k}_2 = k_2\theta_0$, $\bar{k}_4 = k_4\theta_0^3$, $\bar{k}_5 = k_5\theta_0$, $\bar{k}_6 = k_6\theta_0$ and $\bar{m}_i = m_i/\theta_0$ for $i = 1, 2, 3$.

7.4.3 Model B

In the derivation of the system, Ψ, ϕ and θ are vertically averaged quantities. However, taking the vertical average of the height function would not make physical sense, and so the variable h is not vertically averaged.

To represent this, we consider a free energy split into two; the first, Ψ_1 relating to the vertically averaged quantities and the second, Ψ_2 containing the h terms. To account for the fact that Ψ_2 is not vertically averaged, we multiply this term by a factor of $1/h$ resulting in

$$\frac{\Psi}{\theta} = \Psi_1(\theta, \phi, \nabla\phi) + \frac{1}{h}\Psi_2(h, \nabla h). \tag{7.4.11}$$

We define

$$\Psi_1 = -c\ln\left(\frac{\theta}{\theta_0}\right) + \frac{1}{\theta}\left(1 - \frac{\theta}{\theta_0}\right)w(\phi) + \frac{W_1(\phi)}{\theta_0} + \frac{\sigma_1^2}{2\theta_0}|\nabla\phi|^2 \tag{7.4.12}$$

and

$$\Psi_2 = \frac{W_2(h)}{\theta_0} + \frac{\sigma_2^2}{2\theta_0}|\nabla h|^2, \tag{7.4.13}$$

where each terms represents the same phenomena as in the choice for Model A. Following the same non-dimensionalisation as for Model A, the the chemical potentials for the new choice of free energy become

$$\mu_h = \frac{1}{\theta_0}\left(\Psi_1 + W_2'(h) - \sigma_2^2\Delta h\right) \tag{7.4.14}$$

and

$$\mu_\phi = \frac{1}{\theta_0}\left(h\frac{(1-\bar{\theta})}{\bar{\theta}}w'(\phi) + hW_1'(\phi) - \nabla\cdot\left(h\sigma_1^2\nabla\phi\right)\right). \tag{7.4.15}$$

These chemical potentials are combined with the evolution equations to give the final system of equations

$$\begin{aligned}\bar{c}h\dot{\bar{\theta}} = &-\bar{c}\dot{h}\bar{\theta} - hw'(\phi)\dot{\phi} - \dot{h}w(\phi) + \nabla\cdot\left(h\bar{k_2}\nabla\bar{\theta}\right) - \\ &(\bar{\theta}_T - \bar{\theta}_B)\bar{\theta}\left[\nabla\cdot(h\bar{k_4}\nabla(\bar{\theta}_T - \bar{\theta}_B))\right] + \bar{k_5}F(\bar{\theta}_T - \bar{\theta}) + \bar{k_6}(\bar{\theta}_B - \bar{\theta}) + hr,\end{aligned} \tag{7.4.16}$$

$$\dot{h} = \nabla\cdot(h\bar{m}_1\nabla\mu_h) - (\bar{m}_2F + \bar{m}_3)\mu_h, \tag{7.4.17}$$

$$\dot{\phi} = -\bar{k_1}\mu_\phi, \tag{7.4.18}$$

with

$$\mu_h = \Psi_1 + W_2'(h) - \sigma_2^2 \Delta h, \tag{7.4.19}$$

and

$$\mu_\phi = h\frac{(1-\bar{\theta})}{\bar{\theta}} w'(\phi) + hW_1'(\phi) - \nabla \cdot (h\sigma_1^2 \nabla\phi). \tag{7.4.20}$$

We now have derived two separate thermodynamically consistent models for simulating the evolution of a solidifying thin film. In the next section, we verify the models in order to assure us of their validity.

7.5 Verification of the Models

In this section we investigate the validity of the two models given in (7.4.6-7.4.10) and (7.4.16-7.4.20). Firstly, we confirm that the 2nd law of Thermodynamics is indeed adhered to. We then proceed by showing that, by fixing certain parameters for a given scenario, the model reduces to each of the models derived in Chapters 4 and 6. For the remainder of this work, we drop the bar from the non-dimensionalised parameters.

7.5.1 Thermodynamical Consistency

The first stage in the verification of the model is to ensure that it is consistent with the second law of thermodynamics. This is equivalent to saying that restriction (7.2.15) holds for all energy functionals Ψ with the constitutive class $\Psi = \Psi(\theta, \phi, \nabla\phi, h, \nabla h)$. The restraint is written as

$$\begin{aligned}&-\nabla\cdot(h\mathbf{K}) - \nabla\cdot(h\mathbf{k}) + \nabla\cdot\left(h\frac{\partial_{\nabla h}\Psi}{\theta}\dot{h}\right) + \nabla\cdot\left(h\frac{\partial_{\nabla\phi}\Psi}{\theta}\dot{\phi}\right)\\ &+\frac{1}{\theta^2}(h\mathbf{q})\cdot\nabla\theta + \frac{1}{\theta}q_T F - \frac{1}{\theta}q_B - \frac{1}{\theta}hr - \frac{q_T F}{\theta_T} + \frac{q_B}{\theta_B} + \int_0^{h(\mathbf{x},t)} \frac{\hat{r}}{\hat{\theta}}\,dz \\ &+\nabla\mu_h\cdot(h\mathbf{j}) - j_T F\mu_h + j_B\mu_h + \mu_\phi\gamma \leqslant 0.\end{aligned} \tag{7.5.1}$$

Substituting the derived forms of $\mathbf{K}, \mathbf{k}, \mathbf{q}, q_T, q_B, \mathbf{J}, j_T, j_B$ and γ into the left hand side of this equation gives

$$\begin{aligned} &-\frac{1}{\theta^2} h k_2 |\nabla\theta|^2 - \frac{k_5 F}{\theta\theta_T}(\theta_T - \theta)^2 - \frac{k_6}{\theta\theta_B}(\theta_B - \theta)^2 \\ &- h m_1 |\nabla\mu_h|^2 - (m_2 F + m_3)\mu_h^2 - k_1 \mu_\phi^2 \leqslant 0. \end{aligned} \tag{7.5.2}$$

Thus we have shown that the choices made within this chapter for a constitutive class of $\Psi = \Psi(\theta, \phi, \nabla\phi, h, \nabla h)$ do indeed result in thermodynamically consistent models.

We now proceed to reduce the system of equations to cases that have previously been modelled.

7.5.2 Thin Film Heat Equation

The first model that Model A and Model B are compared to is the thin film heat equation, as derived in Chapter 6. In this derivation, the film is modelled as a single phase scenario, and so we choose $\phi(\mathbf{x})$ to be constant for all $\mathbf{x}$, resulting in $\dot{\phi} = W_1'(\phi) = w'(\phi) = 0$. Similarly, it is assumed that the film is rigid, and so $h(\mathbf{x}, t) = h_0(\mathbf{x})$ and $\dot{h} = 0$. To achieve this, we set $m_1 = m_2 = m_3 = 0$. Substituting these simplifications into both (7.4.6-7.4.10) and (7.4.16-7.4.20) results in the equation

$$\begin{aligned} c h_0 \dot{\theta} = \nabla \cdot (h_0 k_2 \nabla\theta) - (\theta_T - \theta_B)\theta \left[\nabla \cdot (h_0 k_4 \nabla(\theta_T - \theta_B))\right] + \\ k_5 F(\theta_T - \theta) + k_6(\theta_B - \theta) + h_0 r. \end{aligned} \tag{7.5.3}$$

This is identical to the model (6.3.42), and so the reduced thin film solidification models are consistent with the thin film heat equation derived in Chapter 6.

7.5.3 Thin Film Flow

Next, we look to reduce equations (7.4.6-7.4.10) and (7.4.16-7.4.20) to a model simulating the evolution of a thin film which is not undergoing a change in state of solidification. To negate the consideration of temperature and phase, we set $\Psi_1 = 0$. In addition, as the film is in an isothermal setting, we fix $\theta = \theta_T = \theta_B$ to be constant. Substituting these assumptions into Model A results in

$$\dot{h} = \nabla \cdot (hm_1 \nabla \mu_h), \tag{7.5.4}$$

$$\mu_h = \Psi_2 + hW_2'(h) - \nabla \cdot \left(\sigma_2^2 h \nabla h\right). \tag{7.5.5}$$

It is clear that this is not equivalent to the system (4.3.22-4.3.23), and thus we have provided a new alternative.

Implementing the same assumptions, Model B reduces to

$$\dot{h} = \nabla \cdot (hm_1 \nabla \mu_h), \tag{7.5.6}$$

$$\mu_h = W_2'(h) - \sigma_2^2 \Delta h, \tag{7.5.7}$$

which is equivalent to (4.3.22-4.3.23). As we have shown in Chapter 4 that this model is equivalent to both energetically and asymptotically derived models for non volatile thin film flow, we proceed by studying Model B, as it is a more natural extension from the simpler models. However, it should be noted that Model A is not invalidated, and it, along with other choices for Ψ/θ could prove useful in future work.

We have now shown that Model B is both thermodynamically consistent, and that is it consistent with models that describe less complex scenarios. We thus have provided with system (7.4.16-7.4.20) a valid model for describing the evolution of a solidifying thin film in an non isothermal setting. In the final chapter, we investigate this model by presenting simulations for a variety of cases.

CHAPTER 8

Numerical Simulations

This chapter provides numerical simulations for Model B (system (7.4.16)-(7.4.20)). This model describes a solidifying thin film, and it was derived in Chapter 7 to be thermodynamically consistent. Firstly in this chapter we simulate a non volatile thin film on a flat impermeable substrate and investigate the effect that solidification has on the evolution of the film by comparing it to the results in Chapter 4. We consider films undergoing phase changes from liquid to solid and also from solid to liquid. We then allow for evaporation to occur and investigate how the rate of evaporation effects the final morphology of the film.

8.1 Numerical Methods

To simulate the system of equations, we employ linear finite elements for the spatial discretisation. For the time discretisation, we employ a convex splitting method as described in Section 3.2.2 for the terms containing the energy potential terms. For this system of equations, this involves finding splits for both $W_1(\phi)$ and $W_2(h)$. This process is detailed in Section 8.3. For the remaining non-linear coupling terms, a semi-implicit scheme is implemented. This results in a linear system of equations having to be solved at each time step. The code used for providing these simulations was entirely written for this project, and was based on [50].

For this work, we use a simple fixed mesh spacing, splitting the domain into $N = 100$ equally sized elements. Simulations were carried out starting with a more coarse mesh, and were compared to further simulations performed on a mesh with a greater number of elements. We were satisfied that the mesh was sufficiently refined for our choice of parameters when a further increase in N resulted in no visual changes in the simulations produced at varying time points.

Using these techniques, for the chosen ϵ the simulations took in the range of $1 - 2$ minutes to run. More advanced techniques, such as refining the mesh around interfaces where variables change quickly, would enable smaller values for ϵ to be used; however for the purposes of this work this was deemed unnecessary.

8.2 A Non Volatile Liquid Film on a Substrate

In order to investigate the solidification of a thin film, we start by modelling a simple thin film on a substrate. Initially we make the assumption that $\theta_T = \theta_{T0}$ and $\theta_B = \theta_{B0}$ are constants, although not necessarily the same value. This replicates a scenario such as the manufacture of thin film solar cells: a film is sitting on a substrate heated from below, while the top surface of the film is in contact with the air. We assume the film is not volatile and therefore set $m_2 = m_3 = 0$.

Given that the temperatures on the boundaries are constant, $\nabla(\theta_T - \theta_B) = 0$, and (7.4.16-7.4.20) becomes

$$ch\dot{\theta} = -c\dot{h}\theta - hw'(\phi)\dot{\phi} - \dot{h}w(\phi) + \nabla \cdot (hk_2\nabla\theta) + k_5F(\theta_{T0} - \theta) + k_6(\theta_{B0} - \theta), \tag{8.2.1}$$

$$\dot{h} = \nabla \cdot (hm_1(h, \phi)\nabla\mu_h), \tag{8.2.2}$$

$$\dot{\phi} = -k_1 \mu_\phi, \tag{8.2.3}$$

$$\mu_h = \Psi_1 + W_2'(h) - \sigma_2^2 \Delta h, \tag{8.2.4}$$

$$\mu_\phi = h\frac{(1-\theta)}{\theta} w'(\phi) + hW_1'(\phi) - \sigma_1^2 \nabla \cdot (h\nabla\phi)\,. \tag{8.2.5}$$

To describe a material which is purely liquid at $\phi(\mathbf{x}) = 1$ and purely solid at $\phi(\mathbf{x}) = 0$, it is required that the potential $W_1(\phi)$ is a double well function with minima at both $W_1(\phi) = 0$ and $W_1(\phi) = 1$. We therefore define

$$W_1(\phi) = \phi^2(\phi - 1)^2. \tag{8.2.6}$$

For $W_2(h)$, we refer back to Chapter 4 and make the choice of

$$W_2(h) = -\frac{1}{6}h^{-2}. \tag{8.2.7}$$

We assume that the mobility function $m_1(h, \phi)$ is only linearly dependent on the phase of solidification, and so choose

$$hm_1(h, \phi) = \phi h^3. \tag{8.2.8}$$

This forces the mobility of the film to be zero when it is solid, resulting in there being no flow of material. In addition, when the film is partially solidified at a point $\mathbf{x}$, the mobility is restricted.

8.3 Numerically-Suitable Function Extensions and Convex Splitting

As in Chapter 4, it is required that the functions chosen are regularised to ensure they remain non-negative when, through computational error, the variables h, ϕ or θ become negative. In addition to this, we seek a regularisation of the potentials $W_1(\phi)$ and $W_2(h)$ to functions which can be split into a convex part and a concave part, which is key for employing the Convex Splitting time stepping method described in Chapter 3. It is also required that the regularisation of the function must be continuous with a continuous first derivative.

We first regularise $W_1(\phi)$. The key property of this potential is that it has minima at both $W_1(\phi) = 0$ and $W_1(\phi) = 1$, so this must also hold true for the regularised function. we define the regularised function to be

$$W_1(\phi) = \begin{cases} \phi^2 & \text{if } \phi \leqslant 0, \\ \phi^2(\phi-1)^2, & \text{if } 0 \leqslant \phi \leqslant 1, \\ (\phi-1)^2 & \text{if } \phi \geqslant 1. \end{cases} \tag{8.3.1}$$

The second derivative of $W_1(\phi)$ is

$$W_1''(\phi) = \begin{cases} 2 & \text{if } \phi \leqslant 0, \\ 12\phi^2 - 12\phi + 2 & \text{if } 0 \leqslant \phi \leqslant 1, \\ 2 & \text{if } \phi \geqslant 1, \end{cases} \tag{8.3.2}$$

and it can be seen that $|W_1''(\phi)| \leqslant 2 \ \forall \phi$. Recall that for some function $f(x)$, if $\exists L > 0$ such that $|f''(x)| < L \ \forall x$ then f can be split into the sum of a convex function $f_+(x)$ and a concave function $f_-(x)$ with the convex part given by $f_+(x) = Lx^2/2$ [54]. Given this, we split $W_1(\phi)$ into the convex function

$$W_{1+}(\phi) = \phi^2, \tag{8.3.3}$$

with corresponding concave function

$$W_{1-}(\phi) = \begin{cases} 0 & \text{if } \phi \leqslant 0, \\ \phi^4 - 2\phi^3, & \text{if } 0 \leqslant \phi \leqslant 1, \\ 1 - 2\phi & \text{if } \phi \geqslant 1. \end{cases} \tag{8.3.4}$$

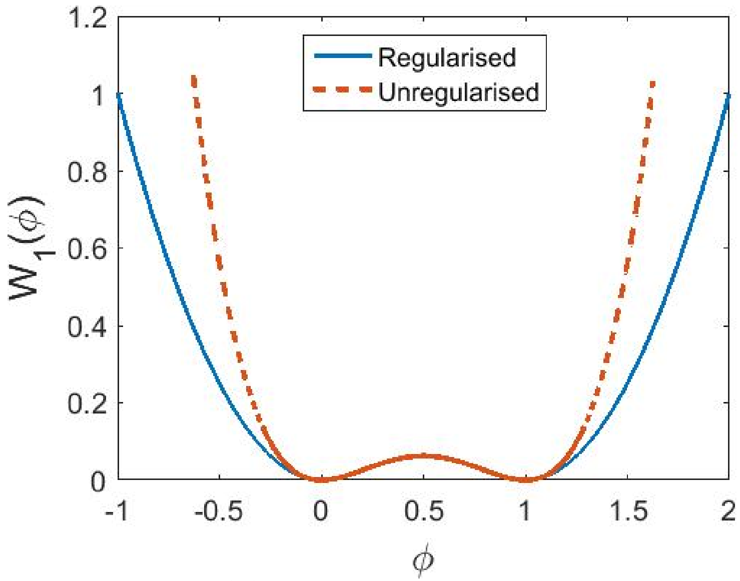

Figure 8.1: Plot of $W_1(\phi)$. The dotted red line is the unregularised function while the blue line represents the regularised function.

The regularised version of $W_1(\phi)$ is shown in Figure 8.3.4 as a solid blue line. The dotted red line shows the unregularised function.

For the function $W_2(h)$ we use the same regularisation as in Chapter 4, by taking a small number $\epsilon > 0$, and by defining

$$W_2(h) = \begin{cases} \frac{1}{6\epsilon^4}h^2 - \frac{1}{3\epsilon^2} & \text{if } h < \epsilon, \\ -\frac{1}{6}h^{-2} & \text{if } h \geq \epsilon. \end{cases} \tag{8.3.5}$$

This regularisation makes $W_2(h)$ quadratic for $h < \epsilon$, and in addition ensures that $W_2(h)$ and $W_2'(h)$ are continuous at all points, in particular $h = \epsilon$. We finally note that the minimum of $W_2(h)$ is found at $h = 0$. A plot of this function can be seen in the bottom panel of Figure 4.6.

Taking the second derivative of $W_2(h)$ results in

$$W_2''(h) = \begin{cases} \frac{1}{3\epsilon^4} & \text{if } h < \epsilon, \\ -\frac{1}{h^4} & \text{if } h \geq \epsilon, \end{cases} \tag{8.3.6}$$

from which it can be seen that $|W_2''(h)| \leqslant \epsilon^{-4}$ and so we take a convex splitting of

$$W_{2+}(h) = \frac{1}{2\epsilon^4}h^2, \tag{8.3.7}$$

with corresponding concave part

$$W_{2-}(h) = \begin{cases} -\frac{1}{3\epsilon^4}h^2 - \frac{1}{3\epsilon^4} & \text{if } h < \epsilon, \\ -\frac{1}{6}h^{-2} - \frac{1}{2\epsilon^4}h^2 & \text{if } h \geq \epsilon. \end{cases} \tag{8.3.8}$$

The next function requiring regularisation is the latent heat function. While this function is already defined such that $w'(0) = w'(1) = 0$, is is important that if numerical inaccuracies lead to either $\phi > 1$ or $\phi < 0$, the energy is unaffected. Thus, we make the regularisation

$$w(\phi) = \begin{cases} -\lambda_0 & \text{if } \phi < 0, \\ \lambda_0(-4\phi^3 + 6\phi^2 - 1) & \text{if } 0 < \phi < 1, \\ \lambda_0 & \text{otherwise.} \end{cases} \tag{8.3.9}$$

This regularised function is plotted in Figure 8.2. From this, it can be seen that when $w(\phi)$ is added to the potential $W_1(\phi)$, the positions of the minima do not change. Having a function $w'(\phi)$ being quadratic is preferable as, for this implemented regularisation, it is continuous for all ϕ.

Finally, for the mobility function we adapt the regularisation made in Chapter 4, and define

$$hm_1(h,\phi) = \begin{cases} 0 & \text{if } h \leqslant 0 \text{ or } \phi \leqslant 0, \\ \phi h^3 & \text{otherwise.} \end{cases} \tag{8.3.10}$$

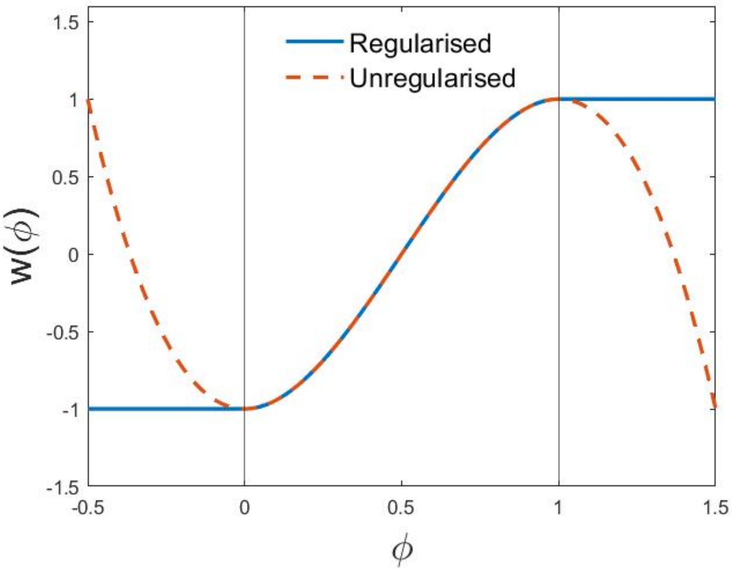

Figure 8.2: Plot of the regularised $w(\phi)$. The dotted red line is the unregularised function while the blue line represents the regularised function.

We now simulate the system for two scenarios; first we look at a liquid thin film undergoing solidification, and secondly we investigate a solid film melting after being heated from below. For both scenarios, we start with a perturbed flat film by setting the initial height function to be

$$h(x,0) = 1 - 0.1\cos\left(\frac{1}{\sqrt{2}}x\right), \tag{8.3.11}$$

and as we are interesting in understanding the behaviour of the film under the chosen conditions, we pick $\epsilon = 0.3$ in the regularisation of $W_2(h)$. If the goal was to produce more realistic results, ϵ would be chosen to be smaller.

8.4 Solidification of a Liquid Film

For a film to undergo solidification from its liquid state, the temperature must be below the melting point of the material. For this reason, we pick $\theta_{T0} = \theta_{B0} = 0.4$. We also take the initial condition of $\theta(x,0) = 0.4$;

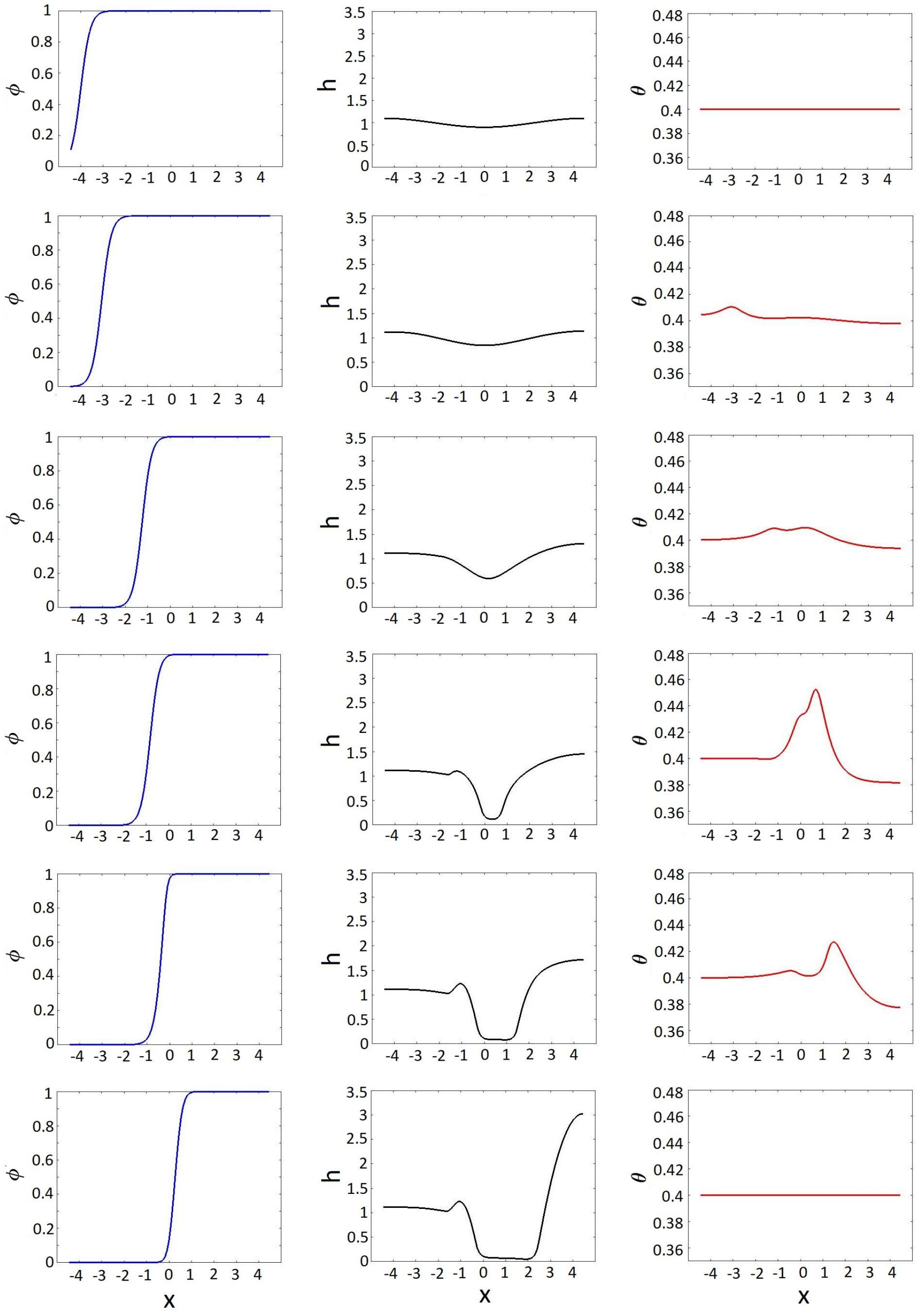

Figure 8.3: The evolution of a solidifying liquid film. The left column shows $\phi(x, t)$, the middle column shows $h(x, t)$ and the right column shows $\theta(x, t)$. The rows show the solutions at times $t = 0, 5, 15, 17.5, 20$ and the equilibrium position. Homogeneous Neumann boundary conditions are used.

this is suggesting that the temperature is in an equilibrium state before the effects of solidification and hole evolution start to contribute. As in Chapter 4, we start with a perturbed flat film, and assume that solidification has nucleated at the left boundary. For this, we set

$$\phi(x,0) = \frac{1}{2} + \frac{1}{2}\tanh\left(\frac{(x+4)}{\sigma_1\sqrt{2}}\right). \tag{8.4.1}$$

We use this initial condition for ϕ as it is a natural choice for an Allen-Cahn type equation.

We set the coefficient of the latent heat $\lambda_0 = 0.1$, and choose $\sigma_1 = 0.3$ and $k_1 = 0.5$. The remaining parameters are set as $\sigma_2 = c = k_2 = k_5 = k_6 = 1$. The results using these parameter settings are shown in Figure 8.3 for times $t = 0, 5, 15, 17.5, 20$ and the equilibrium position. The column on the left shows the evolution of the phase parameter ϕ, the central column depicts the height function of the film above the substrate h, and the right hand column shows the evolution of the average temperature θ.

The top row shows the initial conditions while moving down the rows shows the progression in time. The final row is at a point where h and θ have reached an equilibrium position.

As can be seen from the height function plots, initially the dewetting occurs in a very similar way to the thin film flow modelled in Chapter 4. As the film solidifies, dewetting continues due to the disjoining pressure; however the left boundary becomes fixed, causing a ridge to form. Eventually, hole growth stops as it reaches an equilibrium point. The temperature spike in the second row comes from the latent heat of phase change; as the liquid turns into a solid energy is released as heat. As the film dewets and the height becomes close to zero, additional temperature spikes can be seen (for example in row 4). As the height function of the film height reduces, the average temperature at a point $\mathbf{x}$ increases before it is diffused away, causing this additional spike.

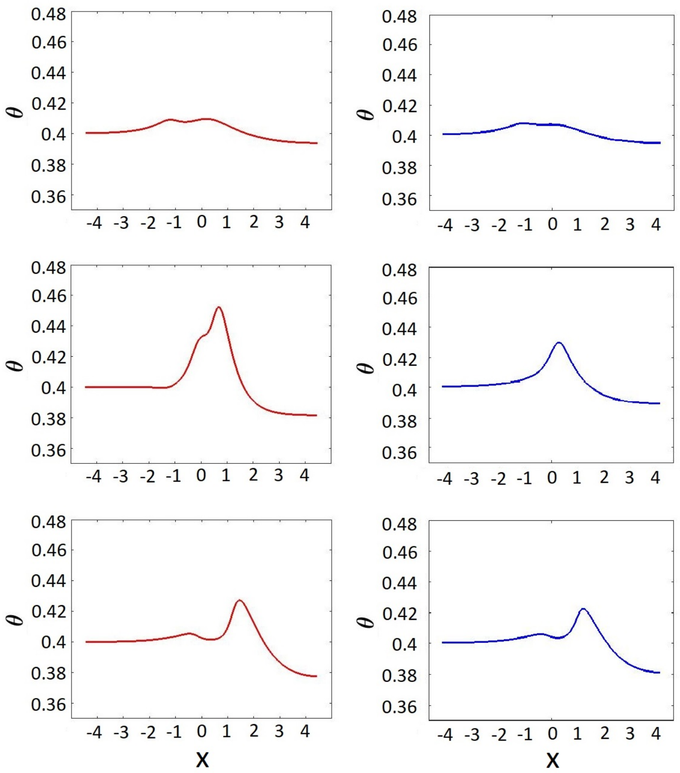

Figure 8.4: The temperature of a solidifying thin film for differing heat diffusion coefficients k_2. In the left hand column, $k_2 = 1$ and in the right hand column $k_2 = 2$. Results are shown at times $t = 15$ (row 1), $t = 17.5$ (row 2) and $t = 20$ (row 3).

This explanation for the origin of this temperature spike can be confirmed by increasing the heat diffusion coefficient k_2 and comparing the results to those shown in Figure 8.3. The left column of Figure **??** shows the temperature at times $t = 15, 17.5$ and 20 when $k_2 = 1$ (as in Figure 8.3), and the right hand column shows the temperature at the same times for $k_2 = 2$. As can be clearly seen, an increase in the heat diffusion coefficient results in a lower spike in temperature as expected.

We now look to vary parameters in order to understand the effect they have on the evolution of the film. In Figure 8.5, we vary the parameter controlling the speed of propagation of solidification, k_1. As can clearly be seen, increasing this parameter results in a smaller hole being formed.

Figure 8.6 demonstrates the effect of varying the coefficient of latent heat.

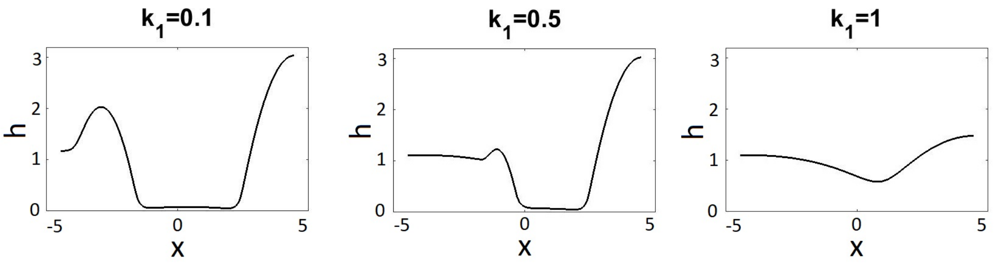

Figure 8.5: The effects on hole growth in a dewetting thin film due to varying the speed of propagation of solidification, k_1.

As with k_1, it can be seen that increasing this value results in the formation of a smaller hole.

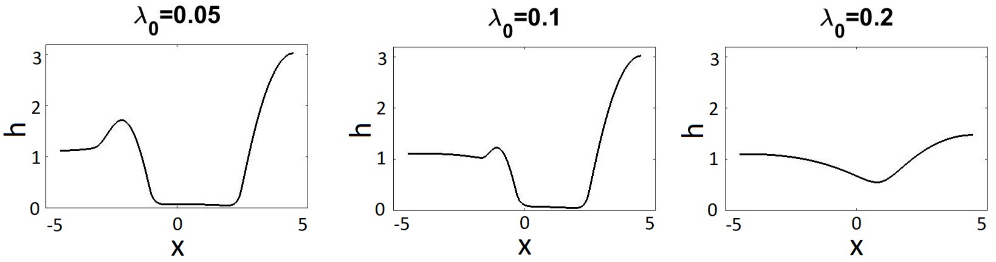

Figure 8.6: The effects on hole growth in a dewetting thin film due to varying the coefficient of latent heat, λ_0

Figure 8.7 shows the effects that the external temperature has on the film formation. When the external temperature is much less than the melting point of the film, as in the left panel, the film solidifies very quickly and very little change in morphology is observed. When the external temperature is close to the melting point, the rate of solidification is greatly reduced, and hole formation is more significant.

8.5 Solid Film Melting on a Heated Substrate

In this section we investigate the effects of putting a solid film with a slight perturbation onto a heated substrate. We set $\theta_{B0} = 2.5$, ensuring that this is above the melting temperature of the film. We set $\theta_{T0} = 2.5$ also - this simulates for example a thin film solar cell being placed

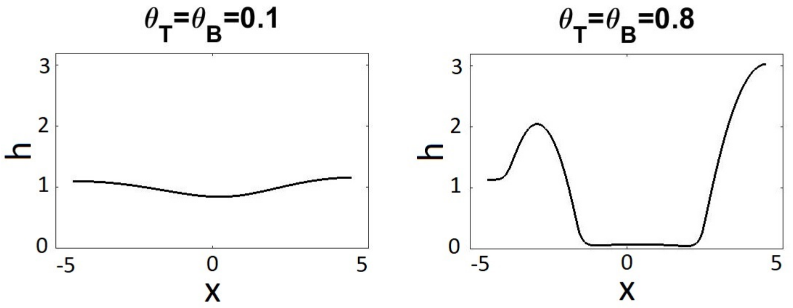

Figure 8.7: The effect on hole growth in a solidifying thin film of varying the boundary temperatures θ_T and θ_B.

into a hot box in which the air temperature has risen to the temperature of the heating plate. For the initial height function, we use the same perturbation used in the previous section, namely

$$h(x,0) = 1 - 0.1\cos\left(\frac{1}{\sqrt{2}x}\right). \tag{8.5.1}$$

For the initial seed for phase-change, we use

$$\phi(x,0) = \frac{1}{2} - \frac{1}{2}\tanh\left(\frac{(x+4)}{\sigma_1\sqrt{2}}\right), \tag{8.5.2}$$

This indicates a liquid film with a seed at the left hand side of the film. Figure 8.8 shows the evolution of a film with these initial conditions, with all parameters set as for Figure 8.3. The time intervals shown are $t = 0, 27.5, 47.5, 55, 60$ and the equilibrium position, reached at approximately $t = 125$. The left column shows the evolution of ϕ and the right column shows the evolution of θ. The black line in the central column shows the evolution of h with the blue line being the initial condition used as a reference. As can be seen, the phase change from a solid into a liquid causes a spike downwards in the temperature as the change from solid to liquid absorbs energy.

Figure 8.9 shows the difference in the evolution of the film when an additional seed for phase change is introduced. In this case, the seed is

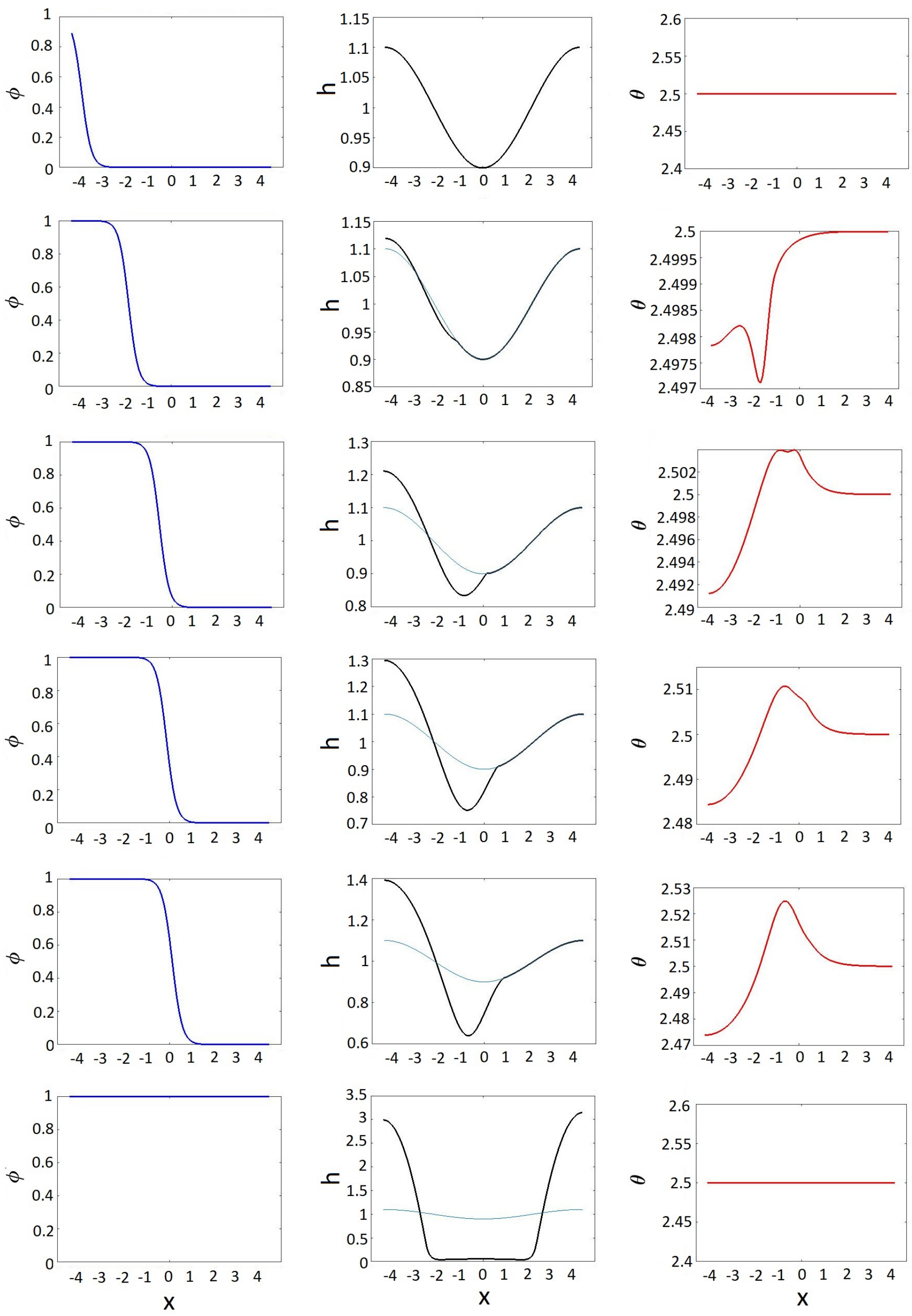

Figure 8.8: The evolution of a melting solid film. The left column shows $\phi(x,t)$, the middle column shows $h(x,t)$ (black line) with the initial condition (blue line) for reference and the right column shows $\theta(x,t)$. The rows show the solutions at times $t = 0, 27.5, 47.5, 55, 60$ and the equilibrium position.

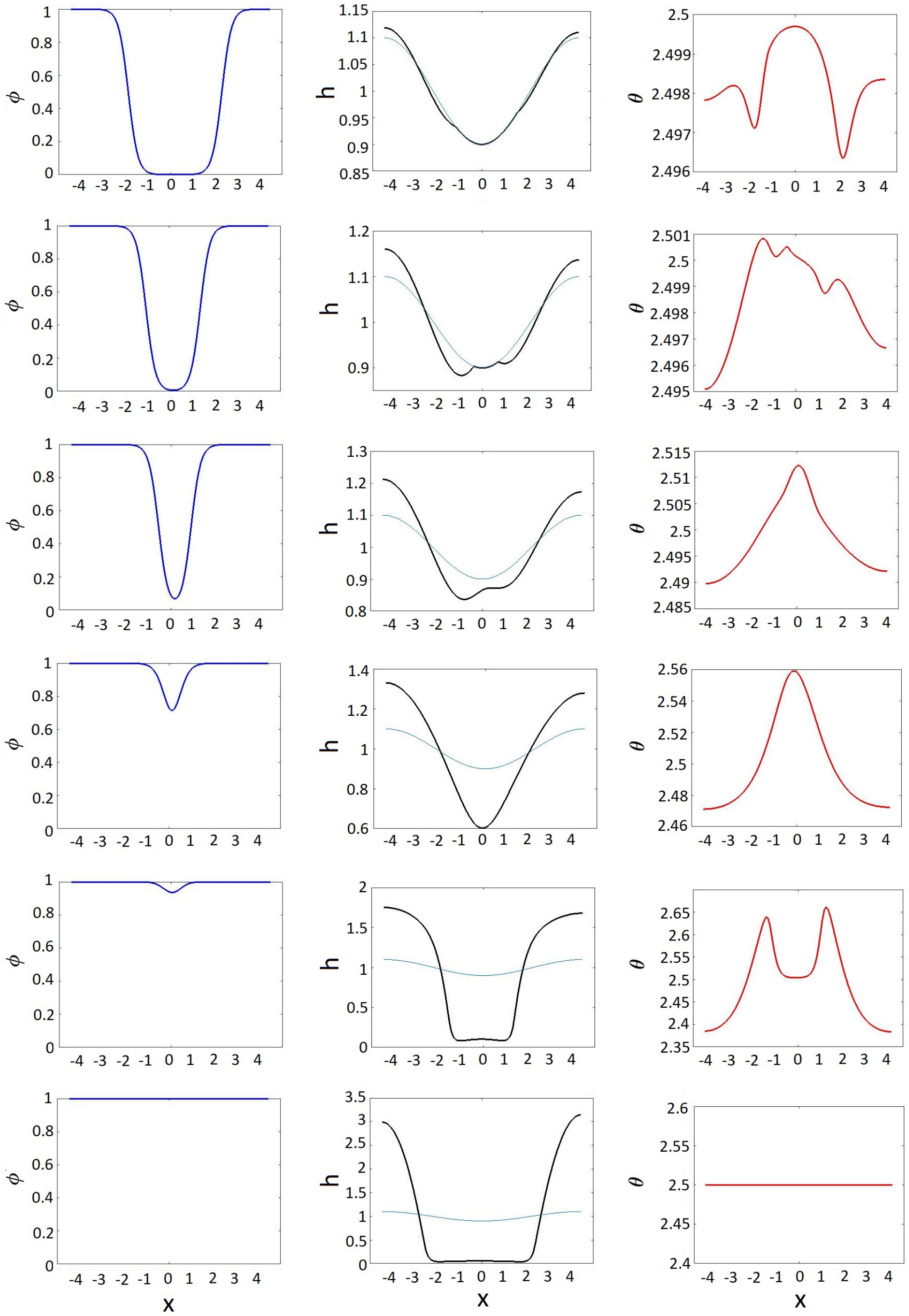

Figure 8.9: The evolution of a melting solid film with two seeds for initiating solidification. The left column shows $\phi(x,t)$, the middle column shows $h(x,t)$ (black line) with the initial condition (blue line) for reference and the right column shows $\theta(x,t)$. The rows show the solutions at times $t = 27.5, 40, 47.5, 55, 60$ and the equilibrium position.

introduced on the right, and the initial condition is given by

$$1 - \frac{1}{2}\tanh\left(\frac{(x+4)}{\sigma_1\sqrt{2}}\right) + \frac{1}{2}\tanh\left(\frac{(x-4.2)}{\sigma_1\sqrt{2}}\right). \tag{8.5.3}$$

The rows in Figure 8.9 show the phase (column 1), height function (column 2) and temperature for times $t = 27.5, 40, 47.5, 55$ and 60. The final row shows the equilibrium position which in this case is reached at around time $t = 87.5$. The equilibrium position reached is the same for both simulations, however the latter simulation reaches this position much quicker.

8.6 Volatile Film on a Heated Substrate

Finally, in this section we investigate the effects of evaporation on a solidifying thin film on a heated substrate. For the temperature on the boundaries, we make the same assumptions as in the previous section that $\theta_T = \theta_{T0}$ and $\theta_B = \theta_{B0}$ are constants. We assume that the substrate that the film is sitting on is non-permeable, and so we still set $m_3 = 0$. However, we now assume that the mobility of the film across the top boundary, m_2 is defined as

$$m_2(\theta, \phi) = k_3\phi \tag{8.6.1}$$

for a positive constant k_3. This makes the assumption that any vapour produced during evaporation is immediately removed. The system of equations that describes the volatile film on a non-permeable heated substrate is now given by

$$ch\dot{\theta} = -c\dot{h}\theta - hw'(\phi)\dot{\phi} - \dot{h}w(\phi) + \nabla \cdot (hk_2\nabla\theta) + k_5F(\theta_{T0} - \theta) + k_6(\theta_{B0} - \theta), \tag{8.6.2}$$

$$\dot{h} = \nabla \cdot (hm_1(h, \phi)\nabla\mu_h) - k_3\phi F\mu_h, \tag{8.6.3}$$

$$\dot{\phi} = -k_1 \mu_\phi, \tag{8.6.4}$$

$$\mu_h = \Psi_1 + W_2'(h) - \sigma_2^2 \Delta h, \tag{8.6.5}$$

$$\mu_\phi = h\frac{(1-\theta)}{\theta} w'(\phi) + hW_1'(\phi) - \sigma_1^2 \nabla \cdot (h \nabla \phi) . \tag{8.6.6}$$

We set the initial film to have the same perturbation as in previous simulations,

$$h(x,0) = 1 - 0.1 \cos\left(\frac{1}{\sqrt{2}} x\right), \tag{8.6.7}$$

and assume there are two seeds of solidification, one on the left and one on the right, by using

$$\phi(x,0) = \frac{1}{2}\tanh\left(\frac{(x+4)}{\sigma_1\sqrt{2}}\right) - \frac{1}{2}\tanh\left(\frac{(x-4)}{\sigma_1\sqrt{2}}\right). \tag{8.6.8}$$

The final height function of the film for varying values of k_3 are shown in Figure 8.10. The remaining parameters for these simulations are set to the same values as for Figure 8.3. The boundary temperatures θ_{T0} and θ_{B0}, and the initial average temperature $\theta(x,0)$ are set at 0.4.

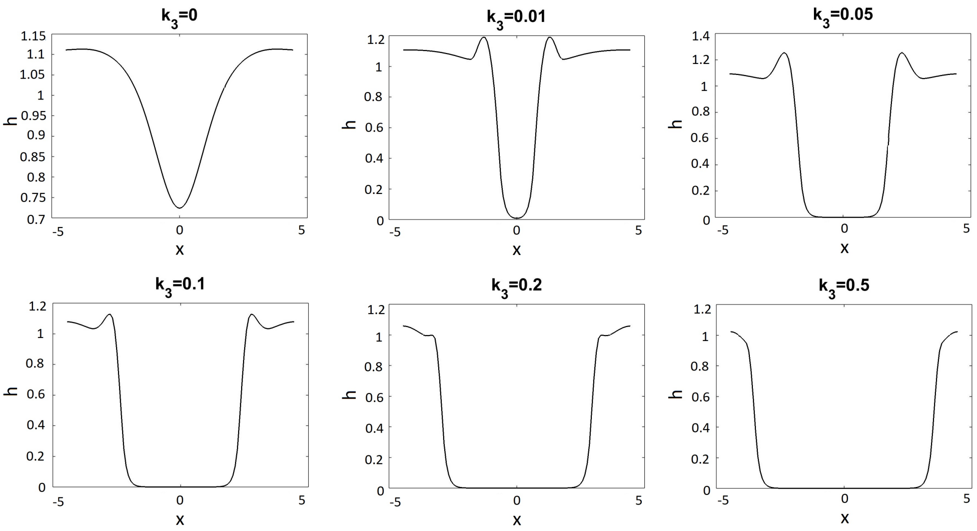

Figure 8.10: The effect changing the rate of evaporation of a solidifying thin film has on hole growth. Each image is shown once the film has fully solidified.

As can be seen, a faster rate of evaporation, represented by a higher value of k_3, results in a much larger hole being formed. This can be explained by more liquid evaporating before the film has a chance to solidify. To investigate the effects on the rate of solidification on a volatile film, we now fix the rate of evaporation $k_3 = 0.1$, and vary the coefficient of solidification propagation, k_1. The results for this are shown in Figure 8.11.

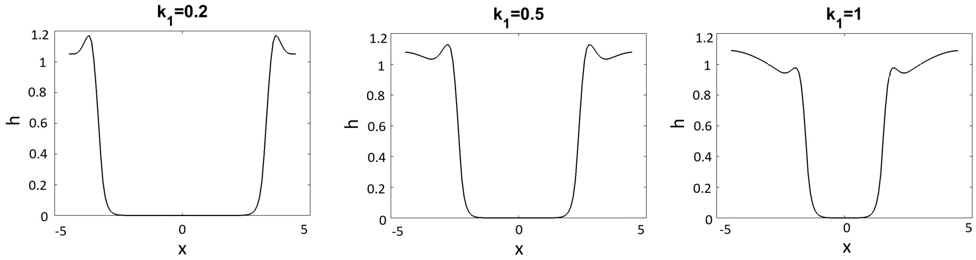

Figure 8.11: The effects on hole growth in a dewetting volatile thin film due to varying the speed of propagation of solidification, k_1.

As can be seen clearly, an increase in the speed of propagation of solidification, k_1, reduces the size of the hole formed in the dewetting thin film. This is due to the fact the film solidifies before it has a chance to dewet fully.

8.7 Conclusions

In this section we have considered Model B derived in Chapter 7 and performed simulations using linear finite elements for the spatial discretisation and a convex splitting algorithm for the time stepping. We have shown how the model can be used to investigate the behaviour of both a non-volatile film and a volatile film when parameters are varied, which will assist in optimising fabrication processes of thin film solar cells, as parameters can be chosen to give the best possible surface coverage.

CHAPTER 9

Conclusions and Recommendations for Future Work

9.1 Conclusions

In this thesis we have presented a rigorous framework for the rational derivation of a family of thermodynamically consistent models describing a number of phenomena: the evolution of the morphology of a thin film; solidification in a bulk material; the transport of heat in a rigid thin film and the solidification of an evolving thin film in a non-isothermal setting. Simulations on the final model have been carried out using an energy stable convex splitting algorithm for the time stepping, and linear finite elements for the spatial discretisation.

We used rational continuum mechanics to derive a family of models for the evolution of an isothermal thin film on a solid substrate. By using this technique, we ensured that the model was thermodynamically consistent, assuming dependent variables were chosen within the constitutive classes specified. In addition, we considered a commonly used model derived using asymptotic assumptions by Burelbach et al. [37]

and showed that, for a non-volatile film, the models are equivalent, as is the model proposed by Thiele [38] by using gradient flow considerations. However, for volatile films, the asymptotically derived model was not necessarily thermodynamically consistent, highlighting an issue with this method of modelling.

Rational arguments were also made to obtain a framework for describing solidification of a material in a non-isothermal setting. Previous work in this area, such as that by Penrose and Fife [47], relies on specifying an entropy functional before initiating the modelling process. We were able to recreate the Penrose and Fife model by saving any choices that needed to be made until the last moment, resulting in a much larger family of potential models.

We then introduced the concept of vertically averaging properties of a thin film to reduce a d-dimensional problem into $d-1$ dimensions. Using this process, we applied rational arguments to derive a thin film heat equation to be used for describing the evolution of temperature in a rigid thin film in a non-isothermal setting. This involved overcoming a closure problem in order to account for variations in the z direction.

Finally, we employed the methods used in all previous chapters to derive a thermodynamically consistent $d-1$-dimensional family of models to describe the evolution of a thin film undergoing solidification-induced phase change in a non-isothermal setting. We then proposed a choice for a free energy functional, based on standard choices made in less complex models, to result in a specific system of equations consistent with the second law of thermodynamics. We performed numerical simulations for this model using the energy stable convex splitting time stepping method for a variety of settings. These consisted of a thin liquid film solidifying, a solid thin film melting, and a volatile thin film experiencing both solidification and evaporation. These scenarios relate directly to the fabrication of a thin film solar cell, which undergoes a process of melting and resolidifying during the annealing stage of fabrication. We validated our choice of model by confirming that it is thermodynamically consistent, and reduces to existing models for more simple scenarios when certain choices are made.

The model provided is of interest to those working with thin films; we have demonstrated that we are able to demonstrate the different effects changing parameters have on the final morphology of the film. In particular, we were able to replicate the findings in [14] that suggested the evaporation rate of a material plays a major role in determining the final surface coverage percentage of a thin film on a substrate.

It can be noted that, while all model families derived in this thesis have dealt with a thin film on a flat substrate, it is simple to simulate an uneven substrate by applying the key result given in (6.1.5-6.1.13) to the bottom surface to project it onto Ω. If the slope of the substrate is sufficiently aggressive, a term handling gravitational effects may be added into the free energy functional Ψ.

9.2 Recommendations for Future Work

We now discuss several recommendations for further research into this topic.

We recommend that the simulations presented in this thesis be extended to two dimensions. One limitation of the simulations provided is that lateral curvature is not present in one dimension. The lateral curvature plays a key role in the evolution of a film under Allen-Cahn type equations, and so should be included in the simulations.

The process of fabricating a thin film solar cell involves a solvent mixed with an absorbing chemical being deposited onto a substrate and heated. During this process, the solvent evaporates off while the absorbing material solidifies. We would recommend that future work be undertaken to extend the single constituent model to deal with multiple constituents. Using rational arguments to describe the evolution of mixtures is a well understood process [89, 103–105]. Using this mixture theory coupled with the model produced in this thesis, setting the evaporation rate of the solvent to be much higher than that of the absorbing material, while setting the melting point of the absorbing material to be higher than that of the solvent would give a good description of the full process of thin film solar cells. In addition, the evaporation of the solvent would be sufficient to destablilise the system, and so evolution of the phase, height function and temperature can commence without the need for a seed.

A final area of interest to progress this work would be to use higher order numerical techniques for simulating the evolution of thin films. This, combined with a more refined regularisation of the functions, would allow parameter optimisation to take place. In the context of thin film solar cell manufacture, this would allow the fabricator to optimise the material, deposition technique and annealing temperature and duration in order to produce the most efficient devices for the lowest energetic and financial cost. An extension of this recommendation, would be to calibrate the model against experimental data.

Bibliography

[1] Christopher T Miles, Kristoffer G van der Zee, Matthew E Hubbard, and Roderick MacKenzie. Thermomechanically-consistent phase-field modeling of thin film flows. *Numerical Methods for Flows*, pages 121–129, 2020.

[2] IEA Statistics. Key world energy statistics. *Paris. International Energy Agency*, 2014.

[3] Solar Photovoltaic Energy. Technology roadmap: solar photovoltaic energy. *Internacional Energy Agency(IEA)*, 2014.

[4] Martin A Green, Keith Emery, Yoshihiro Hishikawa, Wilhelm Warta, and Ewan D Dunlop. Solar cell efficiency tables (version 47). *Progress in Photovoltaics*, 24:3–11, 2015.

[5] Mohammad Khaja Nazeeruddin and Henry Snaith. Methylammonium lead triiodide perovskite solar cells: A new paradigm in photovoltaics. *MRS Bulletin*, 40(08):641–645, 2015.

[6] Martin A Green, Anita Ho-Baillie, and Henry J Snaith. The emergence of perovskite solar cells. *Nature Photonics*, 8(7):506–514, 2014.

[7] Jingbi You, Lei Meng, Tze-Bin Song, Tzung-Fang Guo, Yang Michael Yang, Wei-Hsuan Chang, Ziruo Hong, Huajun Chen, Huanping Zhou, Qi Chen, et al. Improved air stability of perovskite solar cells via solution-processed metal oxide transport layers. *Nature Nanotechnology*, 11(1):75–81, 2016.

[8] Laura M Herz. Charge-carrier dynamics in organic-inorganic metal halide perovskites. *Annual Review of Physical Chemistry*, 67: 65–89, 2016.

[9] Wei Zhang, Michael Saliba, David T Moore, Sandeep K Pathak, Maximilian T Hörantner, Thomas Stergiopoulos, Samuel D Stranks, Giles E Eperon, Jack A Alexander-Webber, Antonio Abate, et al. Ultrasmooth organic–inorganic perovskite thin-film formation and crystallization for efficient planar heterojunction solar cells. *Nature Communications*, 6, 2015.

[10] Alexander T Barrows, Andrew J Pearson, Chan Kyu Kwak, Alan DF Dunbar, Alastair R Buckley, and David G Lidzey. Efficient planar heterojunction mixed-halide perovskite solar cells deposited via spray-deposition. *Energy & Environmental Science*, 7(9): 2944–2950, 2014.

[11] Sven Rühle. Tabulated values of the Shockley–Queisser limit for single junction solar cells. *Solar Energy*, 130:139–147, 2016.

[12] Henry J Snaith. Perovskite solar cells; outshining silicon. 2015.

[13] Seong Sik Shin, Eun Joo Yeom, Woon Seok Yang, Seyoon Hur, Min Gyu Kim, Jino Im, Jangwon Seo, Jun Hong Noh, and Sang Il Seok. Colloidally prepared La-doped BaSnO3 electrodes for efficient, photostable perovskite solar cells. *Science*, 356(6334):167–171, 2017.

[14] Giles E Eperon, Victor M Burlakov, Pablo Docampo, Alain Goriely, and Henry J Snaith. Morphological control for high performance, solution-processed planar heterojunction perovskite solar cells. *Advanced Functional Materials*, 24(1):151–157, 2014.

[15] Ben G Streetman and Sanjay K Banerjee. *Solid state electronic devices*. Prentice-Hall, 2005.

[16] Wanyi Nie, Hsinhan Tsai, Reza Asadpour, Jean-Christophe Blancon, Amanda J Neukirch, Gautam Gupta, Jared J Crochet, Manish Chhowalla, Sergei Tretiak, Muhammad A Alam, et al. High-efficiency solution-processed perovskite solar cells with millimeter-scale grains. *Science*, 347(6221):522–525, 2015.

[17] Mingzhen Liu, Michael B Johnston, and Henry J Snaith. Efficient planar heterojunction perovskite solar cells by vapour deposition. *Nature*, 501(7467):395–398, 2013.

[18] Qi Chen, Huanping Zhou, Ziruo Hong, Song Luo, Hsin-Sheng Duan, Hsin-Hua Wang, Yongsheng Liu, Gang Li, and Yang Yang. Planar heterojunction perovskite solar cells via vapor-assisted solution process. *Journal of the American Chemical Society*, 136(2):622–625, 2013.

[19] Haralds Abolins. Controlling the morphology of CH3NH3PbBr3 perovskite films on planar substrates. *Student Undergraduate Research E-journal!*, 1, 2015.

[20] Yanli Ding, Xin Yao, Xiaodan Zhang, Changchun Wei, and Ying Zhao. Surfactant enhanced surface coverage of CH3NH3PbI3-xClx perovskite for highly efficient mesoscopic solar cells. *Journal of Power Sources*, 272:351–355, 2014.

[21] Yan Li, Xue-Long He, Bin Ding, Li-Li Gao, Guan-Jun Yang, Cheng-Xin Li, and Chang-Jiu Li. Realizing full coverage of perovskite film on substrate surface during solution processing: Characterization and elimination of uncovered surface. *Journal of Power Sources*, 320: 204–211, 2016.

[22] Jörg Puetz and Michel A Aegerter. Dip coating technique. In *Sol-Gel Technologies for Glass Producers and Users*, pages 37–48. Springer, 2004.

[23] Lingling Zheng, Danfei Zhang, Yingzhuang Ma, Zelin Lu, Zhijian Chen, Shufeng Wang, Lixin Xiao, and Qihuang Gong. Morphology control of the perovskite films for efficient solar cells. *Dalton Transactions*, 44(23):10582–10593, 2015.

[24] Cong Li, Qiang Guo, Wenyuan Qiao, Qi Chen, Shuang Ma, Xu Pan, Fuzhi Wang, Jianxi Yao, Chunfeng Zhang, Min Xiao, et al. Efficient lead acetate sourced planar heterojunction perovskite solar cells with enhanced substrate coverage via one-step spin-coating. *Organic Electronics*, 33:194–200, 2016.

[25] Bertrand Faure, German Salazar-Alvarez, Anwar Ahniyaz, Irune Villaluenga, Gemma Berriozabal, Yolanda R De Miguel, and Lennart Bergström. Dispersion and surface functionalization of oxide nanoparticles for transparent photocatalytic and uv-protecting coatings and sunscreens. *Science and technology of advanced materials*, 14(2):023001, 2013.

[26] Daniel Bonn, Jens Eggers, Joseph Indekeu, Jacques Meunier, and Etienne Rolley. Wetting and spreading. *Reviews of Modern Physics*, 81(2):739, 2009.

[27] Eric C Larkins. Lecture notes in solid state devices. *Faculty of Engineering at University of Nottingham*, October 2015.

[28] Pablo Docampo and Henry J Snaith. Obviating the requirement for oxygen in SnO2-based solid-state dye-sensitized solar cells. *Nanotechnology*, 22(22):225403, 2011.

[29] Kai Wang, Chang Liu, Pengcheng Du, Long Chen, Jiahua Zhu, Alamgir Karim, and Xiong Gong. Efficiencies of perovskite hybrid solar cells influenced by film thickness and morphology of CH3 NH3 PbI3-xClx layer. *Organic Electronics*, 21:19–26, 2015.

[30] Qing-Yang Xu, Da-Xing Yuan, Hao-Ran Mu, Femi Igbari, Qiaoliang Bao, and Liang-Sheng Liao. Efficiency enhancement of perovskite solar cells by pumping away the solvent of precursor film before annealing. *Nanoscale Research Letters*, 11(1):248, 2016.

[31] Lioz Etgar, Peng Gao, Zhaosheng Xue, Qin Peng, Aravind Kumar Chandiran, Bin Liu, Md K Nazeeruddin, and Michael Gratzel. Mesoscopic CH3NH3PbI3/TiO2 heterojunction solar cells. *Journal of the American Chemical Society*, 134(42):17396–17399, 2012.

[32] James M Ball, Michael M Lee, Andrew Hey, and Henry J Snaith. Low-temperature processed meso-superstructured to thin-film perovskite solar cells. *Energy & Environmental Science*, 6(6):1739–1743, 2013.

[33] Hui-Seon Kim, Chang-Ryul Lee, Jeong-Hyeok Im, Ki-Beom Lee, Thomas Moehl, Arianna Marchioro, Soo-Jin Moon, Robin Humphry-Baker, Jun-Ho Yum, Jacques E Moser, et al. Lead iodide perovskite sensitized all-solid-state submicron thin film mesoscopic solar cell with efficiency exceeding 9%. *Scientific Reports*, 2:591, 2012.

[34] Aswani Yella, Hsuan-Wei Lee, Hoi Nok Tsao, Chenyi Yi, Aravind Kumar Chandiran, Md Khaja Nazeeruddin, Eric Wei-Guang Diau, Chen-Yu Yeh, Shaik M Zakeeruddin, and Michael Grätzel. Porphyrin-sensitized solar cells with cobalt (ii/iii)–based redox electrolyte exceed 12 percent efficiency. *Science*, 334(6056):629–634, 2011.

[35] Carl V Thompson. Solid-state dewetting of thin films. *Annual Review of Materials Research*, 42:399–434, 2012.

[36] Like Huang, Ziyang Hu, Guoqiang Yue, Jinwang Liu, Xiaohong Cui, Jing Zhang, and Yuejin Zhu. CH3 NH3 PbI3- xClx films

with coverage approaching 100% and with highly oriented crystal domains for reproducible and efficient planar heterojunction perovskite solar cells. *Physical Chemistry Chemical Physics*, 17(34): 22015–22022, 2015.

[37] James P Burelbach, Seymour G Bankoff, and Stephen H Davis. Nonlinear stability of evaporating/condensing liquid films. *Journal of Fluid Mechanics*, 195:463–494, 1988.

[38] Uwe Thiele. Thin film evolution equations from (evaporating) dewetting liquid layers to epitaxial growth. *Journal of Physics: Condensed Matter*, 22(8):084019, 2010.

[39] Morton E Gurtin, Eliot Fried, and Lallit Anand. *The mechanics and thermodynamics of continua*. Cambridge University Press, 2010.

[40] Bernard D Coleman and Walter Noll. The thermodynamics of elastic materials with heat conduction and viscosity. *Archive for Rational Mechanics and Analysis*, 13(1):167–178, 1963.

[41] Geralf Hütter. Coleman–Noll procedure for classical and generalized continuum theories. *Encyclopedia of Continuum Mechanics*, pages 1–8, 2017.

[42] Morton E Gurtin. *Configurational forces as basic concepts of continuum physics*, volume 137. Springer Science & Business Media, 1999.

[43] Mauro Fabrizio, Claudio Giorgi, and Angelo Morro. A thermodynamic approach to non-isothermal phase-field evolution in continuum physics. *Physica D: Nonlinear Phenomena*, 214(2):144–156, 2006.

[44] Samuel M Allen and John W Cahn. Ground state structures in ordered binary alloys with second neighbor interactions. *Acta Metallurgica*, 20(3):423–433, 1972.

[45] John W Cahn and John E Hilliard. Free energy of a nonuniform system. i. interfacial free energy. *The Journal of Chemical Physics*, 28 (2):258–267, 1958.

[46] David J Eyre. Unconditionally gradient stable time marching the cahn-hilliard equation. *MRS online proceedings library archive*, 529, 1998.

[47] Oliver Penrose and Paul C Fife. Thermodynamically consistent models of phase-field type for the kinetic of phase transitions. *Physica D: Nonlinear Phenomena*, 43(1):44–62, 1990.

[48] Adolph Fick. V. on liquid diffusion. *The London, Edinburgh, and Dublin Philosophical Magazine and Journal of Science*, 10(63):30–39, 1855.

[49] Tuncer Cebeci, Jian P Shao, Fassi Kafyeke, and Eric Laurendeau. *Computational fluid dynamics for engineers*. Springer Berlin Heidelberg, 2005.

[50] Mats G Larson and Fredrik Bengzon. *The finite element method: theory, implementation, and applications*, volume 10. Springer Science & Business Media, 2013.

[51] Nele Moelans, Bart Blanpain, and Patrick Wollants. An introduction to phase-field modeling of microstructure evolution. *Calphad*, 32(2):268–294, 2008.

[52] Osborne Reynolds, Arthur William Brightmore, and William Henry Moorby. *The sub-mechanics of the universe*, volume 3. University Press, 1903.

[53] Morton E Gurtin. *An introduction to continuum mechanics*, volume 158. Academic press, 1982.

[54] Hector Gomez and Kristoffer G van der Zee. Computational phase-field modeling. *Encyclopedia of Computational Mechanics Second Edition*, pages 1–35, 2018.

[55] William J Boettinger, James A Warren, Christoph Beckermann, and Alain Karma. Phase-field simulation of solidification. *Annual Review of Materials Research*, 32(1):163–194, 2002.

[56] Michael J Borden, Clemens V Verhoosel, Michael A Scott, Thomas JR Hughes, and Chad M Landis. A phase-field description of dynamic brittle fracture. *Computer Methods in Applied Mechanics and Engineering*, 217:77–95, 2012.

[57] Shunlien Wang, Robert F Sekerka, Adam A Wheeler, Bruce T Murray, Sam R Coriell, Richard J Braun, and Geoffrey B McFadden. Thermodynamically-consistent phase-field models for solidification. *Physica D: Nonlinear Phenomena*, 69(1-2):189–200, 1993.

[58] Uwe Thiele. Note on thin film equations for solutions and suspensions. *The European Physical Journal-Special Topics*, 197(1):213–220, 2011.

[59] Len M Pismen. Spinodal dewetting in a volatile liquid film. *Physical Review E*, 70(2):021601, 2004.

[60] John S Lowengrub, Andreas Rätz, and Axel Voigt. Phase-field modeling of the dynamics of multicomponent vesicles: Spinodal decomposition, coarsening, budding, and fission. *Physical Review E*, 79(3):031926, 2009.

[61] Xiaofeng Yang. Linear, first and second-order, unconditionally energy stable numerical schemes for the phase field model of homopolymer blends. *Journal of Computational Physics*, 327:294–316, 2016.

[62] Jia Zhao, Qi Wang, and Xiaofeng Yang. Numerical approximations for a phase field dendritic crystal growth model based on the invariant energy quadratization approach. *International Journal for Numerical Methods in Engineering*, 110(3):279–300, 2017.

[63] Jie Shen, Jie Xu, and Jiang Yang. The scalar auxiliary variable (SAV) approach for gradient flows. *Journal of Computational Physics*, 353: 407–416, 2018.

[64] Kristoffer G van der Zee, J Tinsley Oden, Serge Prudhomme, and Andrea Hawkins-Daarud. Goal-oriented error estimation for Cahn–Hilliard models of binary phase transition. *Numerical Methods for Partial Differential Equations*, 27(1):160–196, 2011.

[65] Jie Shen, Jie Xu, and Jiang Yang. A new class of efficient and robust energy stable schemes for gradient flows. *SIAM Review*, 61(3):474–506, 2019.

[66] Charles M Elliott and Andrew M Stuart. The global dynamics of discrete semilinear parabolic equations. *SIAM Journal on Numerical Analysis*, 30(6):1622–1663, 1993.

[67] Francisco Guillén-González and Giordano Tierra. On linear schemes for a Cahn–Hilliard diffuse interface model. *Journal of Computational Physics*, 234:140–171, 2013.

[68] Jie Shen, Jie Xu, and Jiang Yang. A new class of efficient and robust energy stable schemes for gradient flows. *SIAM Review*, 61(3):474–506, 2019.

[69] Günter Reiter. Dewetting of thin polymer films. *Physical Review Letters*, 68(1):75, 1992.

[70] F Brochard Wyart and J Daillant. Drying of solids wetted by thin liquid films. *Canadian Journal of Physics*, 68(9):1084–1088, 1990.

[71] David J Srolovitz and Samuel A Safran. Capillary instabilities in thin films. ii. kinetics. *Journal of Applied Physics*, 60(1):255–260, 1986.

[72] Victor M Burlakov, Giles E Eperon, Henry J Snaith, S Jonathan Chapman, and Alain Goriely. Controlling coverage of solution cast materials with unfavourable surface interactions. *Applied Physics Letters*, 104(9):091602, 2014.

[73] David J Srolovitz and Samuel A Safran. Capillary instabilities in thin films. i. energetics. *Journal of Applied Physics*, 60(1):247–254, 1986.

[74] William W Mullins. Flattening of a nearly plane solid surface due to capillarity. *Journal of Applied Physics*, 30(1):77–83, 1959.

[75] Harvey J Palmer. The hydrodynamic stability of rapidly evaporating liquids at reduced pressure. *Journal of Fluid Mechanics*, 75(3): 487–511, 1976.

[76] VS Nikolayev, Denis Chatain, Yves Garrabos, and Daniel Beysens. Experimental evidence of the vapor recoil mechanism in the boiling crisis. *Physical review letters*, 97(18):184503, 2006.

[77] Malcolm B Williams and Stephen H Davis. Nonlinear theory of film rupture. *Journal of Colloid and Interface Science*, 90(1):220–228, 1982.

[78] Oleg E Shklyaev and Eliot Fried. Stability of an evaporating thin liquid film. *Journal of Fluid Mechanics*, 584:157–183, 2007.

[79] Daniel M Anderson and Stephen H Davis. The spreading of volatile liquid droplets on heated surfaces. *Physics of Fluids*, 7(2): 248–265, 1995.

[80] Alexander Oron, Stephen H Davis, and S George Bankoff. Long-scale evolution of thin liquid films. *Reviews of Modern Physics*, 69 (3):931, 1997.

[81] Thomas Erneux and Stephen H Davis. Nonlinear rupture of free films. *Physics of Fluids A: Fluid Dynamics*, 5(5):1117–1122, 1993.

[82] Karl B Glasner and Thomas P Witelski. Coarsening dynamics of dewetting films. *Physical Review E*, 67(1):016302, 2003.

[83] Alexander Oron and S George Bankoff. Dewetting of a heated surface by an evaporating liquid film under conjoining/disjoining pressures. *Journal of Colloid and Interface Science*, 218(1):152–166, 1999.

[84] Len M Pismen and Yves Pomeau. Disjoining potential and spreading of thin liquid layers in the diffuse-interface model coupled to hydrodynamics. *Physical Review E*, 62(2):2480, 2000.

[85] Barend U Felderhof. Dynamics of the diffuse gas-liquid interface near the critical point. *Physica*, 48(4):541–560, 1970.

[86] Pierre Seppecher. Moving contact lines in the Cahn-Hilliard theory. *International Journal of Engineering Science*, 34(9):977–992, 1996.

[87] Francesco Dell'Isola, Henri Gouin, and Giacomo Rotoli. Nucleation of spherical shell-like interfaces by second gradient theory: numerical simulations. *arXiv preprint arXiv:0906.1897*, 2009.

[88] Olga Wodo and Baskar Ganapathysubramanian. Computationally efficient solution to the Cahn–Hilliard equation: Adaptive implicit time schemes, mesh sensitivity analysis and the 3d isoperimetric problem. *Journal of Computational Physics*, 230(15):6037–6060, 2011.

[89] Morton E Gurtin. Generalized Ginzburg-Landau and Cahn-Hilliard equations based on a microforce balance. *Physica D: Nonlinear Phenomena*, 92(3-4):178–192, 1996.

[90] Andrey V Lyushnin, Alexander A Golovin, and Len M Pismen. Fingering instability of thin evaporating liquid films. *Physical Review E*, 65(2):021602, 2002.

[91] Renate Fetzer, Karin Jacobs, Andreas Münch, Barbara Wagner, and Thomas P Witelski. New slip regimes and the shape of dewetting thin liquid films. *Physical Review Letters*, 95(12):127801, 2005.

[92] Haroon S Kheshgi and L Edward Scriven. Dewetting: Nucleation and growth of dry regions. *Chemical Engineering Science*, 46(2):519–526, 1991.

[93] Cornelis Vuik. Some historical notes about the Stefan problem. *Delft University of Technology, Faculty of Technical Mathematics and Informatics*, 1993.

[94] Bruce Chalmers. Principles of solidification. In *Applied solid state physics*, pages 161–170. Springer, 1970.

[95] David P Woodruff. *The solid-liquid interface*. CUP Archive, 1973.

[96] James S Langer. Models of pattern formation in first-order phase transitions. In *Directions in Condensed Matter Physics: Memorial Volume in Honor of Shang-Keng Ma*, pages 165–186. World Scientific, 1986.

[97] Bertrand I Halperin, Pierre C Hohenberg, and Shang-keng Ma. Renormalization-group methods for critical dynamics: I. recursion relations and effects of energy conservation. *Physical Review B*, 10 (1):139, 1974.

[98] Hans W Alt and Irena Pawlow. A mathematical model of dynamics of non-isothermal phase separation. *Physica D: Nonlinear Phenomena*, 59(4):389–416, 1992.

[99] Martin Brokate and Jürgen Sprekels. *Hysteresis and phase transitions*, volume 121. Springer Science & Business Media, 2012.

[100] Kavita Pandey, Pankaj Yadav, Deobrat Singh, Sanjeev Gupta, Yogesh Sonvane, I. Lukačević, Joondong Kim, and Manoj Kumar. First step to investigate nature of electronic states and transport in flower-like mos2: Combining experimental studies with computational calculations. *Scientific Reports*, 6:32690, 09 2016.

[101] Michel C Delfour and Jean-Paul Zolésio. *Shapes and geometries: metrics, analysis, differential calculus, and optimization*, volume 22. Siam, 2011.

[102] Eliot Fried and Morton E Gurtin. Thermomechanics of the interface between a body and its environment. *Continuum Mechanics and Thermodynamics*, 19(5):253–271, 2007.

[103] David Jacqmin. Calculation of two-phase navier–stokes flows using phase-field modeling. *Journal of Computational Physics*, 155(1): 96–127, 1999.

[104] RJ Atkin and RE Craine. Continuum theories of mixtures: basic theory and historical development. *The Quarterly Journal of Mechanics and Applied Mathematics*, 29(2):209–244, 1976.

[105] Ingo Müller. A thermodynamic theory of mixtures of fluids. *Archive for Rational Mechanics and Analysis*, 28(1):1–39, 1968.